Satisficing Nonlinear Spacecraft Rendezvous Under Control Magnitude and Direction Constraints

Shinji Mitani

2013

Abstract

This dissertation concerns the satellite's trajectory control problem subject to constraints on control magnitude and direction.

Firstly, the formation and reconfiguration problem under thrust magnitude and direction constraints is considered. An optimal controller with these constraints is derived using a continuous smoothing method, in which a sequence of unconstrained optimal control problems are solved according to Pontryagin's Minimum Principle by introducing barrier functions to the original performance index. Optimal controllers are successfully formulated in L_1- and L_2-norm problems. The magnitude and direction constrained solution is naturally extended from the solution with only magnitude constraints. Numerical simulations demonstrate that a successive optimal controller subject to such multiple constraints can be obtained by solving a two-point boundary value problem using the shooting method in a non-coplanar circular orbit and a coplanar eccentric orbit.

Secondly, a rendezvous problem under thrust magnitude and direction constraints is considered. Considering the constraints on the parameters in the general quadratic performance index, a control design process is proposed using modal analysis to limit the thrust angle during at the initial and final phases. Subsequently, using a candidate control Lyapunov function by solving the Riccati equation for the considered performance index, a new control applying "satisficing" concepts is devised to meet the constraints strictly from start to finish. A constraint-satisficing scheme has been newly proposed by introducing two barrier functions. For a simple nonlinear controller, a controller generated by projecting a constraint-free optimal controller onto the input constraint is proposed and its stability is investigated. Some numerical simulations treating nonlinear relative orbit systems show that various control sets, which guide the orbit to the origin, can be generated, while the convergence property of the closed-loop system is analyzed by the proposed parameter design with the assistance of a graphical plot.

Acknowledgements

First and foremost, I am obliged to my adviser, Professor Hiroshi Yamakawa who provided helpful comments and suggestions during the course of my study. He introduced me to the subject of control theory and frequently engaged in discussions. He has taught me much more than control theory, and I consider myself very fortunate to have had the opportunity to work with him.

Special thanks are also due to Dr. Mai Bando, whose opinions and information have helped me considerably throughout the production of this study.

I would like to express my appreciation to Professors Takashi Hikihara and Kei Senda for their invaluable comments and suggestions.

Finally, thanks are also due to the co-workers at my company, JAXA for their support and warm encouragement.

Shinji Mitani
Kyoto University

Contents

List of Figures

List of Tables

Nomenclature

a	= Euclidean norm of $\boldsymbol{a}$, $\|\boldsymbol{a}\|$
$\boldsymbol{a}'$	= differential value of $\boldsymbol{a}$ with respect to τ
$\dot{\boldsymbol{a}}$	= differential value of $\boldsymbol{a}$ with respect to t
$\hat{\boldsymbol{a}}$	= unit vector of $\boldsymbol{a}$
$b(\boldsymbol{x})$	= selectivity index
F_u,F_b	= barrier function
H	= Hamiltonian function
J	= nondimensional performance index
L_1	= L_1 norm, u
L_2	= L_2 norm, $u^2/2$
$\mathcal{P}$	= two-point boundary value problem
$p_s(\boldsymbol{u}, \boldsymbol{x})$	= a selectability function
$p_r(\boldsymbol{u}, \boldsymbol{x})$	= a rejectability function
$S_b(\boldsymbol{x})$	= satisficing set with a selectivity index $b(\boldsymbol{x})$
$\boldsymbol{r}$	= position vector from the target to the chaser
$\boldsymbol{u}$	= control acceleration
U_C	= a subset of the control input constraints
V	= control Lyapunov function
$\boldsymbol{x}$	= state of the chaser
β	= angle between $-\boldsymbol{p}$ and $\boldsymbol{u}$
γ	= limitation of the thrust angle
$\theta(\boldsymbol{\xi}, \boldsymbol{u})$	= angle between $-\boldsymbol{\xi}$ and $\boldsymbol{u}$

Chapter 1

Introduction

1.1 Background

1.1.1 Motivation of the Study

This dissertation discusses rendezvous and formation flying trajectory planning where the target moves in circular and elliptic orbits with such practical constraints, and proposes a novel safety guidance approach to the rendezvous problem.

In space applications such as rendezvous and formation flying, approaches to the target and reconfiguring of the formation must be designed under multiple combinations of input constraints. For example, an input magnitude constraint definitely exists to limit thrusting power and the thrust activation direction may also be constrained for cases in which the chaser's attitude must be maintained in a fixed direction due to factors like the sensor field of view (FOV) and sun direction, or whereby the thrust plume must be avoided against the target. These conditions can occur when the injection direction is restricted for cases in which the thrust plume must be avoided or the direction of control with the thrusters fixed on the chaser is restricted, because the target must be visible in the FOV of the camera of the chaser while the chaser moves safely toward the target. These constraints can also be caused by peculiarities of the attitude control system and the stabilization mode of a spacecraft, which are functions of time and the state vector. Therefore it is worth considering problems under a simultaneous combination of input magnitude and directional constraints, which may be functions of time and the state vector. This dissertation treats the rendezvous problem under conditions whereby the chaser's thrust direction relative to the target direction is constrained to some fixed angle in addition to the thruster saturation.

1.1.2 Related Works for the Problem

In flight optimization literature, although constraints on the thrust magnitude value have been extensively investigated, insufficient attention has been applied to constraints on thrust direction. Some of the scarce literature dealing with the thruster direction constraints in rendezvous and formation flying applications include, for example, as follows; an analytic solution was obtained for the effects of continuous radial or vertical thrust on the orbital motion and the mass loss of a vehicle initially in a circular orbit (Boltz, 1991, 1992). A semianalytic method for determining the periodic trajectories of a spacecraft under the influence of a constant small thrust directed from a central station in a circular orbit was presented using the Clohessy-Wiltshire equations by Yamakawa and Funaki (Yamakawa and Funaki, 2008). Woffinden considered the circular orbital rendezvous problem referred to as trigger angle targeting, in which the maneuver start point is restricted to the direction of the target (Woffinden *et al.*, 2008). Sukhanov and Prado (Sukhanov and Prado, 2007, 2008) considered transfers with low thrust subject to constraints imposed on the thrust vector direction and derived some necessary optimal conditions. Richards et al. (Richards *et al.*, 2002) introduced a method for determining fuel-optimal trajectories for spacecraft subject to avoidance requirements. These include avoidance of collision with obstacles or other vehicles and prevention of thruster plumes from one spacecraft impinging on another. The resulting problem is a mixed integer linear program (MILP) that can be solved using available software.

1.1.3 Numerical Approaches to Optimal Control Problem with Constraints

Numerical optimization with constraints is employed in this work. Various numerical optimization techniques can be used to solve such problems under complicated conditions. Betts (Betts, 1998) surveyed numerical methods for a trajectory optimization problem in which path and boundary constraints are imposed. Direct transcription methods using a piecewise polynomial representation for the state and controls are often used to solve optimal control problems in the context of spacecraft transfer trajectories (Conway, 2010). These methods discretize the time horizon and the control and state variables. When no state constraint exists, minimum-fuel problems have sometimes been solved by directly applying Pontryagin's Minimum Principle (PMP) (Pontryagin, 1961; Bryson and Ho, 1975). This approach yields a two-point boundary value problem (TPBVP), which is then solved using a shooting method (Betts, 1998). Enright and Conway (Enright and Conway, 1991) studied a method employing a direct

optimization technique that uses a piecewise polynomial representation for the state, controls, and collocation, which converts the optimal control problem into a nonlinear programming problem.

Irvin, Cobb, and Lovell (Irvin Jr. *et al.*, 2009) investigated strategies to enable a deputy satellite to hover within a defined volume fixed in the vicinity of a chief satellite in a circular orbit for an extended period. The problem of optimizing low-thrust reconfiguration maneuvers for spacecraft flying in formation was addressed by Massari and Bernelli-Zazzera (Massari and Bernelli-Zazzera, 2009). The problem was stated as solving an optimal control problem, in which an objective function related to control was minimized, satisfying a series of constraints on the trajectory that were both differential and algebraic. The problem was treated as a nonlinear programming problem with a parallel multiple-shooting method.

Bertrand and Epenoy (Bertrand and Epenoy, 2002) investigated the solution to bang-bang optimal control problems by shooting methods and proposed a new smoothing approach that yielded a good approximation of the original problem. In this method, a sequence of unconstrained optimal control problems is solved according to PMP by introducing a barrier function to the original performance index. The solutions converge toward the solution of the original problem while strictly satisfying the treated constraints as the perturbation coefficients of the barrier functions approach zero. The orbit transfer problem with a magnitude constraint was first treated in (Bertrand and Epenoy, 2002). Gil-Fernandez also considered this method and solved a practical continuous low-thrust orbit transfer problem (Gil-Fernandez and Gomez-Tierno, 2010). In addition, Epenoy solved a collision avoidance rendezvous problem by introducing new penalty functions (Epenoy, 2011).

Receding horizon (RH) control is a finite horizon open-loop optimal control problem in which the current control is obtained by solving an optimal control problem at each sampling instant using the current state of a nonlinear plant as the initial state and the first control in this sequence is applied to the plant. An important advantage of the RH techniques is its ability to cope with constraints on controls and states (Mayne *et al.*, 2000). Keerthi and Gilbert (Keerthi and Gilbert, 1988) imposed a terminal state equality constraint and first used the value function as the Lyapunov function to ensure the stability of model predictive control (MPC) of constrained nonlinear systems. Several modified nonlinear and stabilized RH formulations have since been proposed; mostly based on a combination of additional constraints or a terminal penalty (Mayne *et al.*, 2000; Maciejowski, 2002). Sznaier (Sznaier *et al.*, 2003) proposed a controller design method, based on a combination of RH and control Lyapunov functions (CLFs), for nonlinear systems subject to input constraints. In principle, stability can be achieved

by simply extending the optimization horizon until the trajectory enters an invariant set where these constraints are no longer binding.

1.2 Approach

In the thesis, a continuous low-thrust formation and reconfiguration problem under control magnitude and direction constraints is treated. Specifically, we herein focus on the condition where the thrust direction of the chaser relative to the direction of the target is constrained. The basic objectives include to drive the chaser vehicle to transfer between the relative periodic orbit around the target under a small thrust magnitude and angle conditions and minimize fuel consumption.

We first discuss the necessary condition of the optimal controller subject to constraints on control magnitude and direction using a smoothing approach. To the best of the authors' knowledge, there has been no report on treating control direction constraints by applying the smoothing method. This approach is based on previous work by Bertrand and Epenoy (Bertrand and Epenoy, 2002) and the necessary condition of the optimal controller is successfully formulated in L_1- and L_2-norm problems respectively by introducing a newly proposed extra barrier function. These solutions are a natural extension of the solution using only a magnitude constraint obtained by Bertrand and Epenoy (Bertrand and Epenoy, 2002). As the perturbation coefficients of the barrier functions approach zero, the smoothed optimal controller approaches the necessary condition whereby the optimal thrust is directed along the projection of Lawden's primer vector (Lawden, 1963) onto the restricting set, while the control, the primer, and the admissible direction vectors are coplanar. This extremal property is completely consistent with the results reported by Sukhanov and Prado (Sukhanov and Prado, 2007, 2008). The method proposed herein is an optimal open-loop controller that emphasizes the performance index.

Secondly, we propose a new approach that considers constraints on thrust angle based on optimal feedback control to introduce a general linear quadratic regulator (LQR), in which the performance index in state and control is designed to align the thrust direction to the relative position vector. A modal analysis method is used to determine the design parameters to make the final thrust angle small. The initial thrust angle can be estimated easily from the optimal control and rendezvous start phase. The transient rendezvous phase, however, may not guarantee constraints on the thrust direction. For the transient phase, this paper proposes a novel method to guarantee closed-loop stability subject to constraints on the thrust angle. Based on a "satisficing" theory proposed by Curtis and Beard (Curtis and Beard, 2002*b*, 2004) that can

deliver a parametric set of stable control inputs, the optimal control designed by modal analysis and contour plots is projected onto a stable domain defined by a candidate control Lyapunov function (CLF). The control applying the satisficing method to the rendezvous problem with control direction constraints is first considered in (Mitani and Yamakawa, 2010). In addition, we show that choosing the candidate CLF generated by solving the Riccati equation for the general performance index easily makes the thrust angle at the final phase small and analytically predictable. In addition, the design process to select parameters to maintain a small-magnitude thrust angle is clarified. The proposed method assumes active rendezvous, involving communication between target and chaser so that chaser's relative states to the target are well estimated.

We consider the elliptic rendezvous problem with constraints on thrust direction using a satisficing method proposed by Curtis and Beard (Curtis and Beard, 2002*b*, 2004) and devise a feedback controller that strictly satisfies the thrust angle constraints (Mitani and Yamakawa, 2010). The idea of introducing a control restriction space to the satisficing set was proposed by Ren and Beard (Ren and Beard, 2004), who treated only control magnitude constraints. Although, in principle, the proposed method can treat added magnitude constraints, this controller does not strictly satisfy the necessary condition of optimality as defined by the L_1 or L_2-norm. The previously proposed method was a feedback controller that emphasizes stability.

Lastly we take over the main results in the satisficing method initially applied to the rendezvous problem with control direction constraints (Mitani and Yamakawa, 2010, 2011). Likewise, a Lyapunov function for the general linear quadratic regulator (LQR) is chosen as a local constrained control Lyapunov function (CCLF) (Sznaier *et al.*, 2003). By performing modal analysis in a linear system (Khalil, 2002), the thrust angle in the final convergent phase can be analytically predicted. The trajectory becomes optimal once the trajectory enters the invariant set where these constraints are no longer binding. To treat the input constraint in the transient phase, a new satisficing set to guarantee closed-loop stability under input constraints on magnitude and direction is proposed, inspired by the idea of a smoothing technique (Bertrand and Epenoy, 2002; Gil-Fernandez and Gomez-Tierno, 2010). Subsequently, a proposed controller is chosen to minimize a pre-Hamiltonian from the given set. The proposed controller in the set resembles that in (Mitani and Yamakawa, 2010) from the perspective of having stability and satisficing constraints, except the magnitude constraint consideration. However, the proposed controller would be more suitable for the following reasons: firstly, since a local CCLF is chosen for the value function in the nonbinding case, the proposed controller becomes a unique optimal control solution where the constraint condition is nonbinding. Secondly, conversely, the proposed controller gives a projection solution

onto the input constraint set where the constraint condition is binding. The projected controller would be sub-optimal because it is guaranteed that the projection vector of a negative signed Lawden's primer vector onto the constraint boundary is optimal (Sukhanov and Prado, 2007, 2008).

1.3 Outline of the Thesis

This dissertation is organized as follows. We propose two new approaches to the problem of controlling the trajectory of a spacecraft safely while reducing fuel consumption subject to constraints on control magnitude and direction. The first approach involves finding an optimal solution in an open loop by introducing a barrier function. The second involves determining a sub-optimal and closed-loop solution by applying a so-called satisficing method. Solving the optimal control problem is largely divided into two approaches: solving a Hamilton-Jacobi-Bellman (HJB) equation based on dynamic programming and solving a Euler-Lagrange equation based on the variational calculus. Chapter 2 describes an approach for solving both classic optimal control problems. We cover some basic properties of a smoothing technique that will jointly apply to both methods and also take into account the constraints. Finally, we describe the concept of control Lyapunov function (CLF), which plays an important role in the so-called satisficing theory. The relevance of the solution of the HJB equation provides the overall outlook.

Chapter 3 states the dynamic equations, which are known as TH equations, and presents the formulation of a two-point boundary value problem (TPBVP) subject to constraints on control magnitude and direction, with a brief reviews of how to adapt the smoothing method to the magnitude constrained problem. The smoothing approach is applied to the optimal control problem subject to constraints on magnitude and direction and the formulation of the sequential optimal controller by extending the results with the magnitude constraint obtained in the previous section is described. Finally, simulation results are presented, and the effectiveness of the proposed method is discussed.

In Chapter 4, the theory of satisficing is briefly reviewed. The basic idea involves defining two utility functions that quantify the benefits and costs of an action. The "selectability" function was chosen as the distance from the predicted state at the next time instant to the origin, while the "rejectability" function was chosen as proportional to the control effort. By linking the "selectability" function to a CLF, closed-loop asymptotic stability is ensured (Curtis and Beard, 2002*a*, 2004), and provides complete parameterization as a generalization of the input-to-state stabilizing (ISS) version of

Sontag's formula (Sontag, 1989) and Freeman and Kokotovic's mini-norm approach (Freeman and Kokotovic, 1996).

Chapter 5 explains the satisficing method in the case of a circular orbit. We formulate the fuel-optimal control problem, which includes the effect of thrust angle constraints as a penalty function, and show how to determine the design parameters to survey the final thrust angle using modal analysis. Using the theory of satisficing, the stable control for the transient phase is constructed. We show how our proposed method can be extended to cases of eccentric orbit. Finally, simulation results are given and the effectiveness of the proposed method is discussed.

Chapter 6 proposes a new representation of the satisficing set by applying two barrier functions and discusses some properties, conditions and differences from the constraint-free satisficing set. The applicability of the control is shown for the rendezvous nonlinear control problem subject to constraints on magnitude and direction and the controller's stability is investigated. Finally, the nonlinear rendezvous simulation results are presented, and the effectiveness of the proposed method is discussed.

Finally, Chapter 7 presents conclusions and future areas of research suggested by this thesis.

Chapter 2

Approaches for Solving Nonlinear Optimal Control Problems

2.1 Introduction

We propose two new approaches to the problem of controlling the trajectory of the spacecraft safely while reducing fuel consumption, subject to constraints on control magnitude and direction. The first involves finding an optimal solution in an open loop by introducing a barrier function. The second involves determining a sub-optimal and closed-loop solution by applying the so-called satisficing method. Solving the optimal control problem is largely divided into two approaches: solving the Hamilton-Jacobi-Bellman (HJB) equation based on dynamic programming and solving the Euler-Lagrange equation based on the variational calculus. Chapter 2 describes an approach for solving both classic optimal control problems. We cover some basic properties of smoothing technique that will jointly apply to both methods to also take into account the constraints. Finally, we describe a concept of control Lyapunov function (CLF), which plays an important role in the satisficing theory. The relevance of the solution of the HJB equation provides an overall prospect in this thesis.

2.2 Trajectory Optimization with Constraints

Typically the system dynamics are defined by a set of ordinary differential equations written in explicit form, which are referred to as the state or system equations

$$\dot{\boldsymbol{x}} = f(t, \boldsymbol{x}(t)) + g(t, \boldsymbol{x}(t))\boldsymbol{u}(t) \tag{2.1}$$

where $\boldsymbol{x} \in \boldsymbol{R}^n$, $f : \boldsymbol{R}^n \to \boldsymbol{R}^n$, $g : \boldsymbol{R}^n \to \boldsymbol{R}^{n\times m}$ and $\boldsymbol{u} \in \boldsymbol{R}^m$. Initial conditions at time t_0 are defined by

$$\boldsymbol{x}(t_0) = \boldsymbol{x}_0 \tag{2.2}$$

and terminal conditions at the final time t_f are defined by

$$\boldsymbol{x}(t_f) = \boldsymbol{x}_f \tag{2.3}$$

In addition, the solution must satisfy algebraic path constraints in the form

$$\boldsymbol{g}[\boldsymbol{x}(t), \boldsymbol{u}(t), t] \leq 0 \tag{2.4}$$

where $\boldsymbol{g}$ is a vector of size N_g. The basic optimal control problem involves determining the control vectors $\boldsymbol{u}(t)$ to minimize the performance index (Betts, 1998)

$$J = \int_{t_0}^{t_f} L[\boldsymbol{x}(t), \boldsymbol{u}(t), t]\mathrm{d}t \tag{2.5}$$

Various index values $L \geq 0$ can be taken according to the considered problems. The case $L = \|\boldsymbol{u}(t)\|$ is the L_1-norm problem, where the performance index Eq. (2.5) represents the minimum fuel consumption, whereas the case $L = \|\boldsymbol{u}(t)\|^2/2$ is the L_2-norm problem, where the performance index Eq. (2.5) represents the minimum energy. When $L = \boldsymbol{x}(t)^T Q\boldsymbol{x}(t) + \boldsymbol{u}(t)^T R\boldsymbol{u}(t) + 2\boldsymbol{x}(t)^T N\boldsymbol{u}(t)$, Eq. (2.5) is the more general performance index of the well-known LQR problem, where Q, R, and N are weight matrices (Bryson and Ho, 1975).

2.3 Nonlinear Optimal Control

Optimal control theory, in its modern sense, began in the 1950s with the formulation of two design optimization techniques: Pontryagin Minimum Principle and Dynamic Programming. While the minimum principle, which represents a far-reaching generalization of the Euler-Lagrange equations from the classical calculus of variations, may be viewed as an outgrowth of the Hamiltonian approach to variational problems, the method of dynamic programming may be viewed as an outgrowth of the Hamilton-Jacobi approach to variational problems (Primbs, 1999; Bryson and Ho, 1975).

2.3.1 Dynamic Programming: Hamilton-Jacobi-Bellman equations

Define $V^*(\boldsymbol{x}_0)$ as the minimum of the performance index taken over all admissible trajectories $(\boldsymbol{x}(t), \boldsymbol{u}(t))$ where $\boldsymbol{x}$ starts at $\boldsymbol{x_0}$:

$$V^*(\boldsymbol{x}_0) = \min_{\boldsymbol{u}} \int_0^\infty (q(\boldsymbol{x}) + \boldsymbol{u}^T\boldsymbol{u})dt \tag{2.6}$$

$$s.t. \qquad \dot{\boldsymbol{x}} = f(\boldsymbol{x}) + g(\boldsymbol{x})\boldsymbol{u} \tag{2.7}$$

$$\boldsymbol{x}(0) = \boldsymbol{x}_0 \tag{2.8}$$

Using the principle of optimality yields one form of the so-called Hamilton-Jacobi-Bellman equation

$$\min_{\boldsymbol{u}} \left\{ [q(\boldsymbol{x}(t)) + \boldsymbol{u}^T(t)\boldsymbol{u}(t)] + \left(\frac{\partial V^*}{\partial \boldsymbol{x}}\right)^T [f(\boldsymbol{x}(t)) + g(\boldsymbol{x}(t))\boldsymbol{u}(t)] \right\} = 0 \tag{2.9}$$

The boundary condition for this equation is given by $V^*(0) = 0$ where $V^*(\boldsymbol{x})$ must be positive for all $\boldsymbol{x}$ (since it corresponds to the optimal cost which must be positive).

In many cases, this is not the final form of the equation. Two more steps can often be performed to reach a more convenient representation of the Hamilton-Jacobi-Bellman equation. First, the indicated minimization is performed, leading to a control law of the form

$$\boldsymbol{u}^* = -\frac{1}{2} g^T(\boldsymbol{x}) \frac{\partial V^*}{\partial \boldsymbol{x}} \tag{2.10}$$

The second step involves substituting Eq. (2.10) back into Eq. (2.9), and solving the resulting nonlinear partial differential equation

$$\left(\frac{\partial V^*}{\partial \boldsymbol{x}}\right)^T f(\boldsymbol{x}) - \frac{1}{4}\left(\frac{\partial V^*}{\partial \boldsymbol{x}}\right)^T g(\boldsymbol{x}) g^T(\boldsymbol{x}) \frac{\partial V^*}{\partial \boldsymbol{x}} + q(\boldsymbol{x}) = 0 \tag{2.11}$$

for $V^*(\boldsymbol{x})$. Equation (2.11) is what we will often refer to as the Hamilton-Jacobi-Bellman (HJB) equation.

2.3.2 Calculus of variations: Euler-Lagrange equations

The Euler-Lagrange solution is based on consideration of the optimal control problem within the framework of constrained optimization:

$$\min_{\boldsymbol{u}} \int_{t_0}^{t_f} (q(\boldsymbol{x}) + \boldsymbol{u}^T\boldsymbol{u})\mathrm{d}t + \varphi(\boldsymbol{x}(t_f)) \tag{2.12}$$

$$s.t. \qquad \dot{\boldsymbol{x}} = f(\boldsymbol{x}) + g(\boldsymbol{x})\boldsymbol{u} \tag{2.13}$$

$$\boldsymbol{x}(0) = \boldsymbol{x}_0 \tag{2.14}$$

The objective function is based on a finite horizon length of terminal weight $\varphi(\cdot)$ applied at the end of the horizon. This cost is equivalent to an infinite horizon cost only when the terminal weight is chosen as the value function, i.e. $\varphi(\cdot) = V^*(\cdot)$, which can only be found from the solution to the HJB equation. Secondly, in addition to viewing the dynamics as a constraint, a specific initial condition is imposed.

The calculus of variations solution can be thought of as a standard application of the necessary conditions for constrained optimization. The first step involves using Lagrange multipliers to adjoin the constraints to the performance index. Since the constraints are determined by the system differential equation and represent equality constraints that must hold at each instant in time, an associated multiplier $\boldsymbol{\lambda}(t) \in \boldsymbol{R}^n$ is a function of time. Defining for convenience, the following scalar function H, called the Hamiltonian,

$$H(\boldsymbol{x}(t), \boldsymbol{u}(t), \boldsymbol{\lambda}(t)) = q(\boldsymbol{x}(t)) + \boldsymbol{u}^T(t)\boldsymbol{u}(t) + \boldsymbol{\lambda}^T(t)(f(\boldsymbol{x}(t)) + g(\boldsymbol{x}(t))\boldsymbol{u}(t)) \quad (2.15)$$

For a stationary point, this must be equal to zero for all allowable variations. The following equations, which represent the necessary conditions for optimality known as Euler-Lagrange equations, are used to design the control $\boldsymbol{u}(t)$ that minimizes the performance index, and can be summarized as follows:

$$\dot{\boldsymbol{x}} = f(\boldsymbol{x}) + g(\boldsymbol{x})\boldsymbol{u} \quad (2.16)$$

$$\dot{\boldsymbol{\lambda}} = -\left(\frac{\partial H}{\partial \boldsymbol{x}}\right) \quad (2.17)$$

$$\frac{\partial H}{\partial \boldsymbol{u}} = 0 \quad (2.18)$$

with boundary conditions

$$\boldsymbol{x}(0) \quad \text{given} \quad (2.19)$$

$$\boldsymbol{\lambda}(T) = \left(\frac{\partial \varphi}{\partial \boldsymbol{x}}\right)\Bigg|_{t=T} \quad (2.20)$$

The optimizing control action $\boldsymbol{u}^*(t)$ is determined by

$$\boldsymbol{u}^*(t) = \arg\min_{\boldsymbol{u}} H(\boldsymbol{x}^*(t), \boldsymbol{u}, \boldsymbol{\lambda}^*(t)) \quad (2.21)$$

where $\boldsymbol{x}^*(t)$ and $\boldsymbol{\lambda}^*(t)$ denote the solution corresponding to the optimal trajectory.

2.4 Smoothing Technique

Smoothing techniques are a useful tool, also used in optimal control to solve problems with discontinuous mixed constraints on state and control (Epenoy and Ferrier, 2001).

Bertrand and Epenoy propose deducing the solution to the initial problem from successive solutions of an auxiliary problem (Bertrand and Epenoy, 2002). This last one is defined by Eqs. (2.1-2.3), constraint (2.4), and the following perturbed performance index

$$J^{\varepsilon} = \int_{t_0}^{t_1} [L(\boldsymbol{x}, \boldsymbol{u}) + \varepsilon F(\boldsymbol{x}, \boldsymbol{u})] \mathrm{d}t = \int_{t_0}^{t_1} h[\boldsymbol{x}, \boldsymbol{u}, \varepsilon] \mathrm{d}t \tag{2.22}$$

where F is a continuous function satisfying

$$F(w) \geq 0 \quad \forall w \in [0, 1] \tag{2.23}$$

We will see below the role of this property. In addition, parameter ε is assumed to be in the interval $(0, 1]$, whereupon the function $h[\boldsymbol{x}, \boldsymbol{u}, \varepsilon]$ is continuous and strictly decreasing for each t in $[t_0, t_1]$ and each $u \in \boldsymbol{\mathcal{U}}$.

The continuation approach consists first of solving the perturbed problem with $\varepsilon = 1$ (i.e. the corresponding TPBVP yields by the minimum principle). Subsequently, after defining a decreasing sequence of ε values ($\varepsilon_1 = 1 > \varepsilon_2 > \cdots > \varepsilon_n$)), the current TPBVP associated with $\varepsilon = \varepsilon_k (k = 2, \cdots, n)$ is solved with the solution of the previous one as a starting point. This iterative process terminates when a certain precision on the performance index has been achieved

$$||J^{\varepsilon_{k+1}} - J^{\varepsilon_k}|| \leq \eta, \quad \eta > 0 \tag{2.24}$$

As a result of the inequality (2.23), we can derive some interesting properties:

Proposition 2.4.1

$$J^{\varepsilon_1}(\boldsymbol{u}^*_{\varepsilon_1}) \leq J^{\varepsilon_2}(\boldsymbol{u}^*_{\varepsilon_2}) \leq \cdots \leq J^{\varepsilon_n}(\boldsymbol{u}^*_{\varepsilon_n}) \leq J(\boldsymbol{u}^*) \leq J(\boldsymbol{u}^*_{\varepsilon_k}), k = 1, \cdots, n \tag{2.25}$$

where $\boldsymbol{u}^*_{\varepsilon}$ denotes the optimal control associated with J^{ε} and $\boldsymbol{u}^*$ is the original optimal control given by Eq. (2.21).

Moreover, under some mild assumptions, and if the existence of a solution for all $\varepsilon \in (0, 1]$ is assumed, we can also write:

Proposition 2.4.2

$$\lim_{\varepsilon \to 0} J^{\varepsilon}(\boldsymbol{u}^*_{\varepsilon}) = J(\boldsymbol{u}^*) \tag{2.26}$$

$$\lim_{\varepsilon \to 0} J(\boldsymbol{u}^*_{\varepsilon}) = J(\boldsymbol{u}^*) \tag{2.27}$$

The proofs of these propositions are given by Gergaud (Gergaud, 1989).

2.5 Control Lyapunov Function Technique

A control Lyapunov function (CLF) is a C^1, proper, positive-definite function V:

$$\inf_{\boldsymbol{u}} \dot{V} = \inf_{\boldsymbol{u}} V_x^T [f(\boldsymbol{x}) + g(\boldsymbol{x})\boldsymbol{u}] < 0 \tag{2.28}$$

for all $\boldsymbol{x} \neq 0$ (Artstein, 1983). Specifically, if $\boldsymbol{u} \in U_C \subset \boldsymbol{R}^m$, $V(\boldsymbol{x})$ is said to be a constrained CLF (CCLF) (Sznaier *et al.*, 2003). We treat a general definition CLF V which depends on time t explicitly from Chapter 4 onward.

If it is possible to make the time derivative $\dot{V}$ negative at every point by an appropriate choice of $\boldsymbol{u}$, then we will have achieved our goal and can stabilize the system with V, a Lyapunov function for the controlled system under the chosen control actions, which is exactly the condition given in the inequality (2.28).

In what follows we develop connections between nonlinear control techniques based on control Lyapunov functions, and the HJB approach to the optimal control problem. When a CLF is viewed beyond a mere Lyapunov stability framework, as an approximation of the value function V^*, many CLF approaches have natural derivations the HJB frame work. We pursue these connections here, focusing the majority of our attention on Sontag's formula and pointwise min-norm controllers.

Rewiring the HJB equation (2.11) as

$$\left(\frac{\partial V^*}{\partial \boldsymbol{x}}\right)^T \left[f - \frac{1}{2} g g^T \frac{\partial V^*}{\partial \boldsymbol{x}}\right] + \frac{1}{4}\left(\frac{\partial V^*}{\partial \boldsymbol{x}}\right)^T g g^T \frac{\partial V^*}{\partial \boldsymbol{x}} + q = 0$$

and recalling that

$$\boldsymbol{u}^* = -\frac{1}{2} g^T \frac{\partial V^*}{\partial \boldsymbol{x}}$$

allows us to reformulate Eq. (2.11) as

$$\left(\frac{\partial V^*}{\partial \boldsymbol{x}}\right)^T [f + g\boldsymbol{u}^*] = -\left[\frac{1}{4}\left(\frac{\partial V^*}{\partial \boldsymbol{x}}\right)^T g g^T \frac{\partial V^*}{\partial \boldsymbol{x}} + q\right] \leq 0 \tag{2.29}$$

Note that now the left-hand side appears as in the definition of a control Lyapunov function (cf. Eq.(2.28)). Hence, if the right-hand side is negative, V^* is a control Lyapunov function. Technically, the right-hand side need only be negative semi-definite, meaning the value function may only be a so-called weak CLF. Of course, for any positive-definite cost parameter q, this equation shows that V^* is in fact a strict CLF. Many CLF-based techniques can be viewed assuming that a CLF is an estimate of the value function, which is ideal for performance purposes.

Chapter 3

Continuous-thrust Transfer with Control Magnitude and Direction Constraints Using Smoothing Techniques

3.1 Introduction

The method proposed herein is an optimal open-loop controller that emphasizes the performance index.

Various numerical optimization techniques can be used to solve such problems under complicated conditions. Direct transcription methods that use a piecewise polynomial representation for the state and controls are often used to solve optimal control problems in the context of spacecraft transfer trajectories (Conway, 2010). These methods discretize the time horizon and the control and state variables. When no state constraint exists, minimum-fuel problems have sometimes been solved by directly applying Pontryagin's minimum principle (PMP) (Pontryagin, 1961; Bryson and Ho, 1975). This approach yields a two-point boundary value problem (TPBVP), which is then solved using a shooting method (Betts, 1998). Few authors have used PMP to solve the inequality constrained optimal control problem that arises when constraints on magnitude and direction are imposed. Bertrand and Epenoy (Bertrand and Epenoy, 2002) investigated the solution of bang-bang optimal control problems by shooting methods. They proposed a new smoothing approach that yields a good approximation of the original problem. In this method, a sequence of unconstrained optimal control problems is solved according to PMP by introducing a barrier function to the original performance index. The solutions converge toward the solution of the original problem while strictly

satisfying the treated constraints as the perturbation coefficients of the barrier functions approach zero. The orbit transfer problem with a magnitude constraint was first treated in (Bertrand and Epenoy, 2002). Gil-Fernandez also considered this method and solved a practical continuous low-thrust orbit transfer problem (Gil-Fernandez and Gomez-Tierno, 2010). In addition, Epenoy solved a collision avoidance rendezvous problem by introducing new penalty functions (Epenoy, 2011).

To the best of the authors' knowledge, there has been no report on treating the control direction constraints by applying the smoothing method. In this chapter, the authors first discuss a necessary condition of the optimal controller under constraints on the control magnitude and direction using a smoothing approach. This contribution owes to the previous work by Bertrand and Epenoy (Bertrand and Epenoy, 2002) and the necessary condition of optimal controller is successfully formulated in L_1- and L_2-norm problems respectively by introducing a newly proposed extra barrier function. These solutions are a natural extension of the solution using only a magnitude constraint obtained by Bertrand and Epenoy (Bertrand and Epenoy, 2002). As the perturbation coefficients of the barrier functions approach zero, the smoothed optimal controller approaches the necessary condition that the optimal thrust is directed along the projection of Lawden's primer vector onto the restricting set, while the control, the primer, and the admissible direction vectors are coplanar. This extremal property is completely consistent with the results reported by Sukhanov and Prado (Sukhanov and Prado, 2007, 2008).

In this chapter, a continuous low-thrust formation and reconfiguration problem under control magnitude and direction constraints is treated. Specifically, the authors herein treat primarily the condition in which the thrust direction of the chaser relative to the direction of the target is constrained. The basic objectives are to drive the chaser vehicle to transfer between the relative periodic orbit around the target under a small thrust magnitude and angle conditions and to minimize fuel consumption.

3.2 Problem Statement

3.2.1 Dynamic Equations

Consider two satellites subject to the gravitational force of the Earth, namely, a chaser satellite equipped with a continuous-thrust propulsion system and a passive target satellite, both flying in elliptical orbits. The analysis does not take into account mass changes of the satellites as a result of propellant usage. Introduce a rotating right-hand reference frame $o - \{\boldsymbol{\mathcal{R}}, \boldsymbol{\mathcal{S}}, \boldsymbol{\mathcal{W}}\}$, where o is the center of mass of the target, $\boldsymbol{\mathcal{R}}$ is in the radial direction, $\boldsymbol{\mathcal{S}}$ is in the flight direction, and $\boldsymbol{\mathcal{W}}$ is the direction outward

from the orbital plane. Let $\boldsymbol{r}$ be the position vector of the chaser relative to the target, and let $\boldsymbol{u}$ be the control acceleration vector. Set $\boldsymbol{r} = x\boldsymbol{\mathcal{R}} + y\boldsymbol{\mathcal{S}} + z\boldsymbol{\mathcal{W}}$ and $\boldsymbol{u} = u_x\boldsymbol{\mathcal{R}} + u_y\boldsymbol{\mathcal{S}} + u_z\boldsymbol{\mathcal{W}}$. The Tschauner-Hempel (TH) equations (Tschauner and Hempel, 1964; Tschauner, 1967; Alfriend *et al.*, 2010) are then given by

$$\ddot{x} - 2\dot{f}\dot{y} - \ddot{f}y - (\dot{f}^2 + 2\frac{\mu}{R_0^3})x = u_x \tag{3.1}$$

$$\ddot{y} + 2\dot{f}\dot{x} + \ddot{f}x - (\dot{f}^2 - \frac{\mu}{R_0^3})y = u_y \tag{3.2}$$

$$\ddot{z} + \frac{\mu}{R_0^3}z = u_z \tag{3.3}$$

where $\dot{\boldsymbol{a}}$ is the derivative with respect to time t, μ is the gravitational parameter of the Earth, $R_0 = \|\boldsymbol{R}_0\| = p_0/\rho(f)$, $\boldsymbol{R}_0$ is the position vector of the target, $p_0 = A_0(1-e^2)$ is the semilatus rectum, $\rho(f) = 1 + e\cos f$, A_0 is the semimajor axis, $e \in [0, 1)$ is the eccentricity of the orbit of the target, and f is the true anomaly. Introducing $\bar{\boldsymbol{r}} = (\bar{x}, \bar{y}, \bar{z}) = (x, y, z)/R_0$ and replacing independent variable t by f, Eqs. (3.1) through (3.3) are transformed into the state-space form, as follows:

$$\bar{\boldsymbol{x}}'(f) = \boldsymbol{A}(f)\bar{\boldsymbol{x}}(f) + \boldsymbol{B}(f)\bar{\boldsymbol{u}}(f) \tag{3.4}$$

where differentiation with respect to f is indicated by $'$, $\bar{\boldsymbol{x}}(f) = [\bar{\boldsymbol{r}}\ \bar{\boldsymbol{r}}']^T \in \mathbf{R}^6$, $\bar{\boldsymbol{u}}(f) = \boldsymbol{u}(f)/\alpha_{\max} \in \mathbf{R}^3$ is the normalized control acceleration vector of the chaser at the true anomaly f, as expressed in the $(\boldsymbol{\mathcal{R}}, \boldsymbol{\mathcal{S}}, \boldsymbol{\mathcal{W}})$ frame, $\bar{\boldsymbol{u}}(f)$ satisfies $\|\bar{\boldsymbol{u}}(f)\| \leq 1$, $\|\cdot\|$ denotes the Euclidean norm, $\alpha_{\max}$ is the maximum control acceleration, and

$$\boldsymbol{A}(f) = \begin{bmatrix} \boldsymbol{O}_{3\times3} & \boldsymbol{I}_{3\times3} \\ \boldsymbol{A}_1(f) & \boldsymbol{A}_2 \end{bmatrix},\ \boldsymbol{B} = \frac{R_0^2(f)}{\rho(f)}\frac{\alpha_{\max}}{\mu}\begin{bmatrix} \boldsymbol{O}_{3\times3} \\ \boldsymbol{I}_{3\times3} \end{bmatrix} \tag{3.5}$$

$$\boldsymbol{A}_1(f) = \begin{bmatrix} 3/\rho(f) & 0 & 0 \\ 0 & 0 & 0 \\ 0 & 0 & -1 \end{bmatrix},\ \boldsymbol{A}_2 = \begin{bmatrix} 0 & 2 & 0 \\ -2 & 0 & 0 \\ 0 & 0 & 0 \end{bmatrix} \tag{3.6}$$

$\boldsymbol{I}_{n\times n}$ is the $n \times n$ identity matrix, and $\boldsymbol{O}_{n\times n}$ is the $n \times n$ zero matrix. The period of the orbit is $T = 2\pi(A_0^3/\mu)^{1/2}$, and the orbital mean motion, which is the average of the orbit rate $\dot{f}$, is $n = (\mu/A_0^3)^{1/2}$.

For convenience, Table 3.1 shows the transformation from true dimensional values preserving the physical meaning into nondimensional values (Yamanaka and Ankersen, 2002). The true anomaly f must be converted to the mean anomaly M in order to obtain dimensional time t (Wie, 1998). In the same table, h and t_p represent the angular momentum of the target and the time of perigee, respectively. Hereinafter, all formulations are executed using the nondimensional values obtained using f. Therefore, the bars over $\boldsymbol{x}$ and $\boldsymbol{u}$ are not shown in Sections 3.3 and 3.4. Note that directions of $\bar{\boldsymbol{r}}$

Table 3.1: Transformation from true dimensional values to nondimensional values.

Physical quantity	The transformation $f(t),\ \bar{\boldsymbol{x}}(f) = [\bar{\boldsymbol{r}}\ \bar{\boldsymbol{r}}']^T,\ \bar{\boldsymbol{u}}(f)$	The inverse transformation $t(f),\ \boldsymbol{x}(t) = [\boldsymbol{r}\ \boldsymbol{v}]^T,\ \boldsymbol{u}(t)$
Time, True anomaly	$f = f(M),\ M = n(t - t_p)$	$t = (1/n) \cdot M(f) + t_p$
Position	$\bar{\boldsymbol{r}} = \boldsymbol{r}/R_0$	$\boldsymbol{r} = R_0 \cdot \bar{\boldsymbol{r}}$
Velocity	$\bar{\boldsymbol{r}}' = -(e \sin f/p_0)\boldsymbol{r} + (p_0/(h\rho))\boldsymbol{v}$	$\boldsymbol{v} = (h/p_0)(e \sin f \bar{\boldsymbol{r}} + \rho \bar{\boldsymbol{r}}')$
Control acceleration	$\bar{\boldsymbol{u}} = \boldsymbol{u}/\alpha_{\max}$	$\boldsymbol{u} = \alpha_{\max} \cdot \bar{\boldsymbol{u}}$

and $\bar{\boldsymbol{u}}$ as expressed in the $(\boldsymbol{\mathcal{R}}, \boldsymbol{\mathcal{S}}, \boldsymbol{\mathcal{W}})$ frame are preserved as the respective directions of the true physical values. However, $\bar{\boldsymbol{r}}'$ and $\boldsymbol{v}$ do not always have the same direction if $e \neq 0$. Therefore, a certain constraint corresponding to the relative angle between $\boldsymbol{r}$ and $\boldsymbol{u}$ is simply converted to the corresponding nondimensional constraint.

3.2.2 Optimal Control Problem Under Control Magnitude and Direction Constraints

Assuming that the initial and final true anomalies (denoted, respectively, as f_0 and f_1) are fixed, with $f_0 < f_1$, the optimal control problems under control magnitude and direction constraints, denoted as $(\mathcal{P}_{mdj})$, can be written as follows:

Problem $(\mathcal{P}_{mdj})$: Find

$$\boldsymbol{u}^*_{mdj} = \arg\min_{u} J_{mdj}(\boldsymbol{u}) \tag{3.7}$$

$$J_{mdj}(\boldsymbol{u}) = \int_{f_0}^{f_1} L_j(\|\boldsymbol{u}(f)\|)\mathrm{d}f \tag{3.8}$$

$$L_j(\|\boldsymbol{u}(f)\|) = \begin{cases} \|\boldsymbol{u}(f)\|, & j = 1 \\ \|\boldsymbol{u}(f)\|^2/2, & j = 2 \end{cases} \tag{3.9}$$

such that

$$\boldsymbol{x}'(f) = \boldsymbol{A}(f)\boldsymbol{x}(f) + \boldsymbol{B}(f)\boldsymbol{u}(f) \tag{3.10}$$

$$\|\boldsymbol{u}(f)\| \leq 1,\ f \in [f_0, f_1] \tag{3.11}$$

$$\|\theta[\boldsymbol{\xi}(f, \boldsymbol{r}), \boldsymbol{u}(f)]\| \leq \gamma,\ f \in [f_0, f_1] \tag{3.12}$$

$$\boldsymbol{x}(f_0) = \boldsymbol{x}_0,\ \boldsymbol{x}(f_1) = \boldsymbol{x}_1 \tag{3.13}$$

Problem $(\mathcal{P}_{md1})$ is the L_1-norm problem, where the performance index $J^*_{md1} = J_{md1}(\boldsymbol{u}^*)$ represents the minimum fuel consumption, and problem $(\mathcal{P}_{md2})$ is the L_2-norm problem,

where the performance index $J^*_{md2} = J_{md2}(\boldsymbol{u}^*)$ represents the minimum energy. The initial and final vectors $\boldsymbol{x}_0$ and $\boldsymbol{x}_1$ in Eq. (3.13) are fixed and can be computed from the original true relative position and velocity using the conversion in Table 3.1.

Equation (3.12) indicates that the control direction, which is defined as the angle between the admissible direction vector $-\boldsymbol{\xi}$ and the control direction vector $\boldsymbol{u}$, is constrained within the angle $\gamma \in (0, \pi]$. The magnitude of the control direction $\|\theta\|$ is defined as

$$\|\theta[\boldsymbol{\xi}(f, \boldsymbol{r}), \boldsymbol{u}(f)]\| = \mathrm{acos}[-\hat{\boldsymbol{\xi}}(f, \boldsymbol{r})^T \hat{\boldsymbol{u}}(f)] \tag{3.14}$$

where $\hat{\boldsymbol{a}}$ is a unit vector of $\boldsymbol{a}$. The polarity of θ is defined later herein based on a discussion and after calculating simulation cases. When taking $\xi(f, \boldsymbol{r}) = \boldsymbol{r}$, $\|\theta[\boldsymbol{r}(f), \boldsymbol{u}(f)]\|$ corresponds to the angle between the direction vector toward the target $-\boldsymbol{r}$ and $\boldsymbol{u}$ from the view of the chaser in the direction away from the target (Mitani and Yamakawa, 2010). Note that the direction of control input $\boldsymbol{u}$ is opposite the direction of injection $-\boldsymbol{u}$. In this case, since the state $\boldsymbol{x}$ and control $\boldsymbol{u}$ are coupled in the inequality condition of Eq. (3.12), it is generally difficult to solve $(\mathcal{P}_{mdj})$. This condition can occur when the direction of injection is restricted because of the thrust plume or when the direction of control with the thrusters fixed on the chaser is restricted because the target must be visible in the FOV of the camera of the chaser as the chaser moves safely toward the target. On the other hand, when taking $\boldsymbol{\xi}(f, \boldsymbol{r}) = \boldsymbol{s}(f)$, $\|\theta[\boldsymbol{s}(f), \boldsymbol{u}(f)]\|$ corresponds to the angle between the sun direction vector $\boldsymbol{s}$ and $\boldsymbol{u}$. In this case, Eq. (3.12) does depend on not the state $\boldsymbol{x}$, but rather depends on f explicitly. In the present chapter, the case in which $\boldsymbol{\xi} = \boldsymbol{r}$ will be primarily treated in Section 3.5.

Here, $(\mathcal{P}_{mdj})$, $j = 1, 2$ are the problems to eventually be solved herein. In a stepwise fashion, define the problems in which inequality conditions are relaxed. For a problem in which the magnitude constraint of Eq. (3.11) is not considered, the subscript m is omitted from the corresponding characters and values, such as $\mathcal{P}$, $\boldsymbol{u}$ and J. In addition, for a problem in which the direction constraint of Eq. (3.12) is not considered, the subscript d is omitted from the corresponding characters and values. For example, $(\mathcal{P}_{mj})$ and $\boldsymbol{u}^*_{mj}$ denote the optimal control problem and the corresponding optimal controller minimizing L_j-norm under the magnitude constraint of Eq. (3.11), while not considering the direction constraint of Eq. (3.12). Likewise, $(\mathcal{P}_2)$ and $\boldsymbol{u}^*_2$ denote the unconstrained optimal control problem and the corresponding optimal controller minimizing the L_2-norm. Note that $(\mathcal{P}_1)$ cannot be defined without the magnitude constraint of Eq. (3.11) because the solution satisfying PMP cannot exist.

3.3 Solving the Control Magnitude Constrained Problem

First, how to solve (P_{m1}) is briefly reviewed. In the following, $\boldsymbol{\lambda}$ denotes the costate corresponding with the $\boldsymbol{x}$ state. Even without the direction constraint, the solution of (P_{m1}) using PMP is not straightforward. Indeed, according to PMP (Pontryagin, 1961; Bryson and Ho, 1975), the optimal control $\boldsymbol{u}^*_{m1}$ takes the following form when $\boldsymbol{p}(f) \triangleq \boldsymbol{B}(f)^T\boldsymbol{\lambda}(f) \neq \boldsymbol{0}$:

$$\boldsymbol{u}^*_{m1}(f) = -u^*_{m1}(f)\hat{\boldsymbol{p}}(f) \tag{3.15}$$

with

$$u^*_{m1}(f) = \begin{cases} 1 & \text{if } \rho_{sw}(f) < 0 \\ 0 & \text{if } \rho_{sw}(f) > 0 \\ w \in [0,1] & \text{if } \rho_{sw}(f) = 0 \end{cases} \tag{3.16}$$

where $\rho_{sw}(f)$ is normally referred to as the switching function:

$$\rho_{sw}(f) = 1 - p(f) \tag{3.17}$$

For the case in which $\boldsymbol{p}(f) = \boldsymbol{0}$, $\boldsymbol{u}^*_{m1}(f) = \boldsymbol{0}$. For convenience, a scalar value $a \triangleq \|\boldsymbol{a}\|$ represents the Euclidean norm of a vector $\boldsymbol{a}$. Denoting $\boldsymbol{p}(f) = \boldsymbol{B}(f)^T\boldsymbol{\lambda}(f)$, the adjoint to $\boldsymbol{r}'(f)$, is referred by Lawden as the primer vector (Lawden, 1963; Conway, 2010). Thus, Eq. (3.16) reveals that the optimal control $\boldsymbol{u}^*_{m1}$ has such a bang-off-bang structure because assuming that no singular arc exists, the interval $[f_0, f_1]$ splits into subintervals in which, alternately, $u^*_{m1}(f) = 1$ (magnitude of control is maximum) and $u^*_{m1}(f) = 0$ (magnitude of control is zero). Then, according to (Bertrand and Epenoy, 2002), the shooting function arising from PMP is not continuously differentiable, and its Jacobian is singular on a large domain. Consequently, solving problem $(\mathcal{P}_{m1})$ by means of the shooting method is very difficult. A novel regularization technique has been developed in (Bertrand and Epenoy, 2002) for solving this type of minimum-fuel problem. The same technique was used in (Gil-Fernandez and Gomez-Tierno, 2010; Epenoy, 2011) and is here again applied to the solution of problem $(\mathcal{P}_{m1})$. Based on (Bertrand and Epenoy, 2002), a regularized control magnitude constrained problem, denoted as $(\mathcal{P}^{\varepsilon}_{m1})$, is established as follows:

Problem $(\mathcal{P}^{\varepsilon}_{m1})$: Find

$$\boldsymbol{u}^{\varepsilon}_{m1} = \arg\min_{u} J^{\varepsilon}_{m1}(\boldsymbol{u}) \tag{3.18}$$

$$J^{\varepsilon}_{m1}(\boldsymbol{u}) = \int_{f_0}^{f_1} u + \varepsilon_u F_u[\boldsymbol{u}(f)]\mathrm{d}f \tag{3.19}$$

such that the conditions of Eqs. (3.10) and (3.13) are satisfied.

Function $\varepsilon_u F_u$ is given hereinafter as

$$\varepsilon_u F_u[\boldsymbol{u}(f)] = -\varepsilon_u \log u(1-u), \quad f \in [f_0, f_1] \tag{3.20}$$

where $\varepsilon_u > 0$, and $\varepsilon_u F_u$ is a continuous function satisfying

$$\varepsilon_u F_u(u) \geq 0, \quad u \in [0, 1] \tag{3.21}$$

Note that Eq. (3.20) is opposite in sign to the definition in (Bertrand and Epenoy, 2002). If $\varepsilon_u F_u(u) \to +\infty$ as u approaches one or zero, then F_u is referred to as a barrier function. Specifically, a barrier function having the form of Eq. (3.20) is referred to as a logarithmic barrier function. For a given $n > 0$, a sequence of values denoted as ε_{ui} $(i = 1, \cdots, n)$ is defined with $(\varepsilon_{u1} > \varepsilon_{u2} > \cdots > \varepsilon_{un} > 0)$. Then, problems $(\mathcal{P}_{m1}^{\varepsilon_i})$ $(i = 1, \cdots, n)$ are solved sequentially using the solution obtained at step $(i-1)$ as an initial guess for step i. Finally, assuming that ε_u is sufficiently small, the solution of $(\mathcal{P}_{m1}^{\varepsilon})$ provides a very accurate approximation of the solution of $(\mathcal{P}_{m1})$ (See (Bertrand and Epenoy, 2002)).

According to PMP (Pontryagin, 1961; Bryson and Ho, 1975), the optimal control $\boldsymbol{u}_{m1}^{\varepsilon}$ takes the following form when $\boldsymbol{p}(f) \neq \boldsymbol{0}$:

$$\boldsymbol{u}_{m1}^{\varepsilon}(f) = -u_{m1}^{\varepsilon}(f)\hat{\boldsymbol{p}}(f) \tag{3.22}$$

The optimal magnitude $u_{m1}^{\varepsilon} \in (0, 1)$ is obtained as the solution of the following equation (Bertrand and Epenoy, 2002):

$$\rho_{sw} - \varepsilon_u \frac{1-2u}{u(1-u)} = 0 \tag{3.23}$$

The solution is

$$u_{m1}^{\varepsilon}(f) \;=\; \frac{2\varepsilon_u}{\rho_{sw}(f) + 2\varepsilon_u + \sqrt{\rho_{sw}(f)^2 + 4\varepsilon_u^2}} \tag{3.24}$$

For the case in which $\boldsymbol{p} = \boldsymbol{0}$, the thrust direction is undetermined. Then, in both cases, the following holds:

$$u_{m1}^{\varepsilon}(f) \in (0, 1); \quad f \in [f_0, f_1] \tag{3.25}$$

The key point in (Bertrand and Epenoy, 2002) is that $\boldsymbol{u}_{m1}^{\varepsilon}$ is a smooth approximation of the bang-off-bang optimal control $\boldsymbol{u}_{m1}^{*}$. In the same way, $\boldsymbol{u}_{m2}^{\varepsilon}$ can be constructed for $(\mathcal{P}_{m2}^{\varepsilon})$ by introducing the same barrier function, i.e., Eq. (3.20). The derivation of the L_2-norm problem is explained in Appendix A.

In addition, the costate differential equations for $(\mathcal{P}_{m1}^{\varepsilon})$ and $(\mathcal{P}_{m2}^{\varepsilon})$ take the same following form:

$$-\boldsymbol{\lambda}' = \frac{\partial H_{mj}^{\varepsilon}}{\partial \boldsymbol{x}} = A(f)^T \boldsymbol{\lambda} \tag{3.26}$$

3.4 Solving the Control Magnitude and Direction Constrained Problem

3.4.1 Introducing an Extra Barrier Function

In the following, the extended smoothing approach to solve $(\mathcal{P}_{mdj})$ is attempted. When $\boldsymbol{u}$ is constrained within the angle γ from an admissible direction vector $-\boldsymbol{\xi}(f,\boldsymbol{r}) \neq \boldsymbol{0}$, an optimal controller can be smoothed by introducing an extra barrier function, in the same manner as in the previous section. For this purpose, a parameter b and a new logarithmic barrier function $\varepsilon_b F_b$ will be introduced as follows:

$$\begin{aligned} b[\boldsymbol{\xi}(f,\boldsymbol{r}),\boldsymbol{u}(f)] &= \frac{-\hat{\boldsymbol{\xi}}^T\hat{\boldsymbol{u}}-\cos\gamma}{1-\cos\gamma} \\ &= \frac{\cos\theta-\cos\gamma}{1-\cos\gamma} \qquad (3.27) \\ \varepsilon_b F_b[\boldsymbol{\xi}(f,\boldsymbol{r}),\boldsymbol{u}(f)] &= -\varepsilon_b u\log b \qquad (3.28) \end{aligned}$$

where $\varepsilon_b > 0$ and Eq. (3.14) is used, $\varepsilon_b F_b$ is a continuous function satisfying

$$\varepsilon_b F_b[\boldsymbol{\xi}(f,\boldsymbol{r}),\boldsymbol{u}(f)] \geq 0, \quad u \leq 1, \quad \|\theta\| \leq \gamma \qquad (3.29)$$

Note that $0 \leq b \leq 1$, and as $\|\theta\|$ approaches γ, b and $\varepsilon_b F_b$ approach $+0$ and $+\infty$, respectively. Therefore, $\varepsilon_b F_b$ satisfies the condition of the barrier function. The coefficient u in front of the logarithmic function is added for two reasons. First, the uncertainty of the direction can be circumvented when $u = 0$. Second, each equation for solving the optimal magnitude and direction can be well separated, and these equations will become extended expressions from the optimal smoothed controller for dealing with the magnitude constraint in the previous section.

In the same manner, adding $\varepsilon_b F_b$ to J^{ε}_{mj}, consider the following $(\mathcal{P}^{\varepsilon}_{mdj})$:

Problem $(\mathcal{P}^{\varepsilon}_{mdj})$: Find

$$\begin{aligned} \boldsymbol{u}^{\varepsilon}_{mdj} &= \arg\min_{u} J^{\varepsilon}_{mdj}(\boldsymbol{u}) \qquad (3.30) \\ J^{\varepsilon}_{mdj}(\boldsymbol{u}) &= \int_{f_0}^{f_1} L_j(\boldsymbol{u}) + \varepsilon_u F_u[\boldsymbol{u}(f)] + \varepsilon_b F_b[\boldsymbol{\xi}(f,\boldsymbol{r}),\boldsymbol{u}(f)]\mathrm{d}f \qquad (3.31) \end{aligned}$$

such that the conditions of Eqs. (3.10) and (3.13) are satisfied.

Using the same PMP approach as in $(\mathcal{P}^{\varepsilon}_{mj})$, build the Hamiltonian function H^{ε}_{mdj}, as follows:

$$H^{\varepsilon}_{mdj} = L_j(u) - \varepsilon_u \log u(1-u) - \varepsilon_b u\log b + \boldsymbol{\lambda}^T(\boldsymbol{A}\boldsymbol{x}+\boldsymbol{B}\boldsymbol{u}) \qquad (3.32)$$

The optimal controller is then given by

$$\boldsymbol{u}^{\varepsilon}_{mdj}(f) = \arg\min_{u} H^{\varepsilon}_{mdj} \tag{3.33}$$

Here, the Cauchy-Schwartz inequality cannot be directly applied to obtain the optimal direction of $\boldsymbol{u}^{\varepsilon}_{mdj}$ because the term $\varepsilon_b F_b$ has $-\hat{\boldsymbol{\xi}}^T \hat{\boldsymbol{u}}$, which depends on the direction of $\boldsymbol{u}$. In the following subsection, the optimal magnitude and direction of $\boldsymbol{u}^{\varepsilon}_{mdj}$ will be derived.

3.4.2 Derivation of Optimal Direction $\hat{\boldsymbol{u}}^{\varepsilon}_{mdj}$

Case in which $\boldsymbol{\xi} \nparallel \boldsymbol{p}$

Introduce a control-space frame $o - \{\boldsymbol{\mathcal{I}}, \boldsymbol{\mathcal{J}}, \boldsymbol{\mathcal{K}}\}$, where o is the zero point of the control, $\boldsymbol{\mathcal{I}} = -\hat{\boldsymbol{\xi}}$, $\boldsymbol{\mathcal{K}} = \hat{\boldsymbol{\xi}} \times \hat{\boldsymbol{p}} / \|\hat{\boldsymbol{\xi}} \times \hat{\boldsymbol{p}}\|$, and $\boldsymbol{\mathcal{J}}$ completes the setup ($\boldsymbol{\mathcal{J}} = \boldsymbol{\mathcal{K}} \times \boldsymbol{\mathcal{I}}$). Then, $\boldsymbol{u}$ is expressed in polar coordinate (u, θ, φ) as follows:

$$\boldsymbol{u} \;=\; u \cdot (\cos\varphi \cos\theta \cdot \boldsymbol{\mathcal{I}} + \cos\varphi \sin\theta \cdot \boldsymbol{\mathcal{J}} + \sin\varphi \cdot \boldsymbol{\mathcal{K}}) \tag{3.34}$$

where $u \in (0, 1)$, $\theta \in (-\gamma, \gamma)$, and $\varphi \in (-\text{acos}[\cos\gamma / \cos\theta], \text{acos}[\cos\gamma / \cos\theta])$ from the

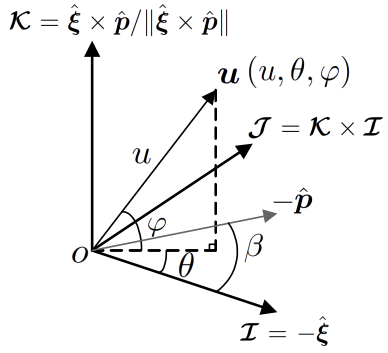

Figure 3.1: Definition of a control-space frame $o - \{\boldsymbol{\mathcal{I}}, \boldsymbol{\mathcal{J}}, \boldsymbol{\mathcal{K}}\}$, control $\boldsymbol{u}$ in polar coordinates (u, θ, φ), and relative angle β between $\hat{\boldsymbol{\xi}}$ and $\hat{\boldsymbol{p}}$.

constraints on control magnitude and direction of Eqs. (3.11) and (3.12). Since θ and φ are linked by the inequality constraint on the direction

$$G(\theta, \varphi) \triangleq (\cos\gamma - \cos\varphi \cos\theta) \leq 0 \tag{3.35}$$

the necessary optimality conditions of constrained problems should be treated analytically by adjoining the inequality (3.35) to H^{ε}_{mdj} in Eq. (3.32). The extremal value of

$H^{\varepsilon}_{mdj} + \nu u G$ indicates that the partial derivatives of θ, φ, and u are zero:

$$\frac{\partial H^{\varepsilon}_{mdj} + \nu u G}{\partial \alpha} = 0 \Rightarrow$$
$$u \cdot \left(-\frac{\varepsilon_b}{\hat{\boldsymbol{\xi}}^T \hat{\boldsymbol{u}} + \cos\gamma} \hat{\boldsymbol{\xi}}^T \hat{\boldsymbol{u}}_\alpha + \boldsymbol{p}^T \hat{\boldsymbol{u}}_\alpha + \nu \frac{\partial G}{\partial \alpha} \right) = 0, \ \alpha = \theta, \varphi \tag{3.36}$$
$$\frac{\partial H^{\varepsilon}_{mdj} + \nu u G}{\partial u} = 0 \Rightarrow$$
$$\frac{\partial L_j(u)}{\partial u} + \boldsymbol{p}^T \hat{\boldsymbol{u}} - \varepsilon_b \log b - \frac{\varepsilon_u (1-2u)}{u(1-u)} + \nu G = 0 \tag{3.37}$$

where $\hat{\boldsymbol{u}}_\alpha = \partial \hat{\boldsymbol{u}} / \partial \alpha$ for simplicity and ν is a Lagrange multiplier corresponding to the inequality $uG \leq 0$

$$\nu \begin{cases} \geq 0, & uG(\theta, \varphi) = 0 \\ = 0, & uG(\theta, \varphi) < 0 \end{cases} \tag{3.38}$$

Choosing the inequality $uG \leq 0$, not $G \leq 0$ is for the same reasons as the case of $\varepsilon_b F_b$. Equation (3.36) corresponds to the condition in which the equality is obtained when the Cauchy-Schwartz inequality is applied, which implicitly determines the optimal direction of $\boldsymbol{u}$. As $u \in (0, 1)$, both sides of Eq. (3.36) can be divided by $u(\neq 0)$. Therefore, the direction α can be derived without any dependence on the magnitude of u. This simplification is possible due to the coefficient u in front of the logarithmic function in Eq. (3.28). Then, Eq. (3.36) reduces to

$$\frac{\partial H^{\varepsilon}_{mdj} + \nu u G}{\partial \theta} = 0 \Rightarrow$$
$$\cos\varphi \left[\{ \sin(\theta - \beta) + \tilde{\nu} \sin\theta \} (\cos\gamma - \cos\varphi \cos\theta) - \tilde{\varepsilon}_b \sin\theta \right] = 0 \tag{3.39}$$
$$\frac{\partial H^{\varepsilon}_{mdj} + \nu u G}{\partial \varphi} = 0 \Rightarrow$$
$$\sin\varphi \left[\{ \cos(\theta - \beta) + \tilde{\nu} \cos\theta \} (\cos\gamma - \cos\varphi \cos\theta) - \tilde{\varepsilon}_b \cos\theta \right] = 0 \tag{3.40}$$

where $\beta \in (0, \pi)$ represents the angle between $-\hat{\boldsymbol{\xi}}$ and $-\hat{\boldsymbol{p}}$, which are defined by the following expressions $\hat{\boldsymbol{\xi}}^T \hat{\boldsymbol{p}} = \cos\beta$ and $\hat{\boldsymbol{\xi}} \times \hat{\boldsymbol{p}} = \sin\beta \cdot \hat{\boldsymbol{k}}$, $\tilde{\varepsilon}_b = \varepsilon_b / p > 0$ and $\tilde{\nu} = \nu / p \geq 0$. From the domain of φ, $\cos\varphi \neq 0$.

If $\sin\varphi \neq 0$, both term of $[\{\sin(\theta - \beta) + \tilde{\nu}\sin\theta\}(\cos\gamma - \cos\varphi\cos\theta) - \tilde{\varepsilon}_b \sin\theta]$ in Eq. (3.39) and term of $[\{\cos(\theta - \beta) + \tilde{\nu}\cos\theta\}(\cos\gamma - \cos\varphi\cos\theta) - \tilde{\varepsilon}_b \cos\theta]$ in Eq. (3.40) must become zero at a certain value of θ. However, such a solution of θ exists only when $\beta = 0, 2\pi$ and $\tilde{\nu} = 0$, which conflicts with the assumption that $\boldsymbol{\xi} \nparallel \boldsymbol{p}$.

If $\sin\varphi = 0$, then $\varphi = 0$, which leads to $\cos\varphi = 1$. Therefore, Eq. (3.40) is automatically satisfied. In the end, Eq. (3.39) reduces to

$$[\sin(\theta - \beta) + \tilde{\nu}\sin\theta](\cos\gamma - \cos\theta) - \tilde{\varepsilon}_b \sin\theta = 0 \tag{3.41}$$

Assume that the constraint is effective ($\nu \geq 0$) at the optimal point, then $\cos\theta = \cos\gamma$ from $\varphi = 0$ and $G = 0$. But the condition can not satisfy Eq. (3.41) as long as $\tilde{\varepsilon}_b > 0$. Therefore, substituting $\nu = 0$ into Eq. (3.41),

$$\sin(\theta^\varepsilon - \beta)(\cos\gamma - \cos\theta^\varepsilon) - \tilde{\varepsilon}_b \sin\theta^\varepsilon = 0 \tag{3.42}$$

determines the optimal θ, denoted by θ^ε. The qualitative property of Eq. (3.42) and the uniqueness of the solution are explained later in this section. Based on Eqs. (3.34) and (3.42) and $\varphi = 0$, $\hat{\boldsymbol{u}}^\varepsilon_{mdj}$ is given as

$$\hat{\boldsymbol{u}}^\varepsilon_{mdj} = (\sin\theta^\varepsilon \cot\beta - \cos\theta^\varepsilon)\hat{\boldsymbol{\xi}} - \sin\theta^\varepsilon \csc\beta \hat{\boldsymbol{p}} \tag{3.43}$$

Case in which $\boldsymbol{\xi} \parallel \boldsymbol{p}$

Take $\hat{\boldsymbol{z}}$ as an arbitrary unit vector vertical to $\hat{\boldsymbol{\xi}}$. Introduce a control-space frame $o - \{\boldsymbol{\mathcal{I}}, \boldsymbol{\mathcal{J}}, \boldsymbol{\mathcal{K}}\}$, where o is the zero point of the control, and $\boldsymbol{\mathcal{I}} = -\hat{\boldsymbol{\xi}}$, $\boldsymbol{\mathcal{K}} = \hat{\boldsymbol{z}}$, and $\boldsymbol{\mathcal{J}}$ completes the setup. As $\boldsymbol{u}$ expressed in polar coordinated (u, θ, φ), Eq. (3.36) reduces to

$$\begin{aligned}
&\frac{\partial H^\varepsilon_{mdj} + \nu u G}{\partial\theta} = 0 \Rightarrow \\
&\cos\varphi \sin\theta[\{(\hat{\boldsymbol{\xi}}^T \hat{\boldsymbol{p}}) + \tilde{\nu}\}(\cos\gamma - \cos\varphi\cos\theta) - \tilde{\varepsilon}_b] = 0 \qquad (3.44) \\
&\frac{\partial H^\varepsilon_{mdj} + \nu u G}{\partial\varphi} = 0 \Rightarrow \\
&\sin\varphi \cos\theta[\{(\hat{\boldsymbol{\xi}}^T \hat{\boldsymbol{p}}) + \tilde{\nu}\}(\cos\gamma - \cos\varphi\cos\theta) - \tilde{\varepsilon}_b] = 0 \qquad (3.45)
\end{aligned}$$

Note that Eqs. (3.44) and (3.45) have the same factor of $[\{(\hat{\boldsymbol{\xi}}^T \hat{\boldsymbol{p}}) + \tilde{\nu}\}(\cos\gamma - \cos\varphi\cos\theta) - \tilde{\varepsilon}_b]$ and $\cos\varphi \neq 0$ from the domain of φ. Assume that the constraint is effective ($\nu \geq 0$) at the optimal point, then $G = (\cos\gamma - \cos\varphi\cos\theta) = 0$. But the condition can not satisfy Eqs. (3.44) and (3.45) simultaneously as long as $\tilde{\varepsilon}_b > 0$. Therefore, $\nu = 0$.

If $\hat{\boldsymbol{\xi}}^T \hat{\boldsymbol{p}} = 1$, then $\cos\gamma - \tilde{\varepsilon}_b \triangleq \cos\gamma'$, $\tilde{\varepsilon}_p > 0$, and $\gamma' > \gamma$. Therefore, $[(\hat{\boldsymbol{\xi}}^T \hat{\boldsymbol{p}})(\cos\gamma - \cos\varphi\cos\theta) - \tilde{\varepsilon}_b] \neq 0$, and $\cos\varphi\sin\theta = \sin\varphi\cos\theta = 0$. In this case, from the domain of θ and φ, $\theta^\varepsilon = \varphi^\varepsilon = 0$ or $\hat{\boldsymbol{u}}^\varepsilon_{mdj} = -\hat{\boldsymbol{p}}$ is the solution. Moreover, in this case, the form of $\hat{\boldsymbol{u}}^\varepsilon_{mdj}$ can be merged to the form for the case in which $\boldsymbol{\xi} \nparallel \boldsymbol{p}$. In fact, taking the limit $\beta \to 0$ or $\hat{\boldsymbol{\xi}} \to \hat{\boldsymbol{p}}$ in Eq. (3.43),

$$\hat{\boldsymbol{u}}^\varepsilon_{mdj} = \lim_{\beta\to 0} -\frac{\sin\theta^\varepsilon - \sin(\theta^\varepsilon - \beta)}{\beta}\frac{\beta}{\sin\beta}\hat{\boldsymbol{p}} = -\cos\theta^\varepsilon \cdot 1 \cdot \hat{\boldsymbol{p}} = -\hat{\boldsymbol{p}} \tag{3.46}$$

where $\theta^\varepsilon = 0$.

If $\hat{\boldsymbol{\xi}}^T \hat{\boldsymbol{p}} = -1$, then Eq. (3.44) and (3.45) can be satisfied when $\cos\varphi\cos\theta = \cos\gamma + \tilde{\varepsilon}_b < 1$ or $\theta = \varphi = 0$. Compare the Hamiltonian values of these two regions. When

$\cos\varphi\cos\theta = \cos\gamma + \tilde{\varepsilon} < 1$, substitute this equation into the Hamiltonian of Eq. (3.32):

$$\tilde{H}/(pu) = -\tilde{\varepsilon}_b \log \frac{\tilde{\varepsilon}_b}{1-\cos\gamma} + \cos\gamma + \tilde{\varepsilon}_b < 1 \tag{3.47}$$

where $\tilde{H} = H^{\varepsilon}_{mdj} - L_j(u) + \varepsilon_u \log u(1-u) - \boldsymbol{\lambda}^T A\boldsymbol{x}$. When $\theta = \varphi = 0$, in the same manner,

$$\tilde{H}/(pu) = 1 \tag{3.48}$$

As a result, Eq. (3.47) always has a smaller Hamiltonian than Eq. (3.48). Therefore, for the case in which $\boldsymbol{\xi} \parallel \boldsymbol{p}$, optimal θ and φ cannot be uniquely identified, but satisfy

$$\cos\varphi^{\varepsilon}\cos\theta^{\varepsilon} = \cos\gamma + \tilde{\varepsilon}_b < 1 \tag{3.49}$$

Putting the cases *1* and *2* together, the optimal direction $\hat{\boldsymbol{u}}^{\varepsilon}_{mdj}$ is summarized as follows:

$$\hat{\boldsymbol{u}}^{\varepsilon}_{mdj}(\theta,\varphi) = \begin{cases} (\sin\theta^{\varepsilon}_1 \cot\beta - \cos\theta^{\varepsilon}_1)\hat{\boldsymbol{\xi}} - \sin\theta^{\varepsilon}_1 \csc\beta\hat{\boldsymbol{p}}, & \hat{\boldsymbol{\xi}} \nparallel \hat{\boldsymbol{p}} \text{ or } \hat{\boldsymbol{\xi}}^T\hat{\boldsymbol{p}} = 1 \\ -\cos\varphi^{\varepsilon}_2\cos\theta^{\varepsilon}_2\hat{\boldsymbol{\xi}} - \cos\varphi^{\varepsilon}_2\sin\theta^{\varepsilon}_2(\hat{\boldsymbol{z}}\times\hat{\boldsymbol{\xi}}) + \sin\varphi^{\varepsilon}_2\hat{\boldsymbol{z}}, & \hat{\boldsymbol{\xi}}^T\hat{\boldsymbol{p}} = -1 \end{cases} \tag{3.50}$$

where $\theta^{\varepsilon}_1 \in [0,\gamma)$ satisfies Eq. (3.42), $(\theta^{\varepsilon}_2, \varphi^{\varepsilon}_2)$ satisfies Eq. (3.49), $\hat{\boldsymbol{\xi}}^T\hat{\boldsymbol{p}} = \cos\beta$, $\hat{\boldsymbol{\xi}}\times\hat{\boldsymbol{p}} = \sin\beta$, and $\hat{\boldsymbol{\xi}}^T\hat{\boldsymbol{z}} = 0$.

In the following, Eq. (3.42) is explained in a little more detail. This equation can be solved explicitly by transforming the equation to a quartic equation of $\chi = \sin\theta^{\varepsilon} \in [0, \sin\gamma)$ and using the Ferrari formula (Burnside and Panton, 2005). For the domain of $\theta^{\varepsilon} \in [0,\gamma)$, a unique solution is found when $\beta \neq 0, \pi$, $\beta > 0$, and $\tilde{\varepsilon}_b > 0$. However, because of the complexity of the analytical form, it is easier to use numerical computation methods such as the Newton-Raphson method to find $\theta^{\varepsilon} \in [0,\gamma)$ (Saaty and Bram, 1981). Based on the form of Eq. (3.42), the qualitative nature is easily found. By adding $\varepsilon_b F_b$ to J^{ε}_{mj}, $\hat{\boldsymbol{u}} = -\hat{\boldsymbol{p}}$ is not always satisfied. Instead, the smoothing approach leads to another interesting property whereby three vectors $\hat{\boldsymbol{u}}^{\varepsilon}_{mdj}$, $\hat{\boldsymbol{\xi}}$, and $\hat{\boldsymbol{p}}$ are coplanar when $\boldsymbol{\xi} \nparallel \boldsymbol{p}$. When $\tilde{\varepsilon}_b = \varepsilon_b/p \to \infty$, $\theta^{\varepsilon} \to 0$, which means that $\boldsymbol{u}$ becomes parallel to $-\boldsymbol{\xi}$. On the other hand, when $\tilde{\varepsilon}_b \to 0$, $\theta \to \beta$, which means $\hat{\boldsymbol{u}}$ approaches $-\hat{\boldsymbol{p}}$ if $\beta \leq \gamma$, and $\theta \to \gamma$, which means $\hat{\boldsymbol{u}}^{\varepsilon}_{mdj}$ approaches the boundary side of the inequality constraint of Eq. (3.12) near $-\boldsymbol{p}$ if $\beta > \gamma$. In the latter case, the thrust angle constraint is activated. In the former case, on the other hand, the constraint is not activated and the property $\hat{\boldsymbol{u}} = -\hat{\boldsymbol{p}}$ is maintained reasonably. This extremal property is completely consistent with the results reported by Sukhanov and Prado (Sukhanov and Prado, 2007, 2008), where the optimal thrust is directed along the projection of Lawden's primer vector onto the boundary restricting the control set.

3.4.3 Derivation of Modified Optimal Magnitude $\|\boldsymbol{u}^{\varepsilon}_{mdj}\|$

Since the optimal direction $\hat{\boldsymbol{u}}^{\varepsilon}_{mdj}$ is given in Eq. (3.50), the optimal magnitude u^{ε}_{mdj} from Eq. (3.37) is obtained, which yields an expression that can be extended to Eq. (3.24). First, in $(\mathcal{P}^{\varepsilon}_{md1})$, define the extended primer vector norm and switching function as follows:

$$\tilde{p}(f) = -\boldsymbol{p}^T\hat{\boldsymbol{u}}^{\varepsilon}_{mdj} + \varepsilon_b \log[b(\hat{\boldsymbol{\xi}}, \hat{\boldsymbol{u}}^{\varepsilon}_{mdj})] \tag{3.51}$$

$$\tilde{\rho}_{sw}(f) = 1 - \tilde{p}(f) \tag{3.52}$$

Based on the properties of $\hat{\boldsymbol{u}}^{\varepsilon}_{mdj}$ in Eq. (3.50) and $\varepsilon_b F_b$ in Eq. (3.29), $\tilde{p} \geq 0$. Then, using $\partial L_1(u)/\partial u = 1$, Eq. (3.37) reduces to

$$\tilde{\rho}_{sw} - \varepsilon_u \frac{1-2u}{u(1-u)} = 0 \tag{3.53}$$

which has the same form as Eq. (3.23). Therefore, u^{ε}_{md1} also has the same form as Eq. (3.24).

$$u^{\varepsilon}_{md1} = \frac{2\varepsilon_u}{\tilde{\rho}_{sw} + 2\varepsilon_u + \sqrt{\tilde{\rho}^2_{sw} + 4\varepsilon^2_u}} \tag{3.54}$$

When $\varepsilon_b = 0$, $\tilde{\rho}_{sw} = \rho_{sw}$, and the solution of Eq. (3.54) of $(\mathcal{P}_{md1})$ naturally reduces to the solution of Eq. (3.24) of $(\mathcal{P}_{m1})$. As in the case of (P^{ε}_{md1}), Eq. (3.37) can be solved for the case of (P^{ε}_{md2}) (See Appendix A). Thus, by introducing $\varepsilon_b F_b$, the formulation of the smoothed optimal controller $\boldsymbol{u}^{\varepsilon}_{mdj}$ can be derived in order to deal with $(\mathcal{P}^{\varepsilon}_{mdj})$ and this form is shown to be a natural extension of the one with only the magnitude constraint in $(\mathcal{P}^{\varepsilon}_{mj})$.

In addition, the explicit forms of the optimal control for (P_{md1}) and (P_{md2}) are given as follows:

$$\hat{\boldsymbol{u}}^*_{mdj} = \begin{cases} -\hat{\boldsymbol{p}}, & \beta \leq \gamma \\ (\sin\gamma\cot\beta - \cos\gamma)\hat{\boldsymbol{\xi}} - \sin\gamma\csc\beta\hat{\boldsymbol{p}}, & \beta > \gamma \end{cases}, \qquad j = 1, 2 \tag{3.55}$$

$$u^*_{md1} = \begin{cases} 1, & \rho_{sw} = 1 + \boldsymbol{p}^T\hat{\boldsymbol{u}}^*_{md1} < 0 \\ 0, & \rho_{sw} > 0 \\ w \in [0,1], & \rho_{sw} = 0 \end{cases} \tag{3.56}$$

$$u^*_{md2} = \begin{cases} -\boldsymbol{p}^T\hat{\boldsymbol{u}}^*_{md2}, & -\boldsymbol{p}^T\hat{\boldsymbol{u}}^*_{md2} \leq 1 \\ 1, & -\boldsymbol{p}^T\hat{\boldsymbol{u}}^*_{md2} > 1 \end{cases} \tag{3.57}$$

In order to obtain a more comprehensive understanding of the results, Fig. 3.2 shows the derived optimal magnitude u^{ε}_{mdj}, the direction $\hat{\boldsymbol{u}}^{\varepsilon}_{mdj}$, and the corresponding

barrier functions $\varepsilon_u F_u$ and $\varepsilon_b F_b$. Note that u^{ε}_{md1} and u^{ε}_{md2} have the same barrier function $\varepsilon_u F_u$. Here, the polarities are appended to β and θ^{ε}. In addition, γ is set to $\pi/2$, for example. Figure 3.2 shows that the optimal u^{ε}_{m1}, u^{ε}_{m2}, and θ^{ε} become steep and saturated as ε approaches $+0$.

Figure 3.3 shows the Hamiltonian H^{ε}_{mdj} contour when $-\boldsymbol{\xi}(f, \boldsymbol{r})$ and $-\boldsymbol{p}(f)$ at a certain f are frozen. Cases **a)** and **b)** are typical two cases for $\beta < \gamma$ and $\beta > \gamma$, where γ is set to $\pi/3$, for example. Since $\boldsymbol{\xi} \nparallel \boldsymbol{p}$, three vectors $\boldsymbol{u}^{\varepsilon}_{mdj}$, $-\boldsymbol{\xi}$, $-\boldsymbol{p}$ are coplanar. In Case **a)**, which corresponds to the case in which the direction constraints are not activated, the optimal θ^{ε} approaches β as $\varepsilon \to 0$. On the other hand, in Case **b)**, which corresponds to the case in which the direction constraint is activated, the optimal θ^{ε} approaches γ as $\varepsilon \to +0$. As shown in Fig. 3.2, $\boldsymbol{u}^{\varepsilon}_{mdj}$ is a single extremal point in H^{ε}_{mdj}, and $\nabla^2 H^{\varepsilon}_{mdj} \geq 0$. In addition, H^{ε}_{mdj} approaches $+\infty$ when $\boldsymbol{u}$ approaches the constraint boundary due to barrier functions. Therefore, $\boldsymbol{u}^{\varepsilon}_{mdj}$ must be a global minimum. The proof of $\nabla^2 H^{\varepsilon}_{mdj} \geq 0$ is given in Appendix B.

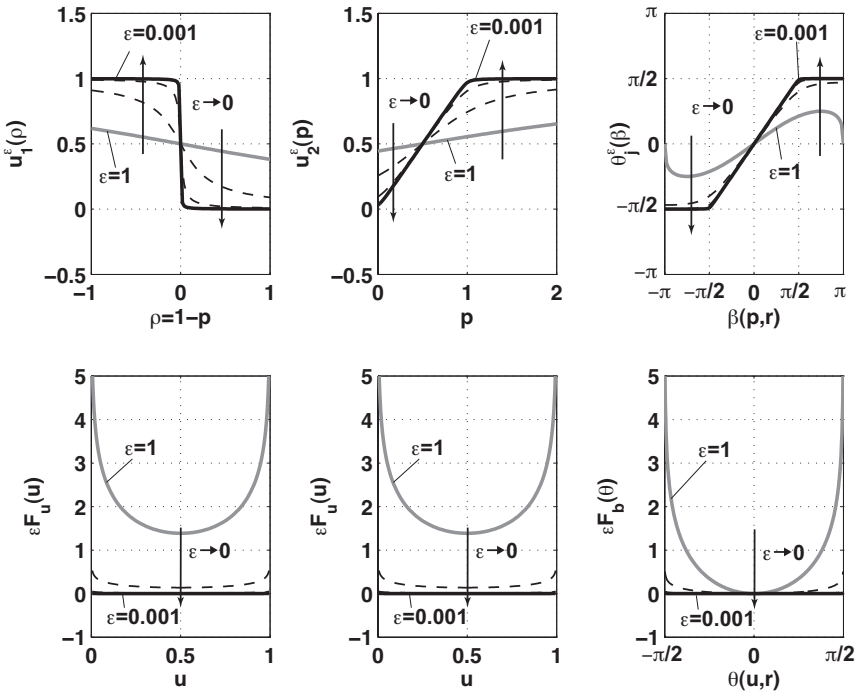

Figure 3.2: Optimal u^{ε}_{m1}, u^{ε}_{m2}, θ^{ε}_{j}, and added costs εF_u, εF_b for ε varying from 1 to 0.001 ($\varepsilon = (1,\ 0.1,\ 0.01,\ 0.001)$.

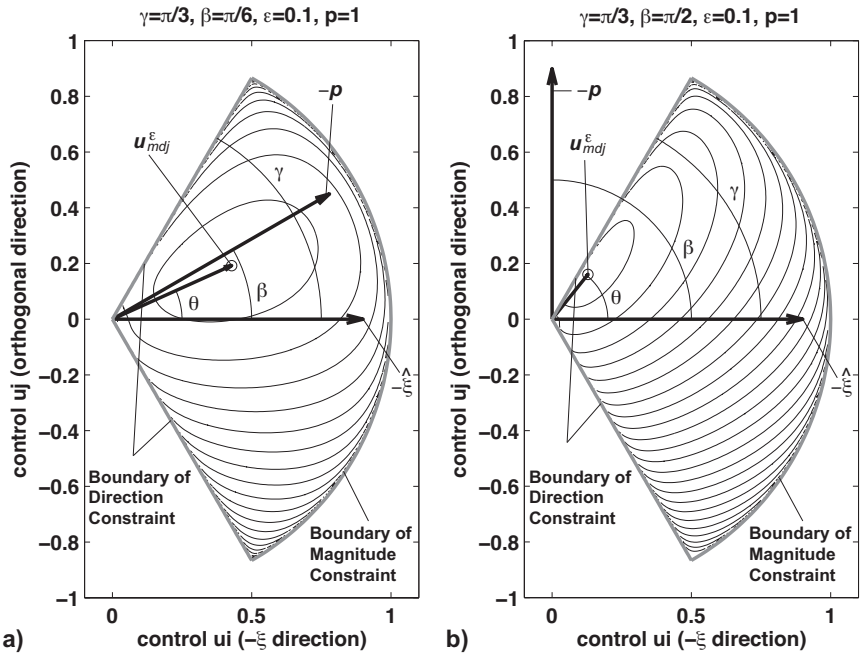

Figure 3.3: Illustration of the Hamiltonian contour in the 2-D control frame $(\boldsymbol{i}, \boldsymbol{j})$. **a)** $\beta < \gamma$, **b)** $\beta > \gamma$.

3.4.4 The Costate Differential Equation

The costate differential equation has the same form as $(\mathcal{P}^{\varepsilon}_{md1})$ and $(\mathcal{P}^{\varepsilon}_{md2})$ because $L_j(u)$ is independent of the state $\boldsymbol{x}$. In both cases, the costate differential equation yields

$$-\boldsymbol{\lambda}' = \frac{\partial H^{\varepsilon}_{mdj}}{\partial \boldsymbol{x}} = \frac{\partial \varepsilon_b F_b[\boldsymbol{u}, \boldsymbol{\xi}]}{\partial \boldsymbol{x}} + A(f)^T \boldsymbol{\lambda} \tag{3.58}$$

Consider two cases, namely, the case in which $\boldsymbol{\xi}$ is independent of the state $\boldsymbol{x}$ and the case in which $\partial(\varepsilon_b F_b)/\partial \boldsymbol{x} = 0$. Thus, the costate differential equation of Eq. (3.58) is exactly the same as Eq. (3.26). When $\boldsymbol{\xi} = \boldsymbol{r}$, Eq. (3.58) reduces to

$$-\boldsymbol{\lambda}' = \frac{\partial H^{\varepsilon}_{mdj}}{\partial \boldsymbol{x}} = \left\{ \begin{array}{c} \dfrac{\varepsilon_b}{\hat{\boldsymbol{r}}^T \hat{\boldsymbol{u}} + \cos\gamma} \cdot \dfrac{1}{r} \left[-\hat{\boldsymbol{u}} + (\hat{\boldsymbol{r}}^T \hat{\boldsymbol{u}}) \hat{\boldsymbol{r}} \right] \\ O_{2\times 1} \end{array} \right\} + A^T \boldsymbol{\lambda} \tag{3.59}$$

Since, in the next section, the case in which $\boldsymbol{\xi} = \boldsymbol{r}$ will be primarily considered, the results of Eq. (3.59) are applied to the numerical simulations.

3.5 Numerical Results

For numerical simulations, a Keplerian orbit of the target of semimajor axis $A_0 = R_e + h_c$ km is considered, in which $h_c = 500$ km, the radius of the Earth R_e, and

Table 3.2: Constants and common parameters.

Constants	Values	Constants	Values
R_e	6378.136 km	$\alpha_{\max}$	0.002 m/s^2
μ	398,601 km^3/s^2	m	500 kg
h_c	500 km	$F_{\max}$	1 N
n	1.1068×10^{-3} rad/s		
T	5,677 s		

the gravitational constant of the Earth μ are given. Then, the period of this orbit is $T = 5677$ s, and the orbital rate $n = 1.1068 \times 10^{-3}$ rad/s is considered (see Table 3.2). In addition, $\alpha_{\max} = 0.002$ m/s^2 is considered to be the maximum acceleration of control, which corresponds to the case in which a chaser of mass $m = 500$ kg has a 1-N actuator, i.e., $F_{\max} = 1$ N.

In this section, for reference, the obtained optimal controller and trajectory with an analytical formulation in $(\mathcal{P}_2)$ are compared. Problem $(\mathcal{P}_2)$ has been solved explicitly based on the circular Hill's equation. For example, Scheeres solved problem $(\mathcal{P}_2)$ using the generating function method (Scheeres, D.J., Park, C. and Guibout, 2003), and Palmer solved problem $(\mathcal{P}_2)$ by the Fourier series expansion approach (Palmer, 2006). In the present chapter, a more general formulation to deal with the elliptic dynamics derived by Cho (Cho *et al.*, 2009), as summarized in Appendix C, is used for comparison.

3.5.1 Proposed Smoothing Process in Circular Orbit

First, the proposed smoothing process is explained in order to demonstrate the validity of the new smoothed solution with respect to the reconfiguration problem. Consider the circular orbit of the target ($e = 0$) and two periodic relative orbits, which have initial and final states $\boldsymbol{x}_0$ and $\boldsymbol{x}_1$, respectively, as the boundary conditions of the chaser satellite:

$$\begin{aligned} \boldsymbol{x}_0 &= [0\text{km},\ 16.0\text{km},\ 0\text{km},\ \ 8.85428\text{m/s},\ 0\text{m/s},\ 0\text{m/s}]^T \\ \boldsymbol{x}_1 &= [0\text{km},\ -8.0\text{km},\ 0\text{km},\ -4.42710\text{m/s},\ 0\text{m/s},\ 0\text{m/s}]^T \end{aligned}$$

where the first three values of each vector refer to the position, and the other values indicate the velocity of the chaser satellite. In addition, the transfer time $t_f = t_1 - t_0$ is set to $2T$ =11353.9 s. Figure 3.4 shows the solution in $(\mathcal{P}_{m1})$ and $(\mathcal{P}_2)$. The solver for the TPBVP used here is *bvp5c* from Matlab®, which provides a C_1-continuous

Table 3.3: Total fuel-consumption ΔV for $(\mathcal{P}^{\varepsilon}_{md1})$ varying with ε and for $(\mathcal{P}_{m1})$ and $(\mathcal{P}_2)$ in example case A.

Problem		$\|\Delta V\|$ m/s
$(\mathcal{P}^{\varepsilon}_{md1})$	$\varepsilon = 1$	13.9508
	$\varepsilon = 0.1$	11.6493
	$\varepsilon = 0.01$	10.1686
	$\varepsilon = 1 \times 10^{-3}$	9.8961
	$\varepsilon = 1 \times 10^{-4}$	9.8823
	$\varepsilon = 5 \times 10^{-5}$	9.8851
$(\mathcal{P}^{\varepsilon}_{m1})$	$\varepsilon = 5 \times 10^{-5}$	7.5495
$(\mathcal{P}_2)$	Analytical solution	9.4633

solution that is fifth-order accurate uniformly in $[f_0, f_1]$. The iterative solution for $(\mathcal{P}_{m1})$ is successfully generated as a bang-off-bang structure. The analytical solution given by Eq. (C.1) is also plotted for reference in Fig. 3.4. The analytical solution and the results of the shooting methods for $(\mathcal{P}_2)$ are completely overlapped. The directions relative to $-\boldsymbol{r}$, denoted by θ is very large. On the other hand, Fig. 3.5 shows the smoothing process when solving $(\mathcal{P}^{\varepsilon}_{md1})$ while varying $\varepsilon = \varepsilon_u = \varepsilon_b$ from 1 to 5×10^{-5}. Here, γ is set to $\pi/3$. The control magnitude and direction are always satisfied by the constraints. Specifically, the magnitude profile approaches the bang-off-bang shape and the relative angle becomes saturated up to the constraint angle. Table 3.3 shows the total fuel consumption, ΔV. ΔV decreases as ε decreases. ΔV in $(\mathcal{P}^{\varepsilon}_{md1})$ when $\varepsilon = 5 \times 10^{-5}$ is 16.6% larger than ΔV in $(\mathcal{P}^{\varepsilon}_{m1})$.

3.5.2 In-plane Transfer in the Eccentric Orbit Case

Next, consider the eccentric orbit of the target ($e = 0.3$) and two periodic relative orbits that have initial and final states $\boldsymbol{x}_0$ and $\boldsymbol{x}_1$, respectively, as the boundary conditions of the chaser satellite:

$$\begin{aligned} \boldsymbol{x}_0 &= [1.0\text{km},\ 0\text{km},\ 0\text{km},\ 0\text{m/s},\ -3.8122\text{m/s},\ 0\text{m/s}]^T \\ \boldsymbol{x}_1 &= [0.5\text{km},\ 0\text{km},\ 0\text{km},\ 0\text{m/s},\ -1.9061\text{m/s},\ 0\text{m/s}]^T \end{aligned}$$

which are also periodic orbit states without control (Ichikawa and Bando, 2009), and the transfer time is set to $T = 5677$ s. Figure 3.6 shows the solution for $(\mathcal{P}^{\varepsilon}_{md1})$ and $(\mathcal{P}_2)$, and Fig. 3.7 shows the solution for $(\mathcal{P}^{\varepsilon}_{md2})$ and $(\mathcal{P}_2)$. The control angle limitation γ is set to $\pi/3$. In both cases, the thrust angle is efficiently suppressed within γ.

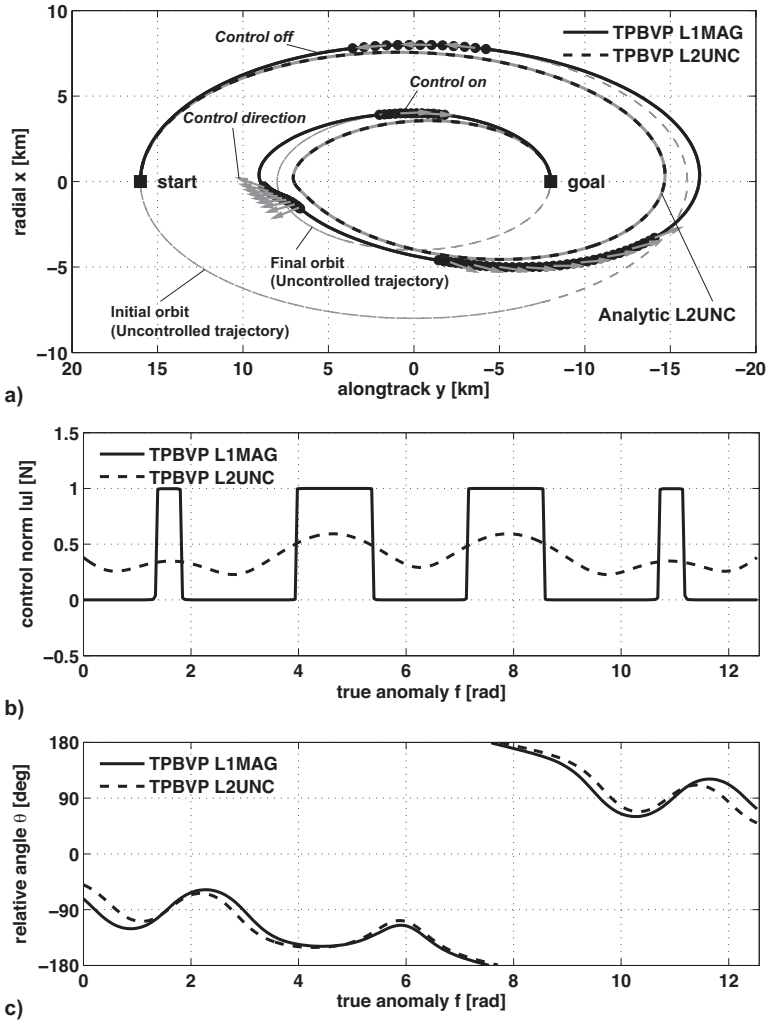

Figure 3.4: Solutions for $(\mathcal{P}^{\varepsilon}_{m1})$. a) trajectory, b) profiles in $\|\boldsymbol{u}\|$, and c) θ.

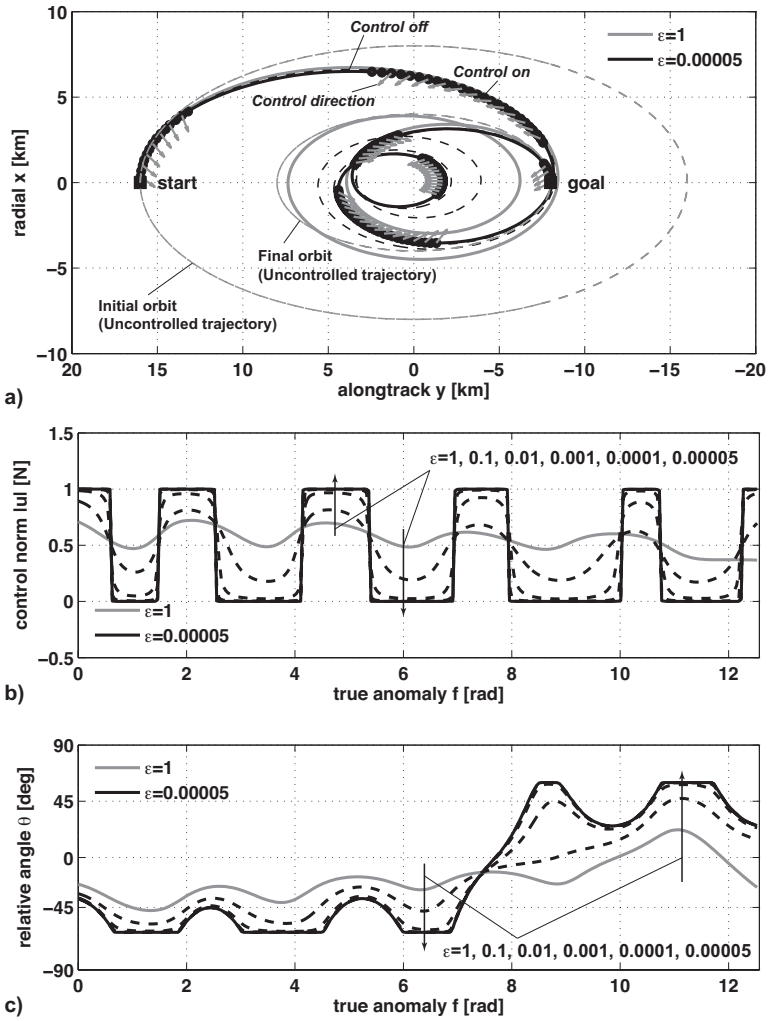

Figure 3.5: Solutions for $(\mathcal{P}^{\varepsilon}_{md1})$. a) trajectory, b) profiles in $\|\boldsymbol{u}\|$, and c) θ.

Table 3.4: Total fuel-consumption ΔV for $(\mathcal{P}^{\varepsilon}_{md1})$ and $(\mathcal{P}^{\varepsilon}_{md2})$ with $\varepsilon = 5 \times 10^{-5}$ and for $(\mathcal{P}_2)$ in example case B.

Problem		$\|\Delta V\|$ m/s
$(\mathcal{P}^{\varepsilon}_{md1})$	$\varepsilon = 5 \times 10^{-5}$	3.34393
$(\mathcal{P}^{\varepsilon}_{md2})$	$\varepsilon = 5 \times 10^{-5}$	4.46839
$(\mathcal{P}_2)$	Analytical solution	0.38887

Figure 3.8 shows that the proximity of the target is magnified in the cases of $(\mathcal{P}^{\varepsilon}_{md1})$ and $(\mathcal{P}^{\varepsilon}_{md2})$. As shown in Figs. 3.6c) and 3.7c), when the direction condition is not applied, θ is coincident with β, which means that $\boldsymbol{u}$ is parallel to $-\boldsymbol{p}$. On the other hand, when the direction condition is applied, θ is saturated with γ, and then β is over $\theta = \gamma$. Table 3.4 shows the total fuel consumption, ΔV. ΔV of $\mathcal{P}^{\varepsilon}_{md1}$ and $\mathcal{P}^{\varepsilon}_{md2}$ become one digit larger than that of $\mathcal{P}_2$, although the control angle becomes suppressed within the direction constraint.

When the barrier terms $\varepsilon_u F_u$ and $\varepsilon_b F_b$ are introduced to deal with $(\mathcal{P}_{md2})$, there is an important difference with the case of $(\mathcal{P}_{md1})$. For $(\mathcal{P}_{m1})$, the control norm is bang-bang and so the use of smoothing techniques is mandatory. In the case of $(\mathcal{P}_{m2})$, the norm of the control is continuous and smoothing techniques are not mandatory from the numerical point of view. The associated shooting function is sufficiently smooth and Newton's method can be used without any problem. The use of barrier functions in the case of $(\mathcal{P}_{m2})$, simply allows to build a sequence of unconstrained problems, the solutions of which converge to the solution of problem $(\mathcal{P}_{m2})$. So, the introduction of barrier terms allows to build a practical algorithm in case of $(\mathcal{P}_{m2})$ but not to face with important numerical difficulties as in the case of problem $(\mathcal{P}_{m1})$. Nevertheless, when introducing the thrust direction constraint, the thrust direction can be discontinuous (even for the L_2-problem so for $(\mathcal{P}_{md2})$) and the use of barrier functions is numerically justified.

3.5.3 Three-dimensional Transfer in the Circular Orbit Case

Finally, consider the reconfiguration problem, including out-of-plane motion. The following boundary conditions of the chaser satellite are considered:

$$\begin{aligned} \boldsymbol{x}_0 &= [-8.0\text{km},\ 0\text{km},\ 13.8564\text{km},\ 0\text{m/s},\ 17.7086\text{m/s},\ 0\text{m/s}]^T \\ \boldsymbol{x}_1 &= [-4.0\text{km},\ 0\text{km},\ 6.9282\text{km},\ 0\text{m/s},\ 8.8543\text{m/s},\ 0\text{m/s}]^T \end{aligned}$$

and the transfer time is set to $2T = 11353.9$ s. Figure 3.9 shows the solution for $(\mathcal{P}^{\varepsilon}_{m1})$ and $(\mathcal{P}_2)$. Solution θ in the unconstrained case exceeds 100° in some parts of

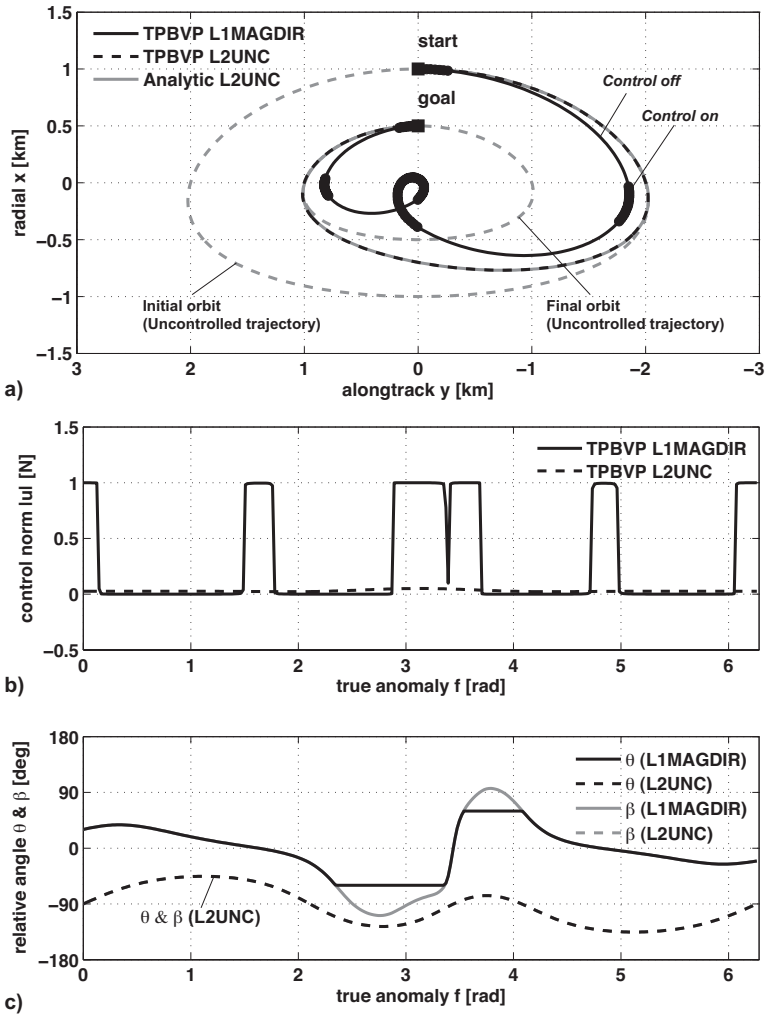

Figure 3.6: Solutions for $(\mathcal{P}^{\varepsilon}_{md1})$. a) trajectory, b) profiles in $\|\boldsymbol{u}^{\varepsilon}_{mdj}\|$, and c) θ and β.

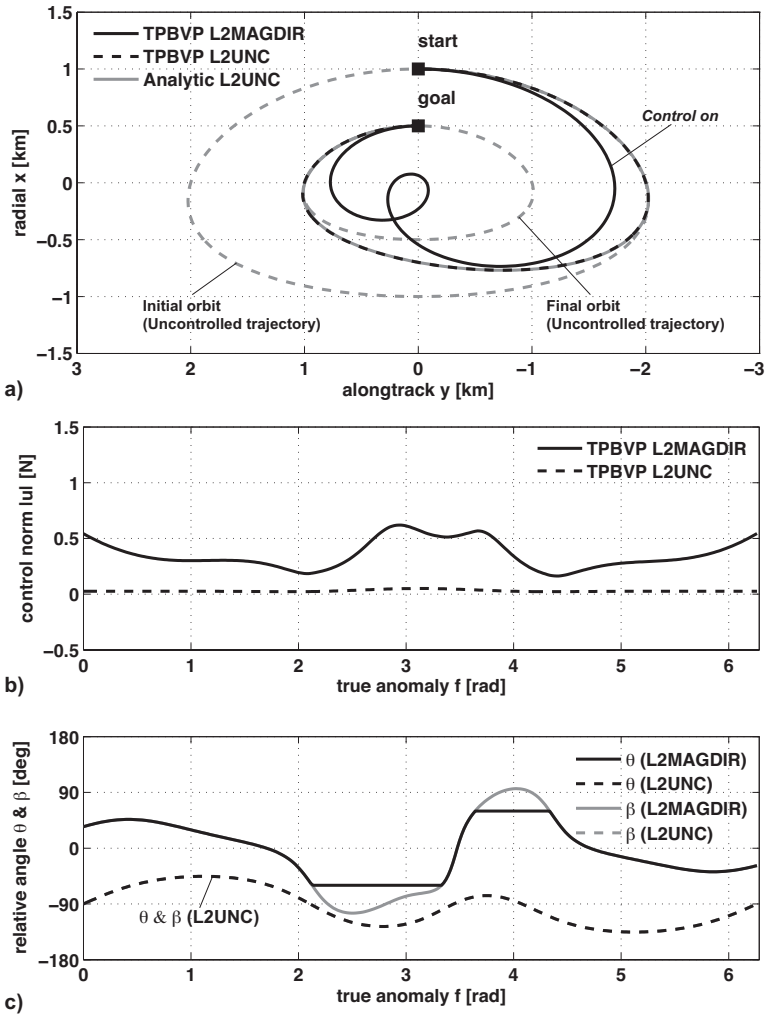

Figure 3.7: Solutions for $(\mathcal{P}^{\varepsilon}_{md2})$. a) trajectory, b) profiles in $\|\boldsymbol{u}^{\varepsilon}_{mdj}\|$, and c) θ and β.

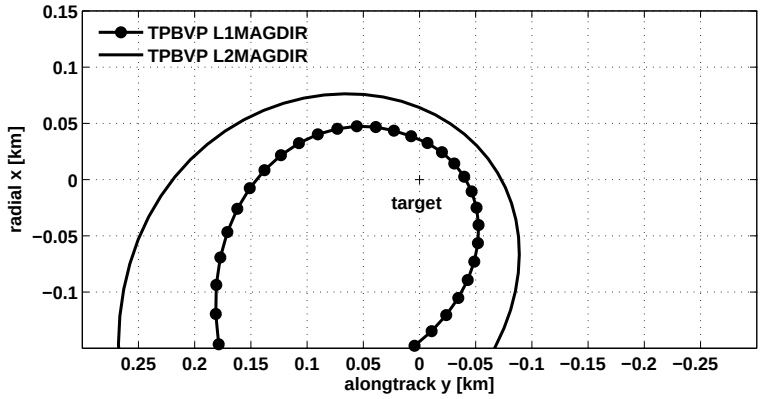

Figure 3.8: Proximity of the target for $(\mathcal{P}^{\varepsilon}_{md1})$ and $(\mathcal{P}^{\varepsilon}_{md2})$.

Table 3.5: Total fuel consumption ΔV for $(\mathcal{P}^{\varepsilon}_{md1})$ and $(\mathcal{P}^{\varepsilon}_{m1})$ with $\varepsilon = 5 \times 10^{-5}$ and for $(\mathcal{P}_2)$ in example case C.

Problem		$\|\Delta V\|$ m/s
$(\mathcal{P}^{\varepsilon}_{md1})$	$\varepsilon = 5 \times 10^{-5}$	9.89213
$(\mathcal{P}^{\varepsilon}_{m1})$	$\varepsilon = 5 \times 10^{-5}$	9.90005
$(\mathcal{P}_2)$	Analytical solution	11.56308

the interval. Figure 3.10 shows the solution for $(\mathcal{P}^{\varepsilon}_{md1})$ and $(\mathcal{P}_2)$. The control angle limitation γ is set to 95°. The thrust angle is suppressed within γ. It is found that thrust direction is hard to be small with the same boundary condition. In the present chapter, the boundary condition for the initial and final positions, the velocity, and the transfer time are fixed determinately. In the future, the authors intend to investigate how to decrease γ and ΔV for various boundary condition. Table 3.5 shows the total fuel consumption, ΔV. ΔV of $\mathcal{P}^{\varepsilon}_{md1}$ is rarely different from that of $(\mathcal{P}^{\varepsilon}_{m1})$. In this case, the solution of $(\mathcal{P}^{\varepsilon}_{md1})$ is shown to be more beneficial than that of $(\mathcal{P}^{\varepsilon}_{m1})$ and $(\mathcal{P}_2)$ in terms of both the control angle and the total fuel consumption.

3.6 Conclusions

The present chapter treated the satellite formation and reconfiguration problem under constraints on the control magnitude and direction. A necessary condition of the op-

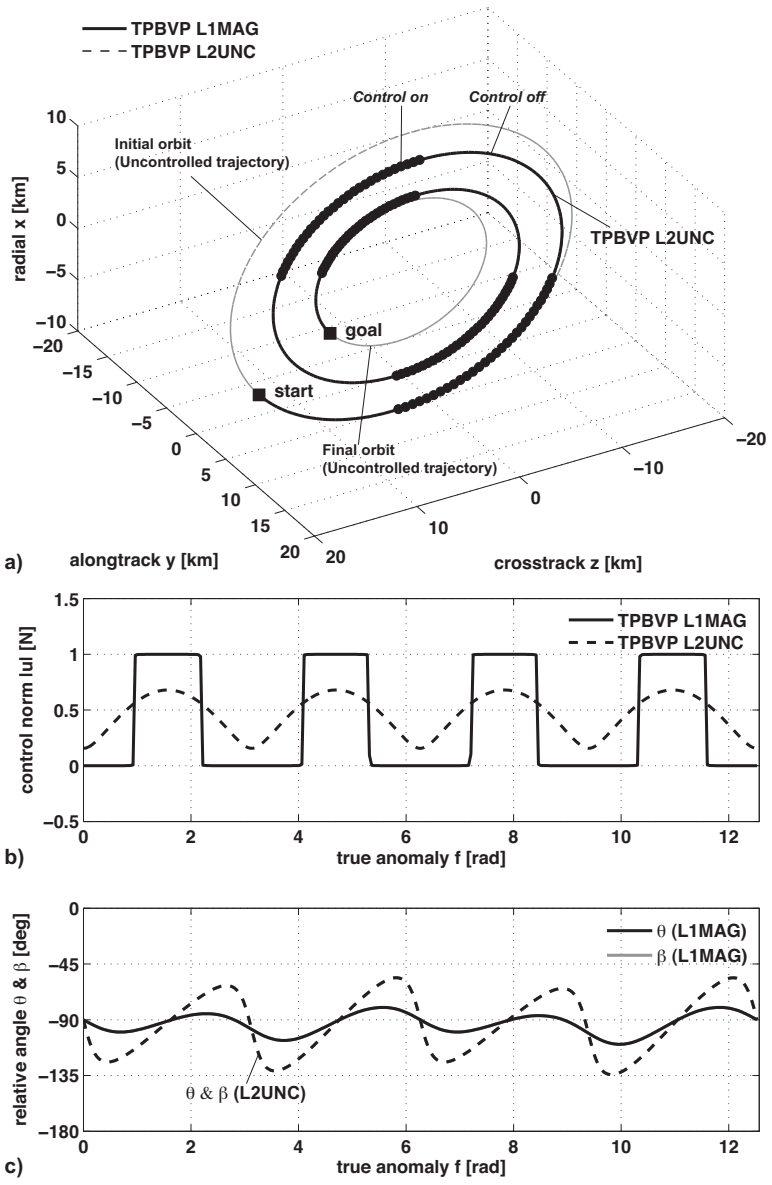

Figure 3.9: Solutions for $(\mathcal{P}^{\varepsilon}_{m1})$. a) 3D-trajectory, b) profiles in $\|\boldsymbol{u}^{\varepsilon}_{mdj}\|$, and c) θ and β.

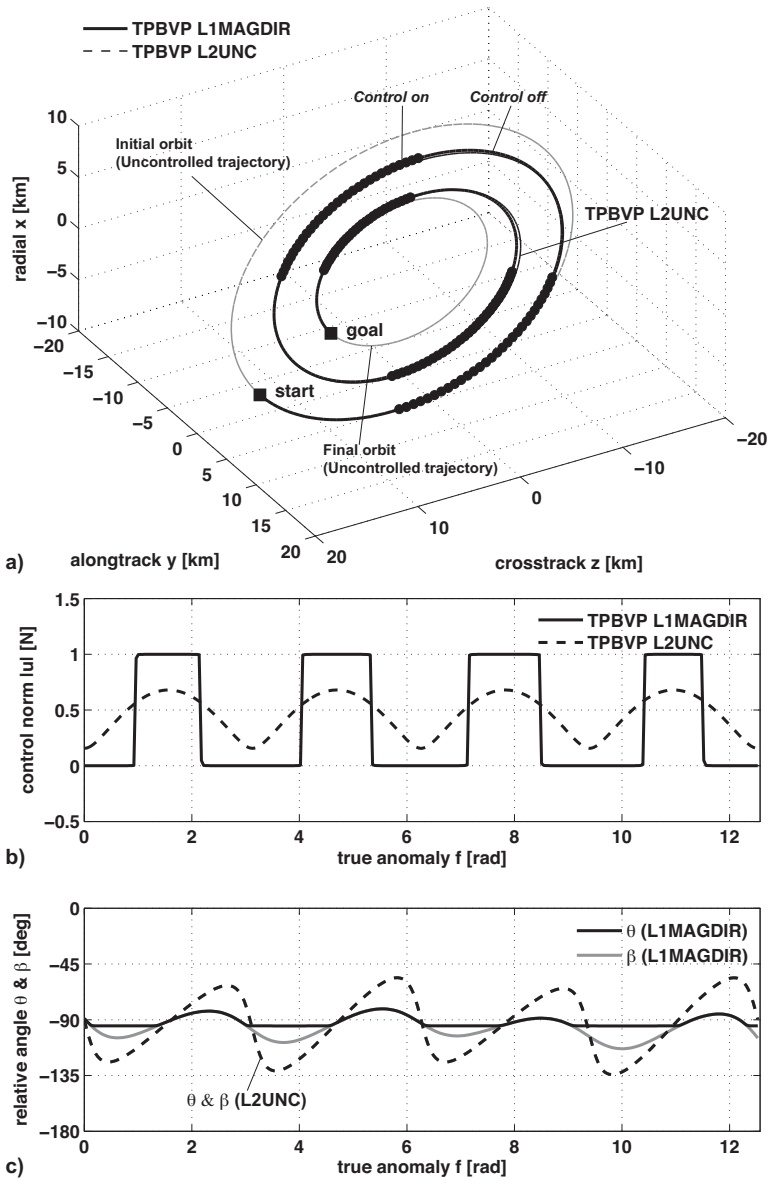

Figure 3.10: Solutions for ($\mathcal{P}^{\varepsilon}_{md1}$). a) 3D-trajectory, b) profiles in $\|\boldsymbol{u}^{\varepsilon}_{mdj}\|$, and c) θ and β.

timal controller under these constraints was first derived using a sequential smoothing method, in which a sequence of unconstrained optimal control problems is solved according to Pontryagin's minimum principle by introducing multiple barrier functions to the original performance index. By introducing the proposed additional barrier function concerning the constraints on the control direction, the derived equations for the necessary condition with respect to optimal control magnitude and direction became decoupled, thereby facilitating their solution. The solutions converged toward to the solution of the original problem and strictly satisfied the treated constraints as the perturbation coefficients of the barrier functions approached zero. Optimal controllers were successfully formulated in the L_1- and L_2-norm problems, and both solutions for the optimal control direction had the same form. These solutions are a natural extension of the solution with only the magnitude constraint. As the perturbation coefficients of the barrier functions approach zero, the smoothed optimal controller approaches the boundary of the inequality constraint near Lawden's primer vector, while the control, the primer, and the admissible direction vectors are coplanar. This extremal property is completely consistent with the result that the optimal thrust is directed along the projection of the primer vector onto the boundary of the restricting set. Numerical simulations demonstrated that the sequential optimal controller with such a mixed-constraint was obtained by solving the two-point boundary value problem with the shooting method in such an non-coplanar circular orbit and a coplanar eccentric orbit. In addition, the control angles of the derived solutions were confirmed to be suppressed within the control direction constraint.

Chapter 4

Satisficing Control Theory

4.1 Introduction

In the following chapters, a new nonlinear control scheme is applied to the problem of satellite rendezvous trajectory planning. Constraints are placed on the thrust angle so as to align the thrust direction with the relative position vector as closely as possible. The control scheme is based on the concept of satisficing. This section explains the concept and the fundamental properties. "Satisficing" is a blended word combining "satisfy" with "suffice". The following definitions of satisficing in Wikipedia are:

- "Aiming to achieve only satisfactory results because the satisfactory position is familiar, hassle-free, and secure, whereas aiming for the best-achievable result would call for costs, effort, and incurring of risks."
- "Optimization where all costs, including the cost of the optimization calculations themselves and the cost of getting information for use in those calculations, are considered."
- "A decision-making strategy that attempts to meet criteria for adequacy, rather than to identify an optimal solution. A satisficing strategy may often be (near) optimal if the costs of the decision-making process itself, such as the cost of obtaining complete information, are considered in the outcome calculus."

Satisficing is a parameterization of universal formulas, which is first derived using the notion of satisficing decision theory (Goodrich *et al.*, 1998; Stirling, 2003). The basic idea involves defining two utility functions that quantify the benefits and costs of an action. The "selectability" function was chosen as the distance from the predicted state at the next time instant to the origin, while the "rejectability" function was chosen as proportional to the control effort. The resulting control strategy is reminiscent

of MPC (Curtis and Beard, 2001). Since then, by linking the "selectability" function to a CLF, closed-loop asymptotic stability is ensured (Curtis and Beard, 2002*a*, 2004), and provides complete parameterization as a generalization of the input-to-state stabilizing (ISS) version of Sontag's formula (Sontag, 1989) and Freeman and Kokotovic's mini-norm approach (Freeman and Kokotovic, 1996). CLF-based satisficing can be modified to parameterize a large class of inverse-optimal (Krstić and Deng, 1998) controllers, which always possess desirable gain margins (Curtis and Beard, 2002*b*, 2004). In (Curtis, 2003, 2005), the constrained stabilizing control value set was proposed in terms of the polytopes-shaped constraint boundary set. The input constraint was first considered in CLF using satisficing theory and the idea was then applied to a practical problem by Ren and Beard (Ren and Beard, 2004), whereby only control magnitude constraints were treated.

In this chapter, we summarize the concept and fundamental properties of the satisficing. The results in this chapter are mainly based on (Curtis and Beard, 2002*b*, 2004). Moreover, the interesting relationship between the Sontag's formula, Min-norm formula and HJB equation are based on (Primbs, 1999). We extend these results in the case of a more general performance index and time-varying nonlinear system.

4.2 Concept of Satisficing

Consider the affine nonlinear time-varying system

$$\dot{\boldsymbol{x}} = f(t, \boldsymbol{x}) + g(t, \boldsymbol{x})\boldsymbol{u} \tag{4.1}$$

where $\boldsymbol{x} \in \boldsymbol{R}^n$, $f : \boldsymbol{R}^n \to \boldsymbol{R}^n$, $g : \boldsymbol{R}^n \to \boldsymbol{R}^{n\times m}$ and $\boldsymbol{u} \in \boldsymbol{R}^m$. We will assume throughout this paper that f and g are locally Lipschitz functions and that $f(\boldsymbol{0}) = \boldsymbol{0}$.

The satisficing scheme involves choosing a control Lyapunov function (CLF) that allows the optimal control input history to be solved. First of all, define the CLF as follows:

Definition 4.2.1 (Curtis and Beard, 2002*b*) C^2 function $V(t,\ \boldsymbol{x}) : \boldsymbol{R}_+ \times \boldsymbol{R}^n \to \boldsymbol{R}$ is said to be a control Lyapunov function (CLF) for the affine nonlinear time-varying system Eq. (4.1) with input constraints $\boldsymbol{u} \in \boldsymbol{U} \subset \boldsymbol{R}^m$ if V is positive-definite, radially unbounded, and if

$$\inf_{\boldsymbol{u}} \dot{V} = \inf_{\boldsymbol{u}} \left\{ \frac{\partial V}{\partial t} + \left(\frac{\partial V}{\partial \boldsymbol{x}}\right)^T (f(t, \boldsymbol{x}) + g(t, \boldsymbol{x})\boldsymbol{u}) \right\} < 0 \tag{4.2}$$

for all $\boldsymbol{x} \neq 0$.

Throughout this thesis, denote the partial derivative with a subscript: $V_t \triangleq \partial V/\partial t$ and $V_x \triangleq \partial V/\partial \boldsymbol{x}$, where V_t is a scalar and V_x is assumed to be a column vector respectively. The satisficing paradigm calls for the definition of two utility functions: the selectability function $p_s(t, \boldsymbol{u}, \boldsymbol{x})$, and the rejectability function $p_r(t, \boldsymbol{u}, \boldsymbol{x})$ (Stirling, 2003). In addition, define $b(t, \boldsymbol{x}) \in (0, \infty)$ to be the selectivity, or boldness, index . Define the satisficing set as follows (Goodrich *et al.*, 1998; Curtis and Beard, 2004):

Definition 4.2.2 (Curtis and Beard, 2004) The satisficing Set $S_b(t, \boldsymbol{x})$ is defined as the set of control values, such that the selectability times the selectivity index exceeds the rejectability, i.e.

$$S_b(t, \boldsymbol{x}) = \left\{ \boldsymbol{u} \in \boldsymbol{R}^m : \; p_s(t, \boldsymbol{u}, \boldsymbol{x}) > \frac{1}{b(t, \boldsymbol{x})} p_r(t, \boldsymbol{u}, \boldsymbol{x}) \right\} \tag{4.3}$$

In other words, the satisficing set is the set of all pointwise control values where the instantaneous benefits of applying that action outweigh the instantaneous costs. If for each $\boldsymbol{x}$, $p_s(t, \boldsymbol{u}, \boldsymbol{x})$ is a concave function of $\boldsymbol{u}$ and $p_r(t, \boldsymbol{u}, \boldsymbol{x})$ is a convex function of $\boldsymbol{u}$, then $S_b(t, \boldsymbol{x})$ is a convex set (Curtis and Beard, 2004).

Note that we only require convexity in $\boldsymbol{u}$ and not $\boldsymbol{x}$. Therefore, we do not impose any convexity restrictions on the system, but only on the incremental measures of benefit and cost.

We will associate the notion of selectability with stability, and that of rejectability with instantaneous cost. In particular, let

$$p_s(t, \boldsymbol{u}, \boldsymbol{x}) = -V_t(t, \boldsymbol{x}) - V_x^T(t, \boldsymbol{x})(f(\boldsymbol{x}) + g\boldsymbol{u}) \tag{4.4}$$

where V is a CLF. Note that stabilizing control values make $p_s(\boldsymbol{u}, \boldsymbol{x})$ positive. We choose the rejectability criterion to be

$$p_r(t, \boldsymbol{u}, \boldsymbol{x}) = l(t, \boldsymbol{x}) + \boldsymbol{u}^T R \boldsymbol{u} + 2\boldsymbol{x}^T N \boldsymbol{u} \tag{4.5}$$

where $R(t, \boldsymbol{x}) = R^T(t, \boldsymbol{x}) > 0$ is a positive-definite matrix function whose elements are locally Lipschitz and $l : \boldsymbol{R}^m \to \boldsymbol{R}$ is a locally Lipschitz non-negative function. For $p_r > 0$,

$$p_r(t, \boldsymbol{u}, \boldsymbol{x}) = [l(t, \boldsymbol{x}) - \boldsymbol{x}^T N R^{-1} N^T \boldsymbol{x}] + (\boldsymbol{u} + R^{-1} N^T \boldsymbol{x}) R (\boldsymbol{u} + R^{-1} N^T \boldsymbol{x}) > 0 \tag{4.6}$$

The second term is always non-negative. The first term is non-negative if

$$l_N \triangleq l(t, \boldsymbol{x}) - \boldsymbol{x}^T N R^{-1} N^T \boldsymbol{x} > 0$$

Note that p_s is a linear function in $\boldsymbol{u}$ and is hence concave in $\boldsymbol{u}$. Additionally, p_r is convex in $\boldsymbol{u}$. For these choices of p_s and p_r the satisficing set becomes

$$S_b(t,\boldsymbol{x}) = \left\{ \boldsymbol{u} \in \boldsymbol{R}^m : \ -V_t - V_x^T(f+g\boldsymbol{u}) > \frac{1}{b}(l + \boldsymbol{u}^T R\boldsymbol{u} + 2\boldsymbol{x}^T N\boldsymbol{u}) \right\} \tag{4.7}$$

which is guaranteed to be a convex set.

The following theorem completely characterizes the satisficing set for the particular selectability and rejectability functions chosen previously.

Theorem 4.2.3 If $p_s(t,\boldsymbol{u},\boldsymbol{x}) = -V_t(t,\boldsymbol{x}) - V_x^T(t,\boldsymbol{x})(f(\boldsymbol{x}) + g\boldsymbol{u})$ and $p_r(t,\boldsymbol{u},\boldsymbol{x}) = l(t,\boldsymbol{x}) + \boldsymbol{u}^T R\boldsymbol{u} + 2\boldsymbol{x}^T N\boldsymbol{u}$, then the satisficing set $S_b(t,\boldsymbol{x})$ at $(t,\boldsymbol{x})$ is nonempty if and only if the design parameter $b(\boldsymbol{x})$ satisfies the inequality

$$b(t,\boldsymbol{x})\omega_N + l_N - \frac{b(t,\boldsymbol{x})^2}{4}\boldsymbol{p}^T R^{-1}\boldsymbol{p} < 0 \tag{4.8}$$

Furthermore, if the inequality Eq. (4.8) holds true, then $S_b(t,\boldsymbol{x}) \subset \boldsymbol{R}^m$ can be described as a perfect parametric form by introducing a new design parameter ν (Curtis and Beard, 2004)

$$\begin{aligned} S_b(t,\boldsymbol{x}) &= \left\{ -R^{-1}\left(\frac{b}{2}\boldsymbol{p} + N^T\boldsymbol{x}\right) + R^{-1/2}\nu\sqrt{\frac{b^2}{4}\boldsymbol{p}^T R^{-1}\boldsymbol{p} - b\omega_N - l_N} : \ |\nu| < 1 \right\} \\ &\triangleq \{-\sigma_1(t,\boldsymbol{x},b) + \sigma_2(t,\boldsymbol{x},b)\cdot\nu : \ |\nu| < 1\} \end{aligned} \tag{4.9}$$

where $\boldsymbol{p} = g^T V_x$, $\omega_N = V_t + V_x^T f - V_x^T g R^{-1} N^T \boldsymbol{x}$ and $l_N = l - \boldsymbol{x}^T N R^{-1} N^T \boldsymbol{x}$.

Note that this formula provides a mapping from the open unit ball (ν is a free parameter whose only constraint is that it lies in the unit ball) to the satisficing set. Note also that when $\boldsymbol{p} = 0$, the satisficing set is well-defined and given by

$$S_b(\boldsymbol{x}) = \left\{ -R^{-1}N^T\boldsymbol{x} + R^{-1/2}\nu\sqrt{-b\omega_N - l_N} : \ |\nu| < 1 \right\}$$

The proof of Theorem depends upon the following lemma, which provides a generalization of the quadratic formula. The following lemma is proven in (Curtis and Beard, 2004).

Lemma 4.2.4 If $A = A^T > 0$, then the set of solutions to the quadratic inequality

$$\boldsymbol{\xi}^T A\boldsymbol{\xi} + \boldsymbol{d}^T\boldsymbol{\xi} + c < 0$$

where $\boldsymbol{\xi} \in \boldsymbol{R}^s$, is nonempty if and only if

$$\frac{1}{4}\boldsymbol{d}^T A^{-1}\boldsymbol{d} - c > 0$$

and is given by

$$\boldsymbol{\xi} = -\frac{1}{2}A^{-1}\boldsymbol{d} + A^{-1/2}\nu\sqrt{\frac{1}{4}\boldsymbol{d}^T A^{-1}\boldsymbol{d} - c}$$

where $\boldsymbol{\nu} \in \{\boldsymbol{\xi} \in \boldsymbol{R}^s : \|\boldsymbol{\xi}\| < 1\}$.

Proof of Theorem 4.2.3: The satisficing set is given by

$$\begin{aligned} S_b(t,\boldsymbol{x}) &= \left\{\boldsymbol{u} \in \boldsymbol{R}^m : -V_t - V_x^T f - V_x^T g\boldsymbol{u} \geq \frac{1}{b}l + \frac{1}{b}\boldsymbol{u}^T R\boldsymbol{u} + \frac{1}{b}2\boldsymbol{x}^T N\boldsymbol{u}\right\} \\ &= \left\{\boldsymbol{u} \in \boldsymbol{R}^m : \boldsymbol{u}^T\left(\frac{R}{b}\right)\boldsymbol{u} + (g^T V_x + \frac{1}{b}2N^T\boldsymbol{x})^T\boldsymbol{u} + (V_t + V_x^T f + \frac{1}{b}l) \leq 0\right\} \end{aligned}$$

The theorem therefore follows from Lemma with $A = R/b$, $\boldsymbol{d} = g^T V_x + 2N^T\boldsymbol{x}/b$, and $c = (1/b)l + V_t + V_x^T f$. □

The theorem shows that the selectivity index $b(t,\boldsymbol{x})$ plays a critical role in the size of $S_b(t,\boldsymbol{x})$. The next lemma shows that for each $\boldsymbol{x} \neq 0$, b can always be chosen such that the satisficing set is nonempty. Toward that end, define

$$\underline{b} = \begin{cases} 2\left(\dfrac{\omega_N + \sqrt{\omega_N^2 + l_N \cdot \boldsymbol{p}^T R^{-1}\boldsymbol{p}}}{\boldsymbol{p}^T R^{-1}\boldsymbol{p}}\right), & \text{if } \boldsymbol{p} \neq \boldsymbol{0} \\ \dfrac{l_N}{-\omega_N}, & \text{if } \boldsymbol{p} = \boldsymbol{0} \end{cases} \tag{4.10}$$

Lemma 4.2.5 If V is a CLF for system Eq. (4.1), $\underline{b}$ is given by Eq. (4.10), and S_b is given by Eq. (4.9), then for each $\boldsymbol{x} \neq 0$

1. $\underline{b}(t,\boldsymbol{x}) \geq 0$
2. $b > \underline{b}(t,\boldsymbol{x})$ implies that $S_b(t,\boldsymbol{x}) \neq \phi$
3. if $l : \boldsymbol{R}^n \Rightarrow \boldsymbol{R}^+$ satisfies the property

$$(g^T V_x \neq 0 \text{ and } \omega_N = 0) \Rightarrow l_N > 0 \tag{4.11}$$

then $\underline{b}(t,\boldsymbol{x})$ is locally Lipschitz on $\boldsymbol{R}^n \backslash 0$.

Proof of Lemma 4.2.5: If $\boldsymbol{p} = \boldsymbol{0}$, then since V is a CLF, $\omega_N = V_t + V_x^T f - V_x^T g R^{-1} N\boldsymbol{x} < 0$, therefore, inequality (4.8) is satisfied if and only if

$$\begin{aligned} & l_N + b\omega_N < 0 \\ \iff \quad & b > \frac{l_N}{-\omega_N} \geq 0 \end{aligned}$$

If $g^T V_z \neq \mathbf{0}$, then inequality (4.8) is satisfied if and only if

$$b^2 - \left(\frac{4\omega_N}{\boldsymbol{p}^T R^{-1}\boldsymbol{p}}\right) b - \left(\frac{4l_N}{\boldsymbol{p}^T R^{-1}\boldsymbol{p}}\right) > 0$$

$$\iff \left(b - \left(\frac{2\omega_N}{\boldsymbol{p}^T R^{-1}\boldsymbol{p}}\right)\right)^2 > \left(\frac{2\omega_N}{\boldsymbol{p}^T R^{-1}\boldsymbol{p}}\right)^2 + \left(\frac{4l_N}{\boldsymbol{p}^T R^{-1}\boldsymbol{p}}\right)$$

Restricting attention to positive solutions, this inequality is true if and only if

$$b > 2\left(\frac{\omega_N + \sqrt{\omega_N^2 + l_N \cdot \boldsymbol{p}^T R^{-1}\boldsymbol{p}}}{\boldsymbol{p}^T R^{-1}\boldsymbol{p}}\right)$$

which clearly exceeds or is equal to zero.

To show that $\underline{b}(\boldsymbol{x})$ is locally Lipschitz on $\boldsymbol{R}^n \backslash 0$, we follow the arguments used in (Krstić and Deng, 1998) to show the continuity of Sontag's formula. Following their arguments, we show that the function

$$\phi(a,c,l) = \begin{cases} -\frac{l}{a}, & \text{if } c = 0 \text{ and } a < 0 \\ \frac{2a + 2\sqrt{a^2+lc}}{c}, & \text{elsewhere} \end{cases}$$

is smooth (C^∞) on the set $P = \{(a,c,l) \in \boldsymbol{R}^3 | l \geq 0 \text{ and } c \geq 0 \text{ and } (c = 0 \Rightarrow a < 0) \text{ and } ((c \neq 0 \text{ and } a = 0) \Rightarrow l > 0)\}$.

Define the function

$$F(a,c,l,p) = l + pa - \frac{1}{4}p^2 c$$

which is smooth on P in all its arguments. By direct substitution, it is straightforward to show that $F(a,c,l,\phi(a,c,l)) = 0$ for all $(a,c,l) \in P$. If $c = 0$, then

$$\frac{\partial F(a,c,l,\phi(a,c,l))}{\partial p} = a$$

which is strictly less than zero since V is a CLF. If $c \neq 0$, then

$$\frac{\partial F(a,c,l,\phi(a,c,l))}{\partial p} = -\sqrt{a^2 + lc}$$

which, by Eq. (4.11), is nonzero on P. Therefore, by the implicit function theorem, $\phi(a,c,l)$ is smooth on P. Since ω_N, $\boldsymbol{p}^T R^{-1}\boldsymbol{p}$, and l_N are locally Lipschitz on $\boldsymbol{R}^2 \backslash \{0\}$, $\underline{b} = \phi(\omega_N, \boldsymbol{p}^T R^{-1}\boldsymbol{p}, l_N)$ is also locally Lipschitz on $\boldsymbol{R}^2 \backslash \{0\}$. □

4.3 Relation to Sontag's Formula and Pointwise Min-norm Solution

This section provides an explanation of the relationship between Sontag's formula (Sontag, 1989), Freeman and Kokotovic's min-norm controls (Freeman and Kokotovic,

1996), and ISS-satisficing controls. It will be shown that the pointwise min-norm control parameterizes a line in $\boldsymbol{R}^m$ for any fixed $\boldsymbol{x}$, and that a point on this line corresponds to Sontag's formula. ISS-satisficing parameterizes a half space in $\boldsymbol{R}^m$ which contains a line corresponding to the min-norm controls as well as all control values with components in the null space of $g^T V_x$.

4.3.1 CLF a substitute for the value function: Sontag's formula

Perhaps the most important formula for producing a stabilizing controller based on the existence of a CLF was introduced in (Sontag, 1989) and has come to be known as Sontag's formula. We will consider a slight variation of Sontag's formula (which we will continue to refer to as Sontag's formula with slight abuse). As described in (Freeman and Kokotovic, 1996), Sontag's formula for input-to-state stability is given by

$$\boldsymbol{u}_{\text{Sontag}} = \begin{cases} -R^{-1}\left[\dfrac{\omega_N + \sqrt{\omega_N^2 + l_N \cdot \boldsymbol{p}^T R^{-1}\boldsymbol{p}}}{\boldsymbol{p}^T R^{-1}\boldsymbol{p}}\boldsymbol{p} + N^T\boldsymbol{x}\right], & \text{if } \boldsymbol{p} \neq \boldsymbol{0} \\ -R^{-1}N^T\boldsymbol{x}, & \text{if } \boldsymbol{p} = \boldsymbol{0} \end{cases} \tag{4.12}$$

Note that this formula corresponds to a point in $\boldsymbol{R}^m$ that lies within the range space of $\boldsymbol{p} = g^T V_x$; $\boldsymbol{u}_{\text{Sontag}} = -R^{-1}[\beta\boldsymbol{p} + N^T\boldsymbol{x}]$ with

$$\beta = \frac{\omega_N + \sqrt{\omega_N^2 + l_N \cdot \boldsymbol{p}^T R^{-1}\boldsymbol{p}}}{\boldsymbol{p}R^{-1}\boldsymbol{p}} > \frac{\omega_N}{\boldsymbol{p}R^{-1}\boldsymbol{p}} \tag{4.13}$$

Since Sontag's formula is continuous and ISS with respect to V, it is also a satisficing control (Curtis and Beard, 2002*a*). Seen alternatively, Eq. (4.9) can be made equal to the ISS version of Sontag's formula when $R = I$, $N = O$, $l = \boldsymbol{p}^T\boldsymbol{p}$, $\nu = 0$, and $b(\boldsymbol{x}) = \underline{b}(\boldsymbol{x})$.

Figure 4.1 shows the point corresponding to Sontag's formula in a snapshot of a two-dimensional control space at a fixed state. The values in the figure are as follows: $\omega_N = -2$, $l = 4$, $R = I_{2\times 2}$, $N = [I_{2\times 2}\ O_{2\times 2}]^T$, $\boldsymbol{x} = [1\ -0.5\ 0\ 0]^T$ and $g^T V_x = [1\ 1]^T$.

Optimality, Sontag's formula and level curves

Below, we unravel some key connections between level curves of the value function V^* and Sontag's formula Eq. (4.12). It is shown that Sontag's formula, in essence, uses the directional information supplied by a CLF, V, and scales it properly to solve the HJB equation. In particular, if V has level curves that match those of the value function, then Sontag's formula produces the optimal controller (Freeman and Primbs, 1996; Primbs, 1999).

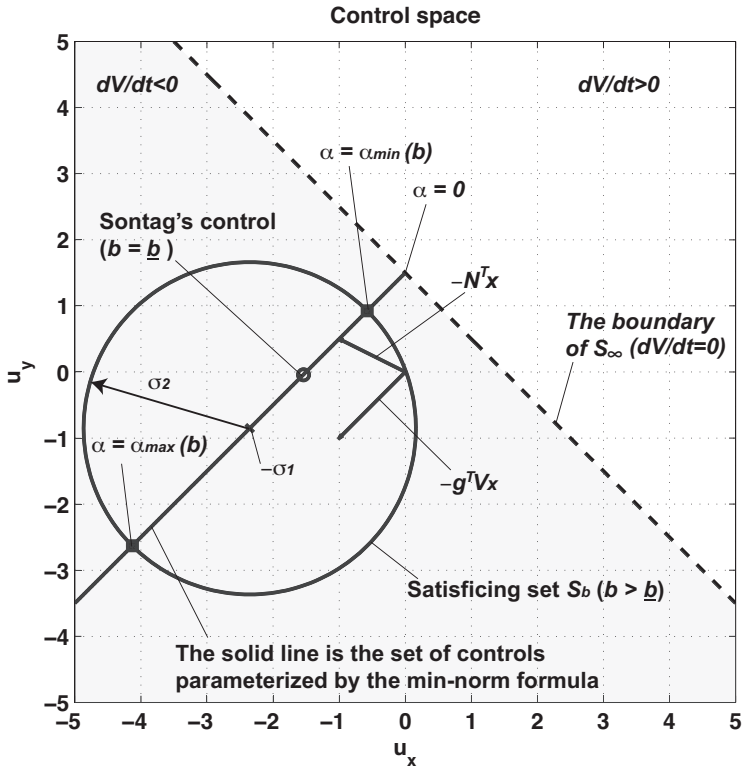

Figure 4.1: Control space at a fixed state and time.

Define $V^*(t_0, \boldsymbol{x}_0)$ to be the minimum of the performance index taken over all admissible trajectories $(\boldsymbol{x}(t), \boldsymbol{u}(t))$ where $\boldsymbol{x}$ starts at $(t_0, \boldsymbol{x_0})$:

$$\begin{aligned} V^*(t_0, x_0) = \quad & \min_{\boldsymbol{u}} \int_{t_0}^{\infty} (l(t, \boldsymbol{x}) + 2\boldsymbol{x}N\boldsymbol{u} + \boldsymbol{u}^T R\boldsymbol{u})dt \\ \text{s.t.} \quad & \dot{\boldsymbol{x}} = f(t, \boldsymbol{x}) + g(t, \boldsymbol{x})\boldsymbol{u} \\ & \boldsymbol{x}(t_0) = \boldsymbol{x}_0 \end{aligned}$$

Using the principle of optimality yields one form of the so-called Hamilton-Jacobi-Bellman equation

$$-V_t^* = \min_{\boldsymbol{u}} \left\{ [l(t, \boldsymbol{x}) + 2\boldsymbol{x}N\boldsymbol{u} + \boldsymbol{u}^T R\boldsymbol{u}] + V_x^{*T}[f(t, \boldsymbol{x}(t)) + g(t, \boldsymbol{x}(t))\boldsymbol{u}(t)] \right\} \quad (4.14)$$

The boundary condition for this equation is given by $V^*(t, \mathbf{0}) = 0$, $\forall t > 0$ where $V^*(t, \boldsymbol{x})$ must be positive for all $(t, \boldsymbol{x})$ (since it corresponds to the optimal cost which must be positive). The indicated minimization is performed, leading to a control law of the form

$$\boldsymbol{u}^* = -R^{-1} \left(\frac{1}{2} g^T V_x^* + N^T \boldsymbol{x} \right) \quad (4.15)$$

Substitute Eq. (4.15) back into Eq. (4.14), and solve the resulting HJB equation

$$-V_t^* = V_x^{*T} f - V_x^{*T} g R^{-1} N^T \boldsymbol{x} - \frac{1}{4} V_x^{*T} g R^{-1} g^T V_x^* + l - \boldsymbol{x}^T N R^{-1} N^T \boldsymbol{x} \quad (4.16)$$

for $V^*(t, \boldsymbol{x})$.

Now, assume that V is a CLF for the system (4.1). For the sake of motivation, assume that V possesses the same shape level curves as those of the value function V^*. Even though in general V would not be the same as V^*, this does imply a relationship between their gradients. We may assert that there exists a scalar function $\lambda(t, \boldsymbol{x})$ such that $V_t^* = \lambda(t, \boldsymbol{x}) V_t$ and $V_x^* = \lambda(t, \boldsymbol{x}) V_x$ for every $(t, \boldsymbol{x})$ (i.e. the gradients point in the same direction at every point). In this case, the optimal control can be written in terms of the CLF V,

$$\boldsymbol{u}^* = -R^{-1} \left(\frac{1}{2} g^T V_x^* + N^T \boldsymbol{x} \right) = -R^{-1} \left(\frac{\lambda(t, \boldsymbol{x})}{2} g^T V_x + N^T \boldsymbol{x} \right) \quad (4.17)$$

Additionally, the HJB equation can be used to determine $\lambda(t, \boldsymbol{x})$ by substituting $V_t^* = \lambda(t, \boldsymbol{x}) V_t$ and $V_x^* = \lambda(t, \boldsymbol{x}) V_x$ into the HJB equation Eq.(4.14)

$$-\lambda V_t = \lambda V_x^T f - \lambda V_x^T g R^{-1} N^T \boldsymbol{x} - \frac{\lambda^2}{4} V_x^T g R^{-1} g^T V_x + l(\boldsymbol{x}) - \boldsymbol{x}^T N R^{-1} N^T \boldsymbol{x} \quad (4.18)$$

This is a quadratic equation in λ. Solving for λ and taking only the positive square root gives

$$\lambda = \begin{cases} 2\left(\dfrac{\omega_N + \sqrt{\omega_N^2 + l_N(\boldsymbol{x})\boldsymbol{p}^T R^{-1}\boldsymbol{p}}}{\boldsymbol{p}^T R^{-1}\boldsymbol{p}}\right), & \text{if } \boldsymbol{p} \neq \boldsymbol{0} \\ \dfrac{l_N(\boldsymbol{x})}{-\omega_N}, & \text{if } \boldsymbol{p} = \boldsymbol{0} \end{cases} \tag{4.19}$$

Substituting this value into the control $\boldsymbol{u}^*$ given in Eq. (4.17) yields $\boldsymbol{u}_{\text{Sontag}}$ Eq. (4.12). In this case, Sontag's formula will result in the optimal controller.

4.3.2 Pointwise min-norm controllers

Given a CLF, $V > 0$, by definition there will exist a control action u such that $\dot{V} = V_t + V_x^T(f + g\boldsymbol{u}) < 0$ for every $(t, \boldsymbol{x})$. In general there are many such $\boldsymbol{u}$ that will satisfy $V_t + V_x^T(f + g\boldsymbol{u}) < 0$. One method of determining a specific $\boldsymbol{u}$ is to pose the following optimization problem (Freeman and Kokotovic, 1996):

Pointwise Min-Norm

$$\text{minimize} \quad l(t, \boldsymbol{x}) + \boldsymbol{u}^T R^{-1}\boldsymbol{u} + 2\boldsymbol{x}^T N\boldsymbol{u} \tag{4.20}$$

$$\text{subject to} \quad V_t + V_x^T(f + g\boldsymbol{u}) \leq -\alpha(t, \boldsymbol{x}) \tag{4.21}$$

where $\alpha(t, \boldsymbol{x})$ is some continuous, positive-definite function satisfying $V_t + V_x^T f \leq -\alpha(t, \boldsymbol{x})$ whenever $g^T V_x = 0$, and the optimization is solved pointwise (i.e. for each $(t, \boldsymbol{x})$). This formula pointwise minimizes the control energy used, while requiring that V be a Lyapunov function for the closed-loop system and decrease by at least $\alpha(t, \boldsymbol{x})$ at every point. The resulting controller can be solved for off-line and in closed form.

In (Freeman and Kokotovic, 1996), it was shown that every CLF V is the value function for some meaningful cost function. In other words, it solves the HJB equation associated with a meaningful cost. This property is commonly referred to as being "inverse-optimal". Note that a CLF V does not uniquely determine a control law because it may be the value function for many different cost functions, the formulation of each which may always produce one of these inverse-optimal control laws.

To intuitively understand why pointwise min-norm controllers possess such strong connections to HJB equations, let us reconsider the optimization in Eq. (4.20), but this time use a Lagrange multiplier to deal with the constraint inequality (4.21). Hence, we can write the Lagrangian for the problem as

$$L(\boldsymbol{u}, \lambda) = l + \boldsymbol{u}^T R\boldsymbol{u} + 2\boldsymbol{x}^T N\boldsymbol{u} + \lambda[V_t + V_x^T(f + g\boldsymbol{u}) + \alpha]$$

where λ is the Lagrange multiplier (required to be positive, etc., in accordance with the Kuhn-Tucker conditions (Kuhn and Tucker, 1961)). Lagrangian duality tells us

that optimizing $\boldsymbol{u}$ should minimize the Lagrangian. Furthermore, we can exploit the fact that adding or subtracting terms to the Lagrangian that do not contain $\boldsymbol{u}$ will not affect the solution. So, we will subtract the term $\lambda\alpha$ to obtain

$$-\lambda V_t = \min_{\boldsymbol{u}} \left\{ l + \boldsymbol{u}^T R \boldsymbol{u} + 2\boldsymbol{x}^T N \boldsymbol{u} + \lambda V_x^T (f + g\boldsymbol{u}) \right\}$$

which is identical to the HJB equation (4.14) except with V_t^* and V_x^* replaced by λV_t and λV_x respectively. Furthermore, by performing the minimization, we find that the resulting state feedback is of the form

$$\boldsymbol{u}_\alpha = -R^{-1} \left(\frac{\lambda}{2} g^T V_x + N^T \boldsymbol{x} \right)$$

This is identical to the relationship used to derive Sontag's formula. Hence, we see that pointwise min-norm formulas resemble Sontag's formula in that they substitute λV_x for the true gradient of the value function V_x^*. The only difference is that pointwise min-norm controllers can use a different criterion to select the scaling λ. This degree of freedom is basically contained in the choice of α. Therefore, we can view pointwise min-norm formulas as a generalization of Sontag's formula.

We now explicitly derive the parameter $\alpha(t, \boldsymbol{x})$ that generates Sontag's formula in the pointwise min-norm formulation. Let us assume that the solution to the above pointwise min-norm problem results in Sontag's formula. It should be clear that for $\boldsymbol{p} \neq \boldsymbol{0}$, the constraint will be active, since $\boldsymbol{u}$ will be reduced as much as possible. Knowing that $\boldsymbol{u}$ will turn out to be Sontag's formula results in the following value for α:

$$\begin{aligned} -\alpha &= V_t + V_x^T (f + g\boldsymbol{u}_\alpha) \\ &= V_t + V_x^T f + V_x^T g[-R^{-1}(\frac{\lambda}{2} g^T V_x + N^T \boldsymbol{x})] \\ &= \omega_N - \frac{\lambda}{2} \boldsymbol{p}^T R^{-1} \boldsymbol{p} \end{aligned}$$

Freeman and Kokotovic's pointwise min-norm formula (Freeman and Kokotovic, 1996) can be written to provide input-to-output stability as follows:

$$\boldsymbol{u}_{FK} = \begin{cases} -R^{-1} \left[\dfrac{\omega_N + \alpha}{\boldsymbol{p} R^{-1} \boldsymbol{p}} \boldsymbol{p} + N^T \boldsymbol{x} \right], & \text{if } \boldsymbol{p} \neq \boldsymbol{0} \\ -R^{-1} N^T \boldsymbol{x}, & \text{otherwise} \end{cases} \tag{4.22}$$

which can be seen as a generalization of Sontag's formula. Indeed, the pointwise min-norm control subsumes Sontag's formula by introducing the positive-definite scalar function α, which parameterizes all ISS controls within the range space of $g^T V_x$. By

choosing $\alpha = \sqrt{\omega_N^2 + l_N \cdot \boldsymbol{p}^T R^{-1} \boldsymbol{p}}$, Sontag's formula is recovered. The region parameterized by the min-norm formula is shown as a solid line in Fig. (4.1). The min-norm is clearly ISS and is thus guaranteed (by Theorem 17 in (Curtis and Beard, 2002*a*)) to be an ISS-satisficing control. The min-norm control values lie in S at every state as shown in Fig. 4.1.

When $b > \underline{b}$, the line where min-norm control values lie crosses the satisficing set boundary circle. By equating $\boldsymbol{u}_{FK}$ Eq. (4.22) and the explicit control form in S_b Eq. (4.9), α at the crossing points can be obtained:

$$\alpha_{\max,\ \min}(b) = \boldsymbol{p}^T R^{-1} \boldsymbol{p} \left[\frac{1}{2} b \pm \frac{\boldsymbol{p}^T R^{1/2} \boldsymbol{p}}{||\boldsymbol{p}||^3} \sqrt{\frac{b^2}{4} \boldsymbol{p}^T R^{-1} \boldsymbol{p} - b\omega_N - l_N} \right] - \omega_N \qquad (4.23)$$

where $\alpha_{\max}$ ($\alpha_{\min}$) takes the sign plus (minus). Apparently, $\boldsymbol{u}_{FK} \in S_b$ for $\alpha_{\min} < \alpha < \alpha_{\max}$. When $b = \underline{b}$, $\alpha_{\max,\ \min}$ are reduced to $\alpha = \sqrt{\omega_N^2 + l_N \cdot \boldsymbol{p}^T R^{-1} \boldsymbol{p}}$ which is the choice for Sontag's formula.

As explained above, control Lyapunov functions are best interpreted in the context of Hamilton-Jacobi-Bellman equations, especially a variation of Sontag's formula that naturally arises from HJB equations and furthermore is a special case of a more general class of CLF-based controllers known as pointwise min-norm controllers.

Additionally, Eq. (4.9) can be thought of as a generalization of the input-to-state form of both Sontag's formula and Freeman and Kokotovic's min-norm formula. The satisficing approach subsumes both Sontag's formula and the min-norm formula by completely parameterizing the entire region of the control space that renders $V_t + V_x^T(f + g\boldsymbol{u})$ negative for an arbitrary non-zero state. The region of control space parameterized by the satisficing approach is the shaded region shown in Fig. 4.1. Note that it differs pointwise from Freeman and Kokotovic's min-norm solutions in that satisficing permits a component of the control to be orthogonal to $g^T V_x$ thus offering maximal freedom for the control designer to choose a high performance controller that is guaranteed to be ISS with respect to V.

4.4 Illustrative Example

Consider the problem of rendezvous to try the satisficing method. A Keplerian orbit of the target of the semimajor axis $A_0 = R_e + h_c$ km is considered, in which $h_c = 5,000$ km, the radius of the Earth R_e, and the gravitational constant of the Earth μ are given. The chaser flies around at 3,413.4 km in an eccentricity axis (eccentricity is 0.3). We

consider the in-plane relative dynamic equation

$$\begin{aligned} \bar{\boldsymbol{x}}'(\tau) &= f(\bar{\boldsymbol{x}}) + g\bar{\boldsymbol{u}}(\tau) \\ f(\bar{\boldsymbol{x}}) &= A\bar{\boldsymbol{x}} + f_2(\bar{\boldsymbol{x}}) \\ g &= B \end{aligned} \tag{4.24}$$

and

$$\begin{aligned} A &= \begin{bmatrix} 0 & 0 & 1 & 0 \\ 0 & 0 & 0 & 1 \\ 3 & 0 & 0 & 2 \\ 0 & 0 & -2 & 0 \end{bmatrix}, \; B = \begin{bmatrix} 0 & 0 \\ 0 & 0 \\ 1 & 0 \\ 0 & 1 \end{bmatrix} \\ f_2(\bar{\boldsymbol{x}}) &= B \begin{bmatrix} -3\bar{x} - \left(\frac{1}{\sigma} + \bar{x}\right)\left(\frac{1}{\sigma^3 \bar{R}^3} - 1\right) \\ -\bar{y}\left(\frac{1}{\sigma^3 \bar{R}^3} - 1\right) \end{bmatrix} \end{aligned}$$

where $\bar{R} = [(1/\sigma + \bar{x})^2 + \bar{y}^2]^{1/2}$. $f(\bar{\boldsymbol{x}})$ and $g(\bar{\boldsymbol{x}})$ are locally Lipschitz functions and $f(\mathbf{0}) = \mathbf{0}$. The derivation of the equation and the mean of physical parameters are explained in Chapter 6.

In the system, (A, B) is controllable. Let Q be a symmetric, positive semi-definite matrix such that $(A, \sqrt{Q})$ is observable, let R be a symmetric positive-definite matrix, and let P be the symmetric positive-definite solution to the Riccati equation

$$A^T S + SA + Q - SBR^{-1}B^T S = 0$$

(A, B) controllable implies that $V(\boldsymbol{x}) = \boldsymbol{x}^T S \boldsymbol{x}$ is a CLF for system Eq. (4.24) since

$$\inf_{\boldsymbol{u}} \dot{V} = \inf_{\boldsymbol{u}} \{-\boldsymbol{x}^T Q \boldsymbol{x} + \boldsymbol{x}^T SB(B^T S\boldsymbol{x} + 2\boldsymbol{u})\} < 0$$

for all $\boldsymbol{x} \neq \mathbf{0}$. In this example, we set $Q = I_{4\times 4}$ and $R = I_{2\times 2}$ (Note that $N = O_{4\times 2}$ and $V_t = 0$).

Figure 4.2 shows the rendezvous trajectories of the closed-loop system using four different controllers. The portrait in Fig. 4.2a corresponds to the LQR controller, while that in Fig. 4.2b corresponds to Sontag's formula. It may be desirable in some applications to have high-gain, which can be achieved by judicious choices of $b(\boldsymbol{x})$ and $\boldsymbol{\nu}$. The portrait in Fig. 4.2c shows the response to satisficing control with

$$\begin{aligned} b(\boldsymbol{x}) &= \frac{3}{2}\underline{b}(\boldsymbol{x}) \\ \boldsymbol{\nu} &= \mathbf{0} \end{aligned}$$

It is interesting to note, that since $b(\boldsymbol{x})$ increases the gain in the direction of $R^{-1}g^T V_x$, the direction of the Eigen spaces are retained in the nonlinear region. The direction of the Eigen spaces can be shaped by the function $\boldsymbol{\nu}$. In the plot in Fig. 4.2d, $b(\boldsymbol{x})$ is chosen similarly to the plot in Fig. 4.2c, but $\boldsymbol{\nu}$ is chosen to maximize the rate of decrease along the function $W(\boldsymbol{x}) = \boldsymbol{x}^T\boldsymbol{x}$, i.e.

$$\begin{aligned} \min_{\boldsymbol{\nu}} \dot{W} &= \min_{\boldsymbol{\nu}} 2\boldsymbol{x}^T\dot{\boldsymbol{x}} = \min_{\boldsymbol{\nu}}[2\boldsymbol{x}^T f + 2\boldsymbol{x}^T g(-\sigma_1 + \sigma_2\boldsymbol{\nu})] \\ &\Longrightarrow \quad \boldsymbol{\nu} = -\frac{\sigma_2 g^T\boldsymbol{x}}{||\sigma_2 g^T\boldsymbol{x}||} \end{aligned}$$

4.5 Conclusions

The main result of this chapter is the development of input-to-state satisficing as a tool to construct nonlinear controllers. The satisficing set is defined point-wise, and includes all control values whose benefits exceed cost. By defining benefits and costs in terms of control Lyapunov functions, both local and global properties of the system are addressed. One way of looking at satisficing is that it bridges the gap between local and global concerns; it is built upon comparison of instantaneous cost with instantaneous benefit, but by defining the benefit of a control action in terms of a CLF this local decision inherits global consequences. This satisficing set of control values is completely parameterized by two selection functions b and ν. If these selection functions are continuous and satisfy the constraints $b > \underline{b}$ and $||\nu|| \leq 1$, then the resulting control strategy globally input-to-state stabilizes the system. Satisficing was shown to completely parameterize the class of continuous controls which render the closed-loop system input-to-state stable with respect to a known CLF V. This result was illustrated graphically in Fig. 4.1. It was noted that many CLF-based 'universal formulas' ignore control values that are pointwise orthogonal to the vector $-g^T V_x$, and the relationship between the satisficing approach and Sontag's formula and Freeman and Kokotovic's min-norm formula was illustrated.

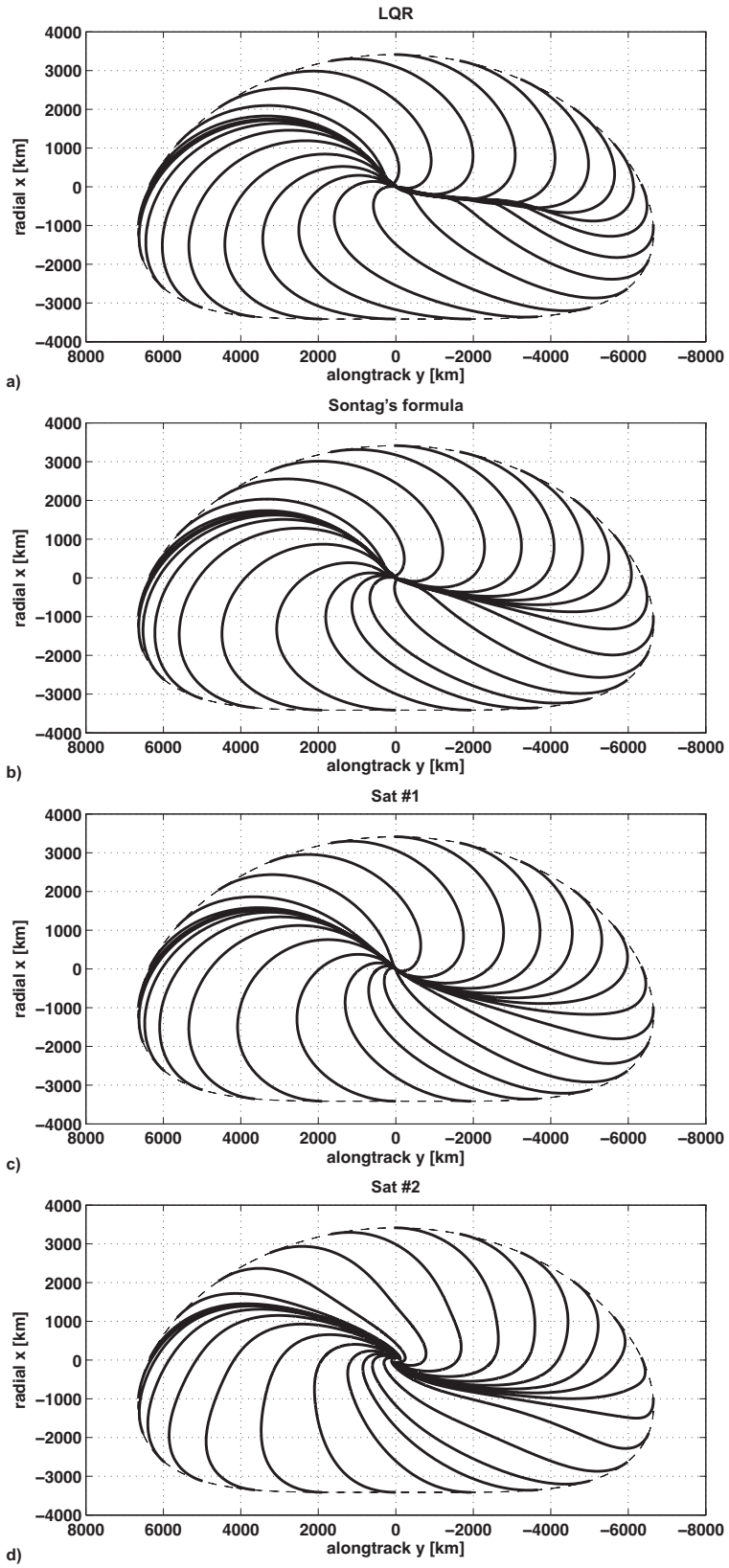

Figure 4.2: Rendezvous trajectories under the control of a) LQR, b) Sontag's formula, c) satisficing #1, and d) satisficing #2.

Chapter 5

Novel Nonlinear Rendezvous Guidance Scheme under Constraints on Thrust Direction

5.1 Introduction

In this chapter, a rendezvous problem under control constraints that may be imposed in actual missions is considered. In particular, this chapter treats the condition that the chaser's thrust direction relative to the target's direction is constrained. The basic objective is to drive the chaser vehicle to rendezvous with the target under a small thrust angle condition and to minimize fuel consumption using a stable feedback controller without solving a numerical optimization problem.

This chapter proposes a new approach that considers constraints on thrust angle based on optimal feedback control to introduce a general linear quadratic regulator (LQR), in which the performance index in state and control is designed to align the thrust direction to the relative position vector. A modal analysis method is used to determine the design parameters to make the final thrust angle small. The initial thrust angle can be estimated easily from the optimal control and rendezvous start phase. The transient rendezvous phase, however, may not guarantee the constraints on the thrust direction. For the transient phase, this chapter proposes a novel method to guarantee closed-loop stability under constraints on the thrust angle. Based on a "satisficing" theory proposed by Curtis and Beard (Curtis and Beard, 2002*b*, 2004) that can deliver a parametric set of stable control inputs, the optimal control designed by modal analysis and contour plots is projected onto a stable domain defined by a candidate control Lyapunov function (CLF). The control applying the satisficing method to the rendezvous problem with control direction constraints is first considered in Ref. (Mi-

tani and Yamakawa, 2010). In addition, this chapter shows that choosing the candidate CLF generated by solving the Riccati equation for the general performance index easily makes the thrust angle at the final phase small and analytically predicted. In addition, the design process to select parameters to maintain a small-magnitude thrust angle is clarified. The proposed method assumes active rendezvous, involving communication between target and chaser so that chaser's relative states to the target is well estimated.

5.2 Rendezvous with Practical Constraints

5.2.1 Equations of Relative Motion

Consider a satellite subject to the gravitational force of the Earth and control input (Fig. 5.1). Then, the equation of motion is given by Newton's equation

$$\ddot{\boldsymbol{R}} = -\frac{\mu}{R^3}\boldsymbol{R} + \boldsymbol{u} \tag{5.1}$$

where $\boldsymbol{R}$ is the position vector of the satellite from the center of the Earth, μ is the gravitational parameter of the Earth, $R = |\boldsymbol{R}|$, and $\boldsymbol{u}$ is the control acceleration. Let the orbit of the target be eccentric, which is given by

$$R_0 = \frac{p}{1 + e\cos\theta} \tag{5.2}$$

where $R_0 = |\boldsymbol{R}_0|$, $\boldsymbol{R}_0$ is the position vector of the target, $p = A_0(1-e^2)$ is the semilatus rectum, A_0 is the semimajor axis, e is the eccentricity of the orbit, and θ is the true anomaly. The period of the orbit is $T = 2\pi(A_0^3/\mu)^{1/2}$, and the orbital mean motion, which is the average of the orbit rate $\dot{\theta}$, is $n = (\mu/A_0^3)^{1/2}$. It is known that (Wie, 1998)

$$\ddot{R}_0 - R_0\dot{\theta}^2 = -\frac{\mu}{R_0^2} \tag{5.3}$$

$$R_0\ddot{\theta} + 2\dot{R}_0\dot{\theta} = 0 \tag{5.4}$$

$$\dot{\theta} = \left(\frac{\mu}{p^3}\right)^{1/2}(1 + e\cos\theta)^2 \tag{5.5}$$

Introduce a rotating right-hand reference frame $o - \{\boldsymbol{i}, \boldsymbol{j}, \boldsymbol{k}\}$, where o is the center of mass of the target, $\boldsymbol{i}$ is in the radial direction, $\boldsymbol{j}$ is in the flight direction, and $\boldsymbol{k}$ is outwards of the orbit plane. Let $\boldsymbol{r}$ be the position vector of the chaser relative to the target, and set $\boldsymbol{r} = x\boldsymbol{i} + y\boldsymbol{j} + z\boldsymbol{k}$. Then the position vector of the chaser is $\boldsymbol{R} = \boldsymbol{R}_0 + \boldsymbol{r}$, and the linearized Eqs. (5.3-5.5) at the origin are given by

$$\ddot{x} - 2\dot{\theta}\dot{y} - \ddot{\theta}y - (\dot{\theta}^2 + 2\frac{\mu}{R_0^3})x = u_x \tag{5.6}$$

$$\ddot{y} - 2\dot{\theta}\dot{x} - \ddot{\theta}x - (\dot{\theta}^2 - \frac{\mu}{R_0^3})y = u_y \tag{5.7}$$

$$\ddot{z} + \frac{\mu}{R_0^3}z = u_z \tag{5.8}$$

which are referred to as Tschauner-Hempel (TH) equations (Yamanaka and Ankersen, 2002).

Introduce $(\bar{x},\ \bar{y},\ \bar{z}) = 1/R_0(x,\ y,\ z)$ and replace independent variable t by θ, then Eqs. (5.6) and (5.7) are transformed respectively into

$$(1 + e\cos\theta)(\bar{x}'' - 2\bar{y}') - 3\bar{x} = \bar{u}_x \tag{5.9}$$

$$(1 + e\cos\theta)(\bar{y}'' + 2\bar{x}') = \bar{u}_y \tag{5.10}$$

where the differentiation with respect to θ is denoted by $'$, and $(\bar{u}_x(\theta), \bar{u}_y(\theta)) = (R_0^2/\mu)(u_x, u_y)$ (Ichikawa and Bando, 2009). The state-space form of Eqs. (5.9) and (5.10) is

$$\bar{\boldsymbol{x}}' = \bar{A}(\theta)\bar{\boldsymbol{x}} + \frac{1}{\rho}B\bar{\boldsymbol{u}},\ \bar{\boldsymbol{x}}(\theta_0) = \bar{\boldsymbol{x}} \tag{5.11}$$

where $\bar{\boldsymbol{x}} = [\bar{x}\ \bar{y}\ \bar{x}'\ \bar{y}']^T$, $\bar{\boldsymbol{u}} = [\bar{u}_x\ \bar{u}_y]^T$, $\theta_0 = \bar{\theta}(\tau_0)$, $\rho = 1 + e\cos\theta$, and

$$\bar{A}(\theta) = \begin{bmatrix} 0 & 0 & 1 & 0 \\ 0 & 0 & 0 & 1 \\ 3/\rho & 0 & 0 & 2 \\ 0 & 0 & -2 & 0 \end{bmatrix},\ B = \begin{bmatrix} 0 & 0 \\ 0 & 0 \\ 1 & 0 \\ 0 & 1 \end{bmatrix} \tag{5.12}$$

If the target's orbit is circular (i.e. $e = 0$), then $\theta = nt,\ R_0 = A_0,\ \rho = 1$. Equations (5.9) and (5.10) yield non-dimensional Hill-Clohessy-Wiltshire (HCW) equations (Clohessy and Wiltshire, 1960)

$$\bar{x}'' - 2\bar{y}' - 3\bar{x} = \bar{u}_x \tag{5.13}$$

$$\bar{y}'' + 2\bar{x}' = \bar{u}_y \tag{5.14}$$

and the state-space form is given by

$$\bar{\boldsymbol{x}}' = A\bar{\boldsymbol{x}} + B\bar{\boldsymbol{u}} \tag{5.15}$$

where

$$A = \begin{bmatrix} 0 & 0 & 1 & 0 \\ 0 & 0 & 0 & 1 \\ 3 & 0 & 0 & 2 \\ 0 & 0 & -2 & 0 \end{bmatrix} \tag{5.16}$$

After this section, the bars over $\boldsymbol{x}$ and $\boldsymbol{u}$ are dropped and the subscript $\boldsymbol{a}'$ is replaced by $\dot{\boldsymbol{a}}$. For convenience, Table 5.1 shows the conversion from nondimensional quantities to dimensional ones. Notice that nondimensional time corresponds to true anomaly θ. θ must be converted to mean anomaly M to get dimensional time t. In the same table, h and t_p represent angular momentum of the target and time of perigee respectively.

Table 5.1: The conversion from nondimensional quantities to dimensional ones.

Physical quantity	Nondimensional quantity	Dimensional quantity	
		$0 \leq e < 1$	$e = 0$ (circular case)
Time	θ	$(1/n) \cdot M(\theta) + t_p$	$(1/n) \cdot \theta + t_p$
Position	$\bar{\boldsymbol{x}}$	$R_0 \cdot \bar{\boldsymbol{x}}$	$A_0 \cdot \bar{\boldsymbol{x}}$
Velocity	$\bar{\boldsymbol{x}}'$	$(h/p)(\rho\bar{\boldsymbol{x}}' - \rho'\bar{\boldsymbol{x}})$	$nA_0 \cdot \bar{\boldsymbol{x}}'$
Control acceleration	$\bar{\boldsymbol{u}}$	$(\mu/R_0^2) \cdot \bar{\boldsymbol{u}}$	$n^2 A_0 \cdot \bar{\boldsymbol{u}}$

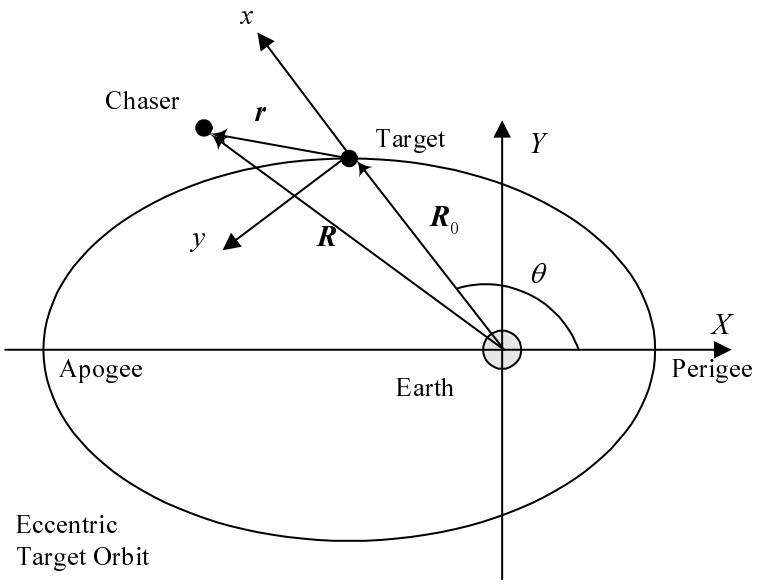

Figure 5.1: Relative motion between chaser and target.

5.2.2 Description of Free Trajectory

The section states analytical solution of free motion trajectory. Periodic (i.e. non-drifting) orbit is often chosen as a station-keeping orbit because of the collision avoidance safety. In Section 5.6, some examples of rendezvous problem which start from a periodic orbit are examined. Including $e \neq 0$, free trajectory without control can be described using Yamanaka-Ankersen's state transition matrix (Yamanaka and Ankersen, 2002)

$$\begin{aligned} \boldsymbol{x}(\theta) &= \begin{bmatrix} s & c & 2-3esJ_\rho & 0 \\ (1+1/\rho)c & -(1+1/\rho)s & -3\rho^2 J_\rho & 1 \\ \dot{s} & \dot{c} & -3e(\dot{s}J_\rho + s/\rho^2) & 0 \\ -2s & -2c+e & -3(1-2esJ_\rho) & 0 \end{bmatrix} \boldsymbol{K} \\ &\triangleq \phi(\theta)\boldsymbol{K} \end{aligned} \tag{5.17}$$

where $\boldsymbol{K} = [K_1\ K_2\ K_3\ K_4]^T$ is constant, $s = \rho\sin\theta$, $c = \rho\cos\theta$, and $J_\rho(\theta) = \int_{\theta_0}^{\theta}(\mathrm{d}\theta/\rho^2)$. If $\boldsymbol{x}(\theta_0)$ is specified, $\boldsymbol{K}$ is given by $\boldsymbol{K} = \phi^{-1}(\theta_0)\boldsymbol{x}(\theta_0)$, where

$$\phi^{-1}(\theta_0) = \frac{1}{1-e^2}\begin{bmatrix} -3(s/\rho)(1+e^2/\rho) & 0 & c-2e & -s(1+1/\rho) \\ -3(c/\rho+e) & 0 & -s & -c(1+1/\rho)-e \\ 3\rho+e^2-1 & 0 & es & \rho^2 \\ -3e(s/\rho)(1+1/\rho) & 1-e^2 & ec-2 & -es(1+1/\rho) \end{bmatrix}_{\theta=\theta_0} \tag{5.18}$$

The solution $\boldsymbol{x}(\theta)$ is periodic if and only if $K_3 = 0$. The parameter K_4 gives a translation of y, and hence we set $K_4 = 0$ for simplicity. Therefore, when (x_0, y_0), θ_0 and e are given, the conditions $K_3 = K_4 = 0$ specifies $(\dot{x}_0, \dot{y}_0)$ uniquely. In the special case where the target's orbit is circular, a periodic trajectory that starts from $(x_0, y_0) = r_0(\cos\varphi_0/2, -\sin\varphi_0)$ is reduced to

$$\boldsymbol{x}(\theta) = [r_0\cos(\theta-\theta_0+\varphi_0)/2,\ -r_0\sin(\theta-\theta_0+\varphi_0),\ y(\theta)/2,\ -2x(\theta)]^T \tag{5.19}$$

where φ_0 $(0 < \varphi_0 < 2\pi)$ is the initial phase angle. In numerical simulations, r_0 is set to be 1 for simplicity.

5.2.3 Control Direction Constraints

Consider the problem that a chaser at time t_0 and in the initial state x_0 is guided towards the target. The terminal time is free. The thrust direction, which represents the angle between the direction vector toward the target $-\boldsymbol{r}$ and the control direction vector $\boldsymbol{u}$, is constrained within the angle $\pm\alpha$ $(0 \leq \alpha \leq \pi)$ from the view of the chaser in the direction away from the target. Notice that the direction of control input $\boldsymbol{u}$ is

opposite to the direction of injection $-\boldsymbol{u}$. This condition can occur when the direction of injection is restricted because of the thrust plume or when the direction of control with the thrusters fixed on the chaser is restricted because the target must be visible in the FOV of the chaser's camera while the chaser moves safely toward the target. Figure 5.2 illustrates this condition. The definition of the thrust angle and control input constraints are given by

$$|\delta| \leq \alpha \tag{5.20}$$

$$|\delta| \triangleq \arccos(-\boldsymbol{u}^T \cdot \boldsymbol{r} / |\boldsymbol{u}| \cdot |\boldsymbol{r}|) \tag{5.21}$$

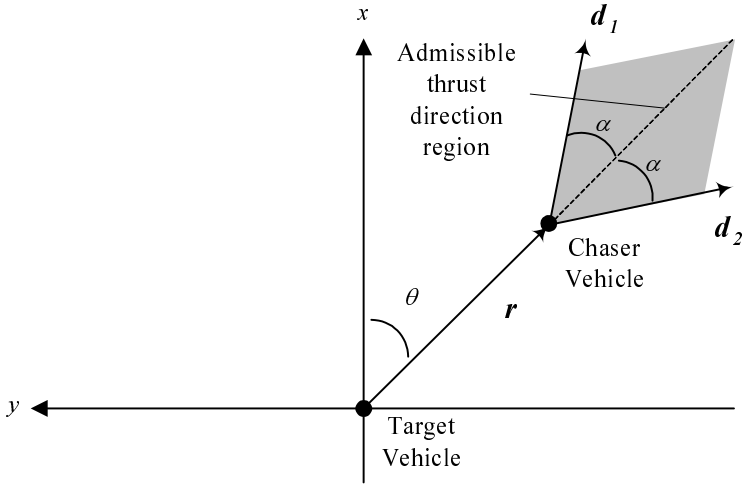

Figure 5.2: Constraints on the thrust direction.

5.3 Optimal Control Including Control Direction Constraints

In this section, we formulate a suboptimal guidance control toward the target under constraints on thrust direction to show the design problem of the LQR weight parameter and initial state of the chaser vehicle. We use modal analysis to show that the thrust angle can be maintained within some constant angle if the initial state meets a certain condition. For a given initial state, parameter design methods are shown to meet the constraints on thrust direction at the initial rendezvous point and final approach phase. First, consider the case where the target's orbit is circular. Section 5.5 explains the extension and limitation of the case where the target's orbit is eccentric.

5.3.1 Optimal Feedback Control Law

First, formulate suboptimal control problems with the constraints on thrust direction by including the effect of the control constraints in a performance index. Then consider the more general performance index of the well-known LQR problem (Bryson and Ho, 1975)

$$J = \int_0^\infty (\boldsymbol{x}^T Q \boldsymbol{x} + \boldsymbol{u}^T R \boldsymbol{u} + 2\boldsymbol{x}^T N \boldsymbol{u}) dt \tag{5.22}$$

where Q, R, and N are weight matrices and the following parameter settings are considered

$$Q = \mathrm{diag}(q_r,\ q_r,\ q_v,\ q_v) \tag{5.23}$$

$$R = I_{2\times 2} \tag{5.24}$$

$$N = \lambda_\alpha \begin{bmatrix} I_{2\times 2} \\ O_{2\times 2} \end{bmatrix} \tag{5.25}$$

$I_{n\times n}$ is $n \times n$ identity matrix, $O_{n\times n}$ is $n \times n$ zero matrix. $q_r,\ q_v,\ \lambda_\alpha \geq 0$ are independent design parameters in the performance index Eq. (5.22). If $\lambda_\alpha = 0$ is set, the integrand in Eq. (5.22) becomes a narrow definition of quadratic form. To transform the integrand, the following expression is used

$$\begin{aligned} & \boldsymbol{x}^T Q \boldsymbol{x} + \boldsymbol{u}^T R \boldsymbol{u} + 2\boldsymbol{x}^T N \boldsymbol{u} \\ = \ & \boldsymbol{x}^T \begin{bmatrix} q_r - \lambda_\alpha^2 & 0 & 0 & 0 \\ 0 & q_r - \lambda_\alpha^2 & 0 & 0 \\ 0 & 0 & q_v & 0 \\ 0 & 0 & 0 & q_v \end{bmatrix} \boldsymbol{x} + (\boldsymbol{u} + C_{\lambda_\alpha}\boldsymbol{x})^T (\boldsymbol{u} + C_{\lambda_\alpha}\boldsymbol{x}) \end{aligned} \tag{5.26}$$

where

$$C_{\lambda_\alpha} \triangleq \lambda_\alpha \cdot C = \begin{bmatrix} \lambda_\alpha & 0 & 0 & 0 \\ 0 & \lambda_\alpha & 0 & 0 \end{bmatrix} \tag{5.27}$$

The term $(\boldsymbol{u}+C_{\lambda_\alpha}\boldsymbol{x})^T(\boldsymbol{u}+C_{\lambda_\alpha}\boldsymbol{x})$ represents the effect of maintaining the angle between $-\boldsymbol{r}$ and $\boldsymbol{u}$ in the expression of quadratic form. In other words, this means that the physical significance of turning the thrust direction to a direction toward the target is included in the penalty function. Optimal feedback control that minimizes Eq. (5.22) is easily obtained by

$$\boldsymbol{u}^* = -K\boldsymbol{x} \tag{5.28}$$

$$K = R^{-1}(B^T S + N^T) \tag{5.29}$$

where K is the state-feedback gain and S is the unique nonnegative solution of the algebraic Riccati equation (ARE)

$$A^T S + SA - (SB + N)R^{-1}(B^T S + N^T) + Q = 0 \tag{5.30}$$

and the closed-loop $A_c = A - BK$ is stabilized if and only if

- The pair $(A,\ B)$ is stabilizable.
- $R > 0$ and $Q - NR^{-1}N^T > 0$.
- $(Q - NR^{-1}N^T,\ A - BR^{-1}N^T)$ has no unobservable mode on the imaginary axis.

If these conditions are satisfied, A_c is stabilized and state-feedback control $\boldsymbol{u} = -K\boldsymbol{x}$ minimizes the quadratic performance function of Eq. (5.22). Because $(A,\ B)$ and $(\bar{A}(\theta),\ B)$ are controllable in the HCW equations Eq. (5.15) and TH equations Eq. (5.11) respectively (Shibata and Ichikawa, 2007; Bando and Ichikawa, 2009; Ichimura and Ichikawa, 2008), in addition to the condition $q_r,\ q_v,\ \lambda_\alpha \geq 0$, the design parameters must satisfy the condition

$$q_r - \lambda_\alpha^2 \ \geq \ 0 \tag{5.31}$$

5.3.2 Modal Analysis

When using optimal control Eq. (5.28), consider by modal analysis how the thrust angle changes to set design parameter $q_r,\ q_v,\ \lambda_\alpha$. When reassigning the poles of A_c with optimal state-feedback control, eigenmodes divide into two groups: slowly damped modes and highly damped modes. Because highly damped modes become zero when they approach the target, slowly damped modes mainly determine the thrust angle at the final approach phase. Such a final thrust angle $|\delta|_\infty$ can be obtained as follows:

If the eigenvalue of the most slowly damped mode has only a real part, let it and the eigenvector be $\lambda_s,\ \boldsymbol{v}_s$ respectively. The final $\boldsymbol{x}$ is

$$\boldsymbol{x} = C_s e^{\lambda_s t}\boldsymbol{v}_s \tag{5.32}$$

where C_s is the integral constant, which depends on the initial state. Therefore, the trajectories become tangent to the slow eigenvector $\boldsymbol{v}_s$ as they approach the origin (Khalil, 2002). By substituting Eq. (5.32) into Eq. (5.28), the control input is then

$$\boldsymbol{u} = -KC_s e^{\lambda_s t}\boldsymbol{v}_s \tag{5.33}$$

By substituting Eqs. (5.32) and (5.33) into Eq. (5.21), $|\delta|$ approaches the constant thrust angle $|\delta|_\infty$ as the vehicle converges on the target

$$|\delta|_\infty = \arccos\left[\frac{\boldsymbol{v}_s^T C^T K \boldsymbol{v}_s}{|C\boldsymbol{v}_s| \cdot |K\boldsymbol{v}_s|}\right] \tag{5.34}$$

Meanwhile, if the eigenvalue of the most slowly damped mode has an imaginary part, let the eigenvalue and eigenvector be $\alpha + j\omega,\ \boldsymbol{w}_1 + j\boldsymbol{w}_2,\ \alpha,\ \omega \in \boldsymbol{R}^1,\ \boldsymbol{w}_1,\ \boldsymbol{w}_2 \in \boldsymbol{R}^4$, respectively. The final $\boldsymbol{x}$ is

$$\boldsymbol{x} = C_1\boldsymbol{x}_1(t) + C_2\boldsymbol{x}_2(t) \tag{5.35}$$

where $C_1,\ C_2$ are also integral constants that depend on the initial state, and

$$\boldsymbol{x}_1(t) = e^{\alpha t}(\cos\omega t\boldsymbol{w}_1 - \sin\omega t\boldsymbol{w}_2) \tag{5.36}$$

$$\boldsymbol{x}_2(t) = e^{\alpha t}(\sin\omega t\boldsymbol{w}_1 + \cos\omega t\boldsymbol{w}_2) \tag{5.37}$$

In this case, thrust angle $|\delta|_\infty$ oscillates with frequency $\omega/2\pi$. By substituting Eq. (5.35) into Eq. (5.21), maximum thrust angle $|\delta|_{\infty,\max}$ is

$$|\delta|_{\infty,\max} = \max_{\omega t=\omega t_1,\ \omega t_1+\pi/2} \arccos\left(\frac{\boldsymbol{z}^T C_w^T K_w \boldsymbol{z}}{|C_w\boldsymbol{z}| \cdot |K_w\boldsymbol{z}|}\right) \tag{5.38}$$

$$\boldsymbol{z}(\omega t) = [\cos\omega t,\ -\sin\omega t]^T \tag{5.39}$$

$$\omega t_1 = -\arctan\left(\frac{2b}{a-c}\right)/2 \tag{5.40}$$

$$\begin{bmatrix} a & b \\ b & c \end{bmatrix} = C_w^T K_w + K_w^T C_w \tag{5.41}$$

where $C_w = [C\boldsymbol{w}_1\ C\boldsymbol{w}_2]$, and $K_w = [K\boldsymbol{w}_1\ K\boldsymbol{w}_2]$. In either case, $|\delta|_\infty$ does not depend on integral constants. This means the thrust angle at the final approach phase is independent of the initial state value.

In general, all modes can be excited according to the initial state and the thrust angle in the transient phase can be large. To avoid such a condition, a simple idea is that initial velocity can be determined for a certain initial position to excite only modes that maintain a small-magnitude thrust angle. If increased velocity direction to get such an initial velocity satisfies the constraints on thrust direction, it is possible to rendezvous with the target with a small thrust angle during the entire flight after performing an impulsive ΔV at the initial point to kill other "undesired "modes.

If the eigenvalue of the most slowly damped mode has only a real part, final trajectory approaches Eq. (5.32) and a pair of (C_s, φ_0) exist in such a way that the initial state has the form

$$\boldsymbol{x}_0(\varphi_0) = C_s\boldsymbol{v}_s \tag{5.42}$$

Eq. (5.42) has a one-dimensional subspace for each eigenvalue, so some initial positions will work in such a mode for rendezvous.

If the eigenvalue of the most slowly damped mode has an imaginary part, the initial state is written in modal form

$$\boldsymbol{x}_0 = [\boldsymbol{w}_1\ \boldsymbol{w}_2\ \boldsymbol{w}_3\ \boldsymbol{w}_4] \cdot [C_1\ C_2\ C_3\ C_4] \tag{5.43}$$

Therefore, the required initial velocity for any initial position $\boldsymbol{r}_0 = [x_0,\ y_0]^T$ can be achieved and remain only in the slowly damped mode

$$\begin{bmatrix} \dot{x_0}^{M_k} \\ \dot{y_0}^{M_k} \end{bmatrix} = \begin{bmatrix} w_{3,k} & w_{3,k+1} \\ w_{4,k} & w_{4,k+1} \end{bmatrix} \cdot \begin{bmatrix} w_{1,k} & w_{1,k+1} \\ w_{2,k} & w_{2,k+1} \end{bmatrix}^{-1} \begin{bmatrix} x_0 \\ y_0 \end{bmatrix}, \quad k = 1, 2 \tag{5.44}$$

where $w_{i,j}$ is the ith component of the eigenvector $\boldsymbol{w}_j$. In this case, the velocity given by Eq. (5.44) can be obtained for any initial position because the state vector has a two-dimensional subspace for the imaginary mode and its own conjugate mode. Initial velocities determined by Eq. (5.44) approach the target within thrust angle $|\delta|_{\infty,\max}$ as calculated in Eq. (5.38) for each mode. The necessary direction and magnitude of ΔV to change from an arbitrary initial velocity to the required initial velocity given by Eq. (5.44)

$$\Delta \boldsymbol{v} = \begin{bmatrix} \dot{x_0}^{M_k} \\ \dot{y_0}^{M_k} \end{bmatrix} - \begin{bmatrix} \dot{x_0} \\ \dot{y_0} \end{bmatrix} \tag{5.45}$$

Using this equation, the direction and magnitude of the initial impulsive thrust angle, $|\delta|_0^{\text{impulse}}$, which defines the angle between the $\Delta \boldsymbol{v}$ vector and $-\boldsymbol{r}$ vector, is calculated for any initial state.

However, when the direction of impulse cannot satisfy the constraints on thrust direction or $\Delta \boldsymbol{v}$ in Eq. (5.45) is too large to be admissible, a second idea is that the initial state can be chosen so that the thrust angle at the initial phase becomes small. The initial thrust angle for any initial state can be easily calculated from Eq. (5.21) once the design parameters $q,\ \lambda_\alpha$ are fixed. It still holds true that the thrust angle at the final approach phase is maintained within Eqs. (5.34) or (5.38) because the choice of initial start point has no effect on $|\delta|_{\infty,\max}$. In this case, however, the thrust angle at the transient phase possibly overshoots constraint angle α. To improve this problem, our proposed method to maintain a small-magnitude thrust angle at the transient phase is explained in the next section.

5.4 Satisficing Method

A control parameter design approach and suboptimal feedback control making the thrust angle small at the initial and final phases is derived. However, it is not guar-

anteed that this method makes the thrust angle small from start to finish. To solve this problem, a satisficing method is used to satisfy rigidly the constraints on thrust direction. CLF-based satisficing is a complete parameterization of asymptotically stabilizing control laws given a valid CLF for the closed-loop system (Curtis and Beard, 2002*b*, 2004). This method can achieve stabilized and robust control. Consider that the quadratic form Lyapunov function, which is derived from the unique nonnegative solution of solving Eq. (5.30) from the performance index Eq. (5.22) is used as a candidate CLF. Satisficing control can stabilize a system regularly. However, in the transient phase, the constraints on thrust direction are not necessarily guaranteed. In this phase, this chapter proposes that the thrust control input in the satisficing set is derived from the projection of optimal feedback control parallel to the borderline of the stable area. This method has the tendency of making a large input, but a continuous input profile from optimal control can be available from the satisficing set. Because this proposed method is based on the optimal control considered in the previous section, it is still expected that the highly damped mode decays and the slowly damped mode remains until the final phase. Therefore, at the final phase the control returns to optimal and satisfies the constraints on thrust direction, as explained in the previous section.

5.4.1 Concept of Satisficing

This section briefly reviews the concept of satisficing. According to Definition 4.2.1, we define the CLF as follows:

$$\inf_{\boldsymbol{u}} \dot{V} = \inf_{\boldsymbol{u}} \left\{ \frac{\partial V}{\partial t} + \left(\frac{\partial V}{\partial \boldsymbol{x}} \right)^T (f(t,\boldsymbol{x}) + g(t,\boldsymbol{x})\boldsymbol{u}) \right\} < 0 \tag{5.46}$$

for all $\boldsymbol{x} \neq 0$.

If such a CLF exists, the satisficing subset $S_b(t,\boldsymbol{x})$ is defined as follows:

$$S_b(t,\boldsymbol{x}) = \left\{ \boldsymbol{u} \in \boldsymbol{R}^m : \; -V_t - V_x^T(f+g\boldsymbol{u}) > \frac{1}{b}(l + \boldsymbol{u}^T R \boldsymbol{u} + 2\boldsymbol{x}^T N \boldsymbol{u}) \right\} \tag{5.47}$$

From Theorem 4.2.3, the satisficing set $S_b(t,\boldsymbol{x})$ at $(t,\boldsymbol{x})$ is nonempty if and only if design parameter $b(\boldsymbol{x})$ satisfies the inequality

$$b(t,\boldsymbol{x})\omega_N + l_N - \frac{b(t,\boldsymbol{x})^2}{4} \boldsymbol{p}^T R^{-1} \boldsymbol{p} < 0 \tag{5.48}$$

Furthermore, if the inequality Eq. (5.48) holds true, then $S_b(t,\boldsymbol{x}) \subset \boldsymbol{R}^m$ can be

described as a perfect parametric form by introducing new design parameter ν:

$$\begin{aligned} S_b(t,\boldsymbol{x}) &= \left\{ -R^{-1}\left(\frac{b}{2}\boldsymbol{p}+N^T\boldsymbol{x}\right) + R^{-1/2}\nu\sqrt{\frac{b^2}{4}\boldsymbol{p}^TR^{-1}\boldsymbol{p}-b\omega_N-l_N} :\ |\nu|<1 \right\} \\ &\triangleq \{-\sigma_1(t,\boldsymbol{x},b)+\sigma_2(t,\boldsymbol{x},b)\cdot\nu :\ |\nu|<1\} \end{aligned} \tag{5.49}$$

where $\boldsymbol{p}=g^TV_x$, $\omega_N=V_t+V_x^Tf-V_x^TgR^{-1}N^T\boldsymbol{x}$ and $l_N=l-\boldsymbol{x}^TNR^{-1}N^T\boldsymbol{x}$.

When considering the target's orbit as circular, as an example, the system Eq. (5.15) is a linear time-invariant system, and $f=A\boldsymbol{x}, g=B$ and (A,B) are controllable. Therefore, when taking $Q=Q^T\geq 0$ and $R>0$, such that $(A,Q^{1/2})$ is observable, the Riccati equation

$$A^TS+SA-(SB+N)R^{-1}(B^TS+N^T)+Q=0 \tag{5.50}$$

has a unique nonnegative solution $S=S^T>0$, and the quadratic form

$$V=\boldsymbol{x}^TS\boldsymbol{x} \tag{5.51}$$

becomes a CLF for the linear time-invariant system Eq. (5.15) since

$$\begin{aligned} \dot{V} &= (A\boldsymbol{x}+B\boldsymbol{u}^*)^TS\boldsymbol{x}+\boldsymbol{x}^TS(A\boldsymbol{x}+B\boldsymbol{u}^*) \\ &= \boldsymbol{x}^T(-SBR^{-1}B^TS-Q+NR^{-1}N^T)\boldsymbol{x}<0 \end{aligned} \tag{5.52}$$

for all $\boldsymbol{x}\neq 0$, where the condition $Q-NR^{-1}N^T>0$ for a positive integrand in the performance index Eq. (5.22) for all $\boldsymbol{x}\neq 0$ is used. When employing this CLF and setting design parameter $l(\boldsymbol{x})=\boldsymbol{x}^TQ\boldsymbol{x}$, inequality Eq. (5.48) reduces to a simple form $b(\boldsymbol{x})\geq 1$ (Curtis and Beard, 2004). Choose design parameters $b(\boldsymbol{x})=1$, according to Eq. (5.49), to obtain

$$S_1(\boldsymbol{x})=\{-R^{-1}(B^TS+N^T)\boldsymbol{x}\} \tag{5.53}$$

for all $\boldsymbol{x}\neq 0$. This is the optimal control Eq. (5.28) to minimize the performance index Eq. (5.22). As a result, $S_b(\boldsymbol{x})$ represents the control input subspace expanding to nonlinear control input of states to stabilize the system.

Next, the concept of satisficing is graphically explained. The time derivative of the CLF is

$$\begin{aligned} \dot{V} &= \left(\frac{\partial V}{\partial \boldsymbol{x}}\right)^T(A\boldsymbol{x}+B\boldsymbol{u}) \\ &= a-\boldsymbol{b}^T\boldsymbol{u}<0 \end{aligned} \tag{5.54}$$

where

$$a = \left(\frac{\partial V}{\partial \boldsymbol{x}}\right)^TA\boldsymbol{x} = 2\boldsymbol{x}^TSA\boldsymbol{x} \tag{5.55}$$

$$\boldsymbol{b} = -B^T\left(\frac{\partial V}{\partial \boldsymbol{x}}\right) = -2B^TS\boldsymbol{x} \tag{5.56}$$

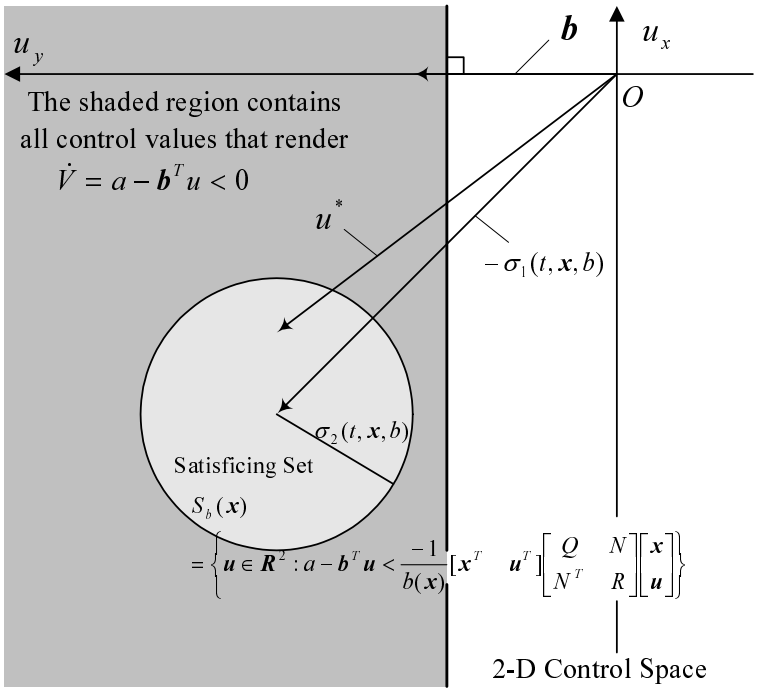

Figure 5.3: The satisficing set in a 2-D control space.

Therefore, a satisficing set that has a CLF Eq. (5.51) can be defined as

$$\begin{aligned} S_b(\boldsymbol{x}) &= \{\boldsymbol{u} \in \boldsymbol{R}^2 : a - \boldsymbol{b}^T\boldsymbol{u} < -\frac{1}{b(\boldsymbol{x})}[\boldsymbol{x}^T \ \boldsymbol{u}^T] \begin{bmatrix} Q & N \\ N^T & R \end{bmatrix} \begin{bmatrix} \boldsymbol{x}^T \\ \boldsymbol{u}^T \end{bmatrix}\} \\ &\triangleq \{\boldsymbol{u} \in \boldsymbol{R}^2 : p_s(\boldsymbol{u}, \boldsymbol{x}) < -p_r(\boldsymbol{u}, \boldsymbol{x})/b(\boldsymbol{x})\} \end{aligned} \tag{5.57}$$

As shown in Fig. 5.3, $S_b(\boldsymbol{x})$ is the subset including control inputs, which decrease the CLF regularly by $p_r(\boldsymbol{u}, \boldsymbol{x})/b(\boldsymbol{x})$ and represent an inner subset of the ellipsoid, which has a center $-\sigma_1$ and major and minor axis eigenvalues of the σ_2 matrix. The satisficing set becomes an optimal control $\boldsymbol{u}^*$ when $b = 1$ as explained above, which corresponds to $\sigma_2 = O_{2\times 2}$. $\boldsymbol{u}^*$ is included in $S_b(\boldsymbol{x})$ set for all $b \geq 1$ as made apparent in Definition 4.2.2. When b approaches infinity, S_b approaches a half plane in the control input space, which has a linear borderline, $a - \boldsymbol{b}^T\boldsymbol{u} = 0$, with a normal vector, $\boldsymbol{b}$ Eq. (5.56). Therefore, a stable half plane that regularly decreases the CLF can be described as

$$S_\infty(\boldsymbol{x}) = \{\boldsymbol{u} \in \boldsymbol{R}^2 : a - \boldsymbol{b}^T\boldsymbol{u} < 0\} \tag{5.58}$$

That is to say, the stability of the system continues to be guaranteed by projecting along the borderline $a - \boldsymbol{b}^T\boldsymbol{u} = 0$ and such a generated vector is in a certain satisficing set with a certain $b \geq 1$. However, the satisficing definition means that a system tends to become unstable with a large b because decreases of V become small and the control

input becomes large. The satisficing theorem also shows that control setting $b = 1$ is a unique one and decreases the CLF the most. The next section explains how to generate a control that meets the input constraints using these facts.

5.4.2 Satisficing with Control Direction Constraints

After selecting Eq. (5.51) as a candidate CLF, consider the constraints on thrust direction. A subset of the control input constraints $U_C(\boldsymbol{x}) \subset \boldsymbol{R}^2$ is described from Eq. (5.20) as

$$U_C(\boldsymbol{x}) = \{\boldsymbol{u} \in \boldsymbol{R}^2 : \arccos(-\boldsymbol{u}^T \cdot \boldsymbol{r}/|\boldsymbol{u}| \cdot |\boldsymbol{r}|) \leq \alpha\} \tag{5.59}$$

Figure 5.4 shows both subsets S_∞ and U_C at the same time. Subset $S_\infty \cap U_C$ denotes a favorable control subspace, which satisfies $\inf \dot{V} < 0$, and the constraints. The condition under which subset $S_\infty \cap U_C$ is nonempty is

$$(-\boldsymbol{r})^T \cdot \boldsymbol{u}^* > |\boldsymbol{r}| \cdot |\boldsymbol{u}^*| \cdot \cos(\pi/2 + \alpha) \tag{5.60}$$

If condition Eq. (5.60) is satisfied for all $\boldsymbol{x} \neq 0$, a new control input $\hat{\boldsymbol{u}}$ near $\boldsymbol{u}^*$ using Eq. (5.28) is proposed

$$\hat{\boldsymbol{u}}(\boldsymbol{x}) = \boldsymbol{u}^* + k\boldsymbol{b}_\perp \tag{5.61}$$

From a geometry point of view, this corresponds to the projection of optimal control to U_C along the satisficing boundary of S_∞ by vector $\boldsymbol{b}_\perp$. However, when the boundary of S_∞ and line segment OP_2 are parallel, $b(\boldsymbol{x})$ becomes too large and the system tends to become unstable. To avoid such a situation, when the angle between the two lines reaches $\boldsymbol{\delta}_{\mathrm{margin}}$, the control input is set to 0. Additionally, if condition Eq. (5.60) is not satisfied for $\exists \boldsymbol{x} \neq 0$, the input control is set to 0

$$\tilde{\boldsymbol{u}}(\boldsymbol{x}) = \begin{cases} \boldsymbol{u}^* + k\boldsymbol{b}_\perp & , \ S_\infty \cap U_C \neq \phi \\ 0 & , \ S_\infty \cap U_C = \phi \end{cases} \tag{5.62}$$

Whether condition Eq. (5.60) is satisfied or not for all $\boldsymbol{x} \neq 0$ depends on thrust angle α. In the case of $\pi/2 < \alpha \leq \pi$, as shown in Fig. 5.5 right, $S_\infty \cap U_C$ is always nonempty, whatever the relation between $\boldsymbol{r}$ and $\boldsymbol{b}$ is. Therefore, the candidate CLF V of Eq. (5.51) is valid. On the other hand, when the thrust angle is $0 < \alpha \leq \pi/2$, as shown in Fig. 5.5 left, $S_\infty \cap U_C$ may be empty with a certain relation between $\boldsymbol{r} = (x, \ y)^T$ and $\boldsymbol{b}$. Then, the candidate CLF V of Eq. (5.51) is not guaranteed as a valid CLF. Numerical validation on whether to converge stably to the origin is examined in Section 5.6.

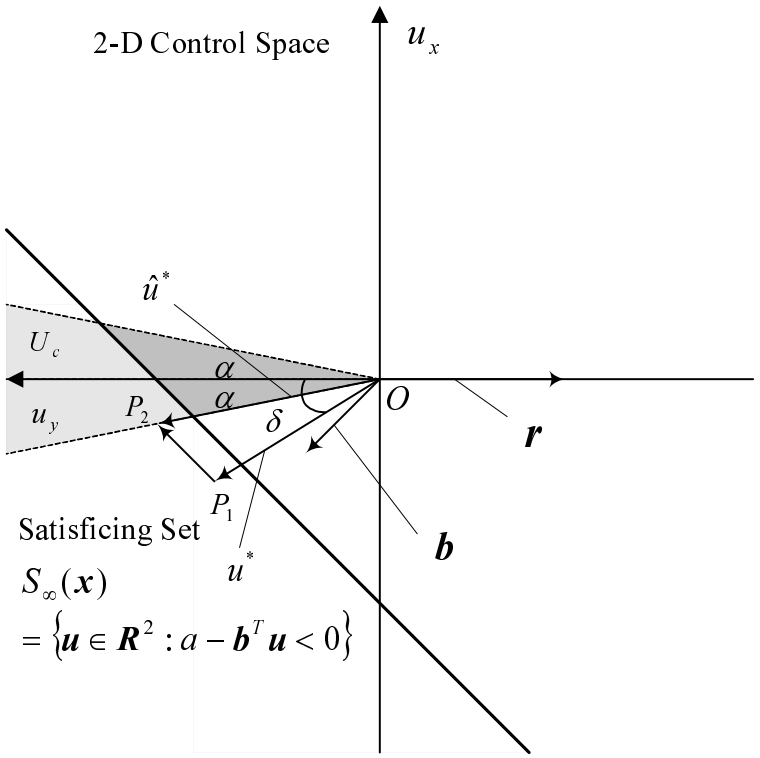

Figure 5.4: Satisficing with constrained condition of input.

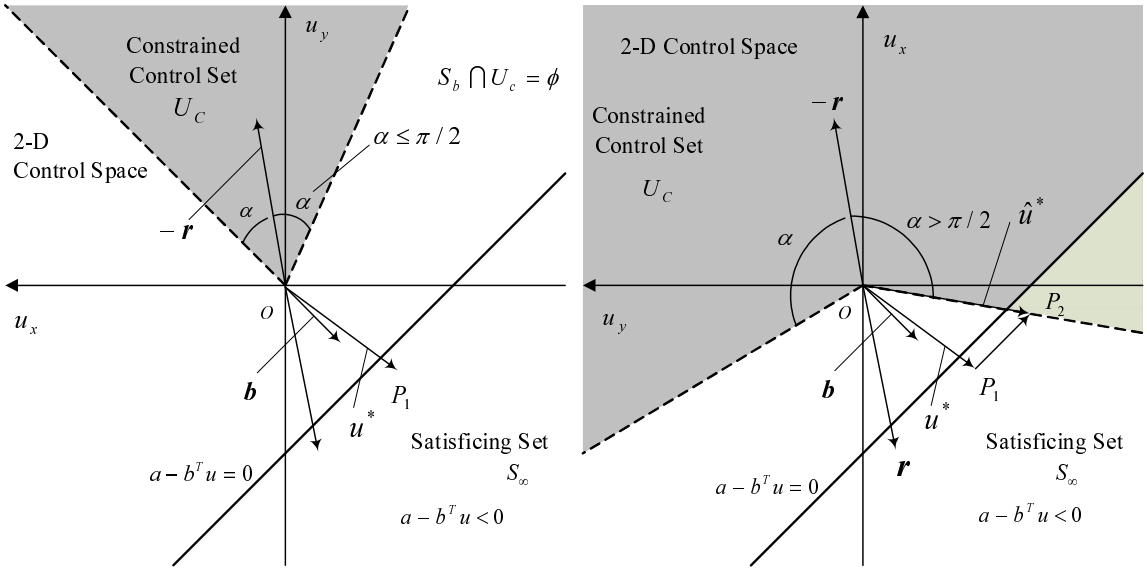

Figure 5.5: Performing projection onto the restricted area.

5.5 Rendezvous with Eccentric orbit

The proposed method is also applicable when the target's orbit is eccentric. This section explains the method.

5.5.1 Optimal Feedback Control Law

In the case of an eccentric orbit, the problem that minimizes the performance index Eq. (5.22) becomes time varying. Yet the formation problem for Eq. (5.22) can be solved essentially in the same way as for the HCW equations. In fact, the feedback control is

$$\tilde{\boldsymbol{u}}^* = -R^{-1}\left(\frac{1}{\rho}B^T\tilde{X}(\theta) + N^T\right)\tilde{\boldsymbol{x}} \tag{5.63}$$

where $\tilde{X}(\theta)$ is the periodic stabilizing solution of the differential Riccati equation (DRE)

$$-\tilde{X}' = \tilde{A}^T\tilde{X} + \tilde{X}\tilde{A} + C^TC - \left(\frac{1}{\rho}\tilde{X}B + N\right)R^{-1}\left(\frac{1}{\rho}B^T\tilde{X} + N^T\right) \tag{5.64}$$

which has a unique nonnegative 2π-periodic stabilizing solution $\tilde{X}(\theta)$ (Ichikawa and Katayama, 2001).

5.5.2 Modal Analysis

With the feedback law Eq. (5.63), the system becomes linear non-homogeneous, and has a closed-loop form $\bar{A}_c = \bar{A}(\theta) - BK(\theta)$. General solutions have the form

$$\boldsymbol{x}(\theta) = \Phi(\theta,\theta_0)\boldsymbol{x}(\theta_0), \Phi(\theta_0,\theta_0) = I_{4\times4} \tag{5.65}$$

which represents a four-dimensional vector subspace. This linear operator $\Phi(\theta,\theta_0)$ is referred to as the state transition matrix. It is known that the state transition matrix differential equation must satisfy

$$\dot{\Phi}(\theta,\theta_0) = \bar{A}_c(\theta)\Phi(\theta,\theta_0),\ \Phi(\theta_0,\theta_0) = I_{4\times4} \tag{5.66}$$

Thus, in the worst-case scenario, Eq. (5.66) can be solved numerically to determine $\Phi(\theta,\theta_0)$. However, when the eccentricity e approaches 0, $\int_{\theta_0}^{\theta}\bar{A}_c(\theta_1)d\theta_1$ and $\bar{A}_c(\theta)$ become commutative. Then $\Phi(\theta,\theta_0)$ reduces to (Schaub and Junkins, 2003)

$$\lim_{e\to0}\Phi(\theta,\theta_0) = \exp\left[\int_{\theta_0}^{\theta}\bar{A}_c(\theta_1)\right]\mathrm{d}\theta_1 \tag{5.67}$$

This solution is identical to the solution in the HCW equations. In this way, the thrust angle estimated in the circular orbit case can be applicable to the eccentric orbit case, which has $e \ll 1$.

5.5.3 Satisficing Method

In the case of an eccentric orbit, the system Eq. (5.11) is linear time-varying, $f = \bar{A}(\theta)\boldsymbol{x}$, $g = B$ and $(\bar{A}(\theta), B)$ is controllable for all θ. Moreover

$$\tilde{V}(\theta, \boldsymbol{x}) = \tilde{x}^T \tilde{X} \tilde{\boldsymbol{x}} \tag{5.68}$$

is a CLF in the system Eq. (5.11). Differentiate Eq. (5.68) with respect to θ

$$\begin{aligned} \tilde{V}' = & \quad \frac{\partial \tilde{V}}{\partial \theta} + \left(\frac{\partial \tilde{V}}{\partial \tilde{\boldsymbol{x}}} \right)^T \tilde{\boldsymbol{x}}' \\ = & \quad \tilde{a}(\theta) - \tilde{\boldsymbol{b}}^T(\theta) \cdot \tilde{\boldsymbol{u}} < 0 \end{aligned} \tag{5.69}$$

where

$$\tilde{a} = \quad \tilde{\boldsymbol{x}}^T \tilde{X}' \tilde{\boldsymbol{x}} + 2\tilde{\boldsymbol{x}}^T \tilde{X} \bar{A}(\theta) \tilde{\boldsymbol{x}} \tag{5.70}$$

$$\tilde{\boldsymbol{b}} = \quad -\frac{2}{\rho} B^T \tilde{X} \tilde{\boldsymbol{x}} \tag{5.71}$$

Therefore, the subspace of the satisficing set that has a CLF Eq. (5.68) can be defined

$$\tilde{S}_\infty(\theta, \tilde{\boldsymbol{x}}) = \{ \tilde{\boldsymbol{u}} \in \boldsymbol{R}^2 : \tilde{a}(\theta) - \tilde{\boldsymbol{b}}(\theta)^T \cdot \boldsymbol{u} < 0 \} \tag{5.72}$$

Likewise, the subspace of $\tilde{S}_\infty(\theta, \tilde{\boldsymbol{x}})$ is a half plane in the control space and the boundary is described as a straight line $\tilde{a}(\theta) - \tilde{\boldsymbol{b}}(\theta)^T \cdot \boldsymbol{u} = 0$ which has a normal vector $\tilde{\boldsymbol{b}}$ Eq. (5.71). The method to generate a control that satisfies both stable space and the constraints and projects optimal control along the boundary of $\tilde{S}_\infty$ is also applicable in Section 5.4.2.

5.6 Numerical Simulation

5.6.1 Circular Orbit Case with Initial Periodic Orbit

This section examines the efficiency of the proposed method. Two parameter setting cases — $q_r = q,\ q_v = 0$, called case 1 and $q_r = q_v = q$, called case 2 — are examined.

Parameter Setting Case 1 : $q_r = q,\ q_v = 0$

First, examine a trajectory of eigenvalues when varying the parameters $q,\ \lambda_\alpha$. Figure 5.6 shows the trajectory of the eigenvalues when varying parameter q. The left and right figures show the case of $\lambda_\alpha = 0,\ \sqrt{0.9q}$ respectively. In this parameter setting case, all the eigenvalues become complex, excluding the points where the eigenvalues degenerate.

For all parameters, λ_1 and the conjugate complex $\bar{\lambda}_1$ become slower modes, so the $\lambda_1,\ \bar{\lambda}_1$ modes become dominant as they approach the origin. As previously mentioned, when eigenvalues are complex, $|\delta|_\infty$ oscillates at ω angular frequency. Figure 5.7 shows the contour plot of the maximum thrust angle at final phase $|\delta|_{\infty,\max}$ using Eq. (5.38) when varying $q,\ \lambda_\alpha$ in the mode of $\lambda_1,\ \lambda_2$, respectively. Figure 5.7 shows that $|\delta|_{\infty,\max}$ becomes smaller for fixed q when a larger λ_α is set. This fact confirms the efficiency of introducing the λ_α parameter to the quadratic performance index. Especially, if the λ_1 mode is dominant, a smaller $|\delta|_{\infty,\max}$ can be set for any q when λ_α is set closer to the boundary (dotted line) $q = \lambda_\alpha^2$. Note that convergence becomes much slower as it approaches $q = \lambda_\alpha^2$ because $q = \lambda_\alpha^2$ corresponds to no penalty of position error in the meaning of the performance index. As for the λ_2 mode, a small $|\delta|_{\infty,\max}$ can be set only when q is large and λ_α is close to the dotted line $q = \lambda_\alpha^2$. Therefore, the λ_1 mode has more favorable characteristics than the λ_2 mode.

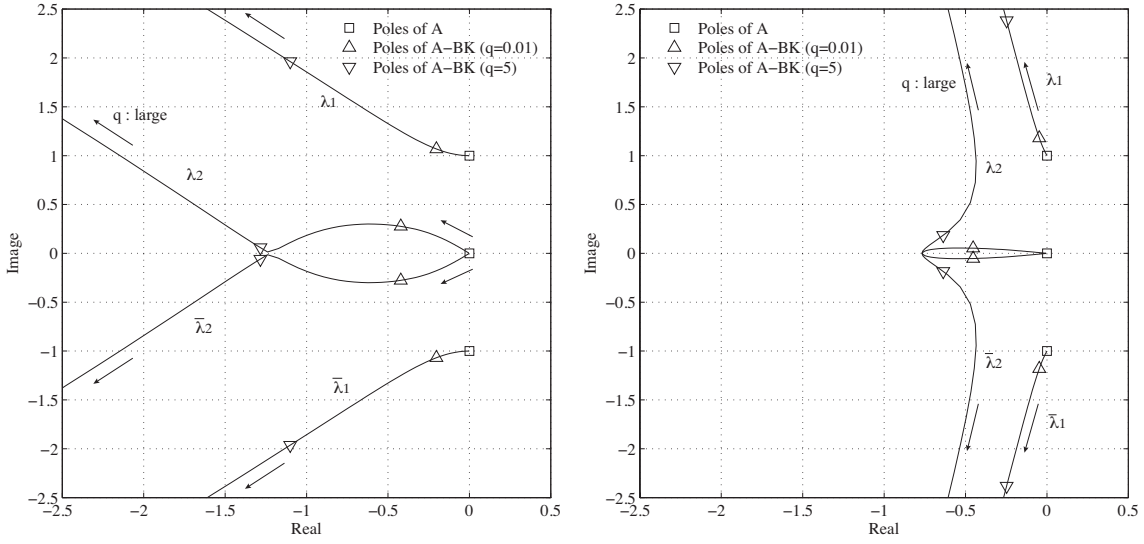

Figure 5.6: Trajectory of closed-loop pole assignment in the case $q_r = q,\ q_v = 0$ (Left: $\lambda_\alpha = 0$, Right: $\lambda_\alpha = \sqrt{0.9q}$).

Consider the case of the initial state of the chaser before rendezvous when it is in a periodic (i.e. non-drifting) relative orbit. In this case, examine whether the rendezvous, in which only each mode remains, is possible. Figure 5.8 shows the contour plot of the necessary magnitude and direction to $-\boldsymbol{r}$ of the impulsive maneuver. These contours depict the magnitude and thrust angle δ between $-\boldsymbol{r}$ and the necessary impulsive maneuver under the condition that rendezvous starts at $\boldsymbol{x}_0(\varphi_0) = (\cos\varphi_0/2, -\sin\varphi_0, y_0/2, -2x_0),\ (0 \le \varphi_0 < 2\pi)$ from Eq. (5.19) and varying design parameter q from 10^{-3} to 10^3. The initial distance from the origin does not

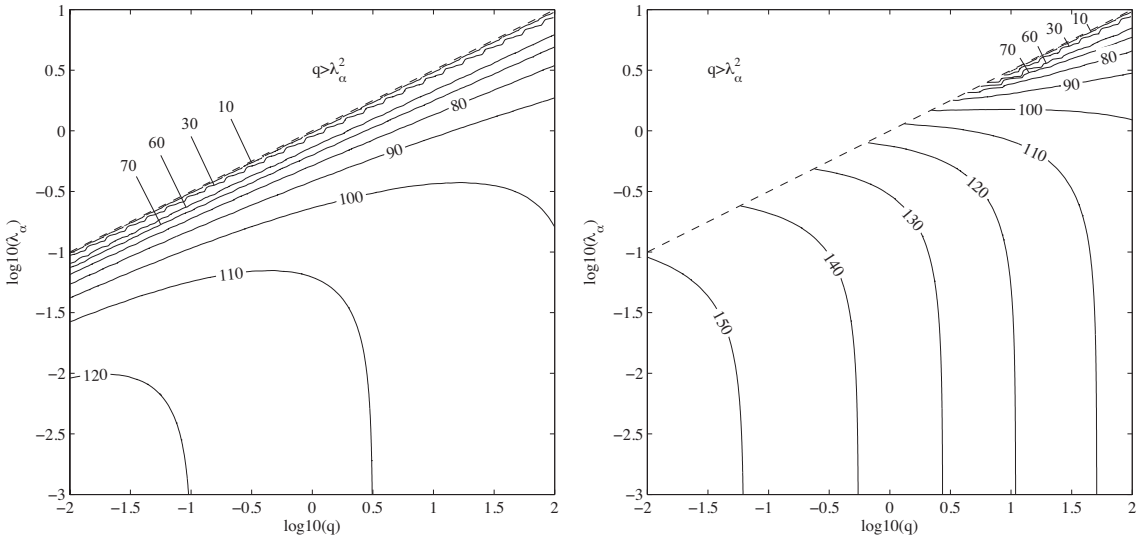

Figure 5.7: Estimation of $|\delta|_{\infty,\max}$ [°] as they approach the origin in the case $q_r = q,\ q_v = 0$ (Left: $\lambda_1,\ \bar{\lambda}_1$ mode, Right: $\lambda_2,\ \bar{\lambda}_2$ mode).

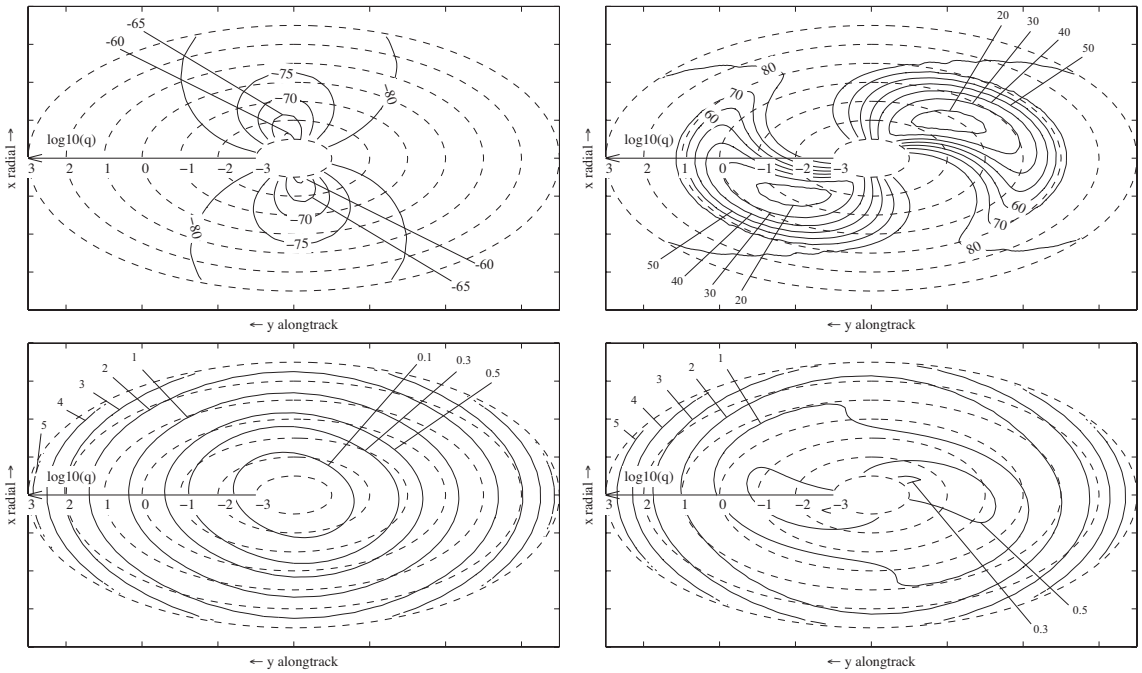

Figure 5.8: Initial δ [°] as an impulsive maneuver when the initial state is in periodic relative orbit (Left top: $\lambda_1,\ \bar{\lambda}_1$ mode, Right top: $\lambda_2,\ \bar{\lambda}_2$ mode) and ΔV for the impulsive maneuver (Left bottom: $\lambda_1,\ \bar{\lambda}_1$ mode, Right bottom: $\lambda_2,\ \bar{\lambda}_2$ mode).

affect the δ profile because of the definition of δ and feedback control. Therefore, the initial distance from the origin is normalized to 1. Instead, the distance from the origin uses the scale of parameter q. For example, the outmost dotted line of the ellipsoid represents δ with $q = 10^3$ when varying the initial phase φ_0 of rendezvous. One views the impulsive maneuver's magnitude contour plot likewise. Figure 5.8 shows that if q is small, a trajectory that makes the thrust angle small can be possible using the λ_1 mode; whereas, the initial impulsive maneuver direction is over 60°. On the other hand, if q is large, the impulsive maneuver direction is also over 60° using the λ_2 mode. Therefore, if thrust angle α is approximately 60°, it is possible to satisfy the constraints. However, if α is smaller than 60°, such a trajectory is impossible, as it excites the single mode by the impulsive maneuver, which satisfies the constraints when the initial state is in periodical orbit in the parameter setting case. Figures 5.9 and 5.10 show examples of the rendezvous trajectory of modes 1 and 2, respectively. In Fig. 5.9a the chaser's initial periodical orbit before control is shown with a dotted line and the rendezvous start point with an impulsive maneuver is shown with a triangle. Without control, the chaser rounds the target periodically since the initial condition satisfies a non-drifting relative orbit. In addition, the velocity vectors before and after the impulsive maneuver are shown. A solid line shows the trajectory profile after rendezvous start. Figure 5.9 shows the profiles of relative position $\boldsymbol{r}$ after an impulsive maneuver in Fig. 5.9b, control $\boldsymbol{u}$ in Fig. 5.9c, and thrust angle δ in Fig. 5.9d. Control mode, initial condition and design parameters are listed in Table 5.2.

Next, consider a rendezvous trajectory design example to choose q, λ_α to satisfy the constraints without the killing mode. Figure 5.11 (following the same convention as Fig. 5.8 shows the contour plot of thrust angle δ between $-\boldsymbol{r}$ and $\boldsymbol{u}^*$ at the initial rendezvous state $\boldsymbol{x}_0(\varphi_0)(0 \leq \varphi_0 < 2\pi)$ when varying design parameter q from 10^{-3} to 10^3. It is possible to set the initial thrust angle to below 10° for any q, as shown in Fig. 5.11.

Figure 5.12a shows an example of a designed rendezvous trajectory, setting the design parameters $q = 1$, $\lambda = \sqrt{0.9q}$, thrust constraint $\alpha = 30°$, and start rendezvous point $\varphi_0 = 120°$. In Fig. 5.12a the chaser's initial periodical orbit before control is shown with a chain line and the rendezvous start point with an impulsive maneuver is shown with a triangle. A solid line and a dotted line show the trajectory profiles with the satisficing control Eq. (5.62) and optimal control Eq. (5.28), respectively. Figure 5.12 shows the profiles of the candidate CLF Eq. (4.14) in Fig. 5.12b, control $\boldsymbol{u}$ in Fig. 5.12c, and thrust angle δ with controls Eqs. (5.62) and (5.28) in Fig. 5.12d. The figure shows that the constraints on thrust direction are satisfied in a rigorous manner using the proposed control, which in turn uses the satisficing method; whereas, the thrust

angle becomes larger than α at the transient phase using optimal control. In addition, δ at both the initial and final state is maintained as estimated from Figs. 5.11 and 5.7.

Parameter Setting Case 2 : $q_r = q_v = q$

Here, examine the case of setting $q_r = q_v = q$. Figure 5.13 shows the trajectory eigenvalues when varying parameter q. The left and right figures show $\lambda_\alpha = 0,\ \sqrt{0.9q}$, respectively. In time, mode λ_2 can have two different real solutions for $\lambda_\alpha \neq 0$. Figure 5.14 shows the contour plot of the maximum thrust angle at final phase $|\delta|_{\infty,\max}$ using Eqs. (5.34) and (5.38) when varying $q,\ \lambda_\alpha$ in the mode of $\lambda_1,\ \lambda_2$ and λ_3, respectively. The figure shows that the thrust angle at the final phase is over 90° in the λ_1 mode. The positional relationship of each mode when varying q in Fig. 5.14 shows that the relationship between the sizes of the real part of the eigenvalue is reversed. Therefore, $\lambda_1, \bar{\lambda}_1$ modes become slowly damped modes if around $q = 0.01$; whereas, $\lambda_1, \bar{\lambda}_1$ modes become highly damped modes if around $q = 1$. Therefore, q should not be set to such a small value that the λ_1 mode becomes a slowly damped mode in this case.

Examine rendezvous trajectory remaining in a single mode. Designing ΔV using the λ_1 mode has no usefulness because the thrust angle at the final phase in this mode becomes large for any q. Using the λ_2 mode, the thrust angle can be designed to be small if λ_α is set larger and q is set for the eigenvalue to become real. Figure 5.15 shows the example trajectory to meet these parameter conditions. The parameter is set to $q = 1,\ \lambda_\alpha = \sqrt{0.9q}$. The magnitude of the initial impulsive maneuver direction is almost the same as that of the initial periodical orbit and the thrust angle becomes about 70°. After that, the thrust angle always becomes almost 0 to the target. Figure 5.16 shows that designing the rendezvous trajectory can be possible using the satisficing control to maintain a small-magnitude thrust angle if q is set larger. There is a span during which generated control becomes zero because thrust angle δ is over the constraint α at the transient phase, but after that the trajectory stabilizes. The case $q_r = q_v = q$ has a favorable characteristic in that it approaches the target quickly compared to the case $q_r = q,\ q_v = 0$. Additionally, the tangential direction to approach is the direction of the eigenvector $\boldsymbol{v}_s$'s positional components, as shown by Eq. (5.32).

Result of Comparing Case 1 and 2

Table 5.3 sums up the result of comparing cases 1 and 2. As shown in the previous section, in case 1, the λ_1 mode becomes dominant as it approaches the origin for any q, λ_α and $|\delta|_\infty$ of λ_1 mode can be set to be small for any q. On the other hand, in case 2, $|\delta|_\infty$ of λ_1 mode becomes large for any q, λ_α. Setting $q \sim 1$ can only meet the condition

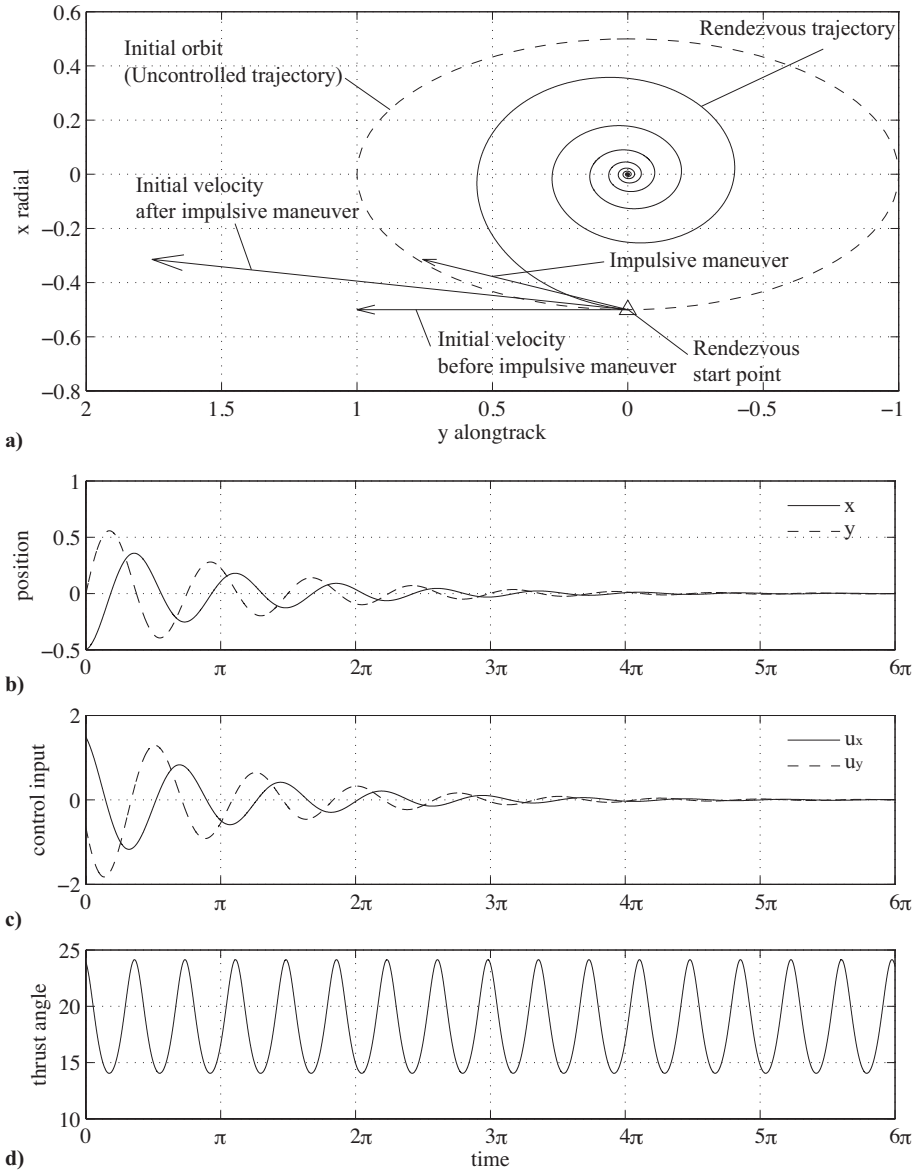

Figure 5.9: a) Rendezvous trajectory leaving $\lambda_1,\ \bar{\lambda}_1$ mode, b) Profiles in position $\boldsymbol{r}$, c) input $\boldsymbol{u}$, and d) thrust angle δ [°]. Parameter setting $q_r = q = 10,\ q_v = 0,\ \lambda_\alpha = \sqrt{0.9q},\ \varphi_0 = 180°$.

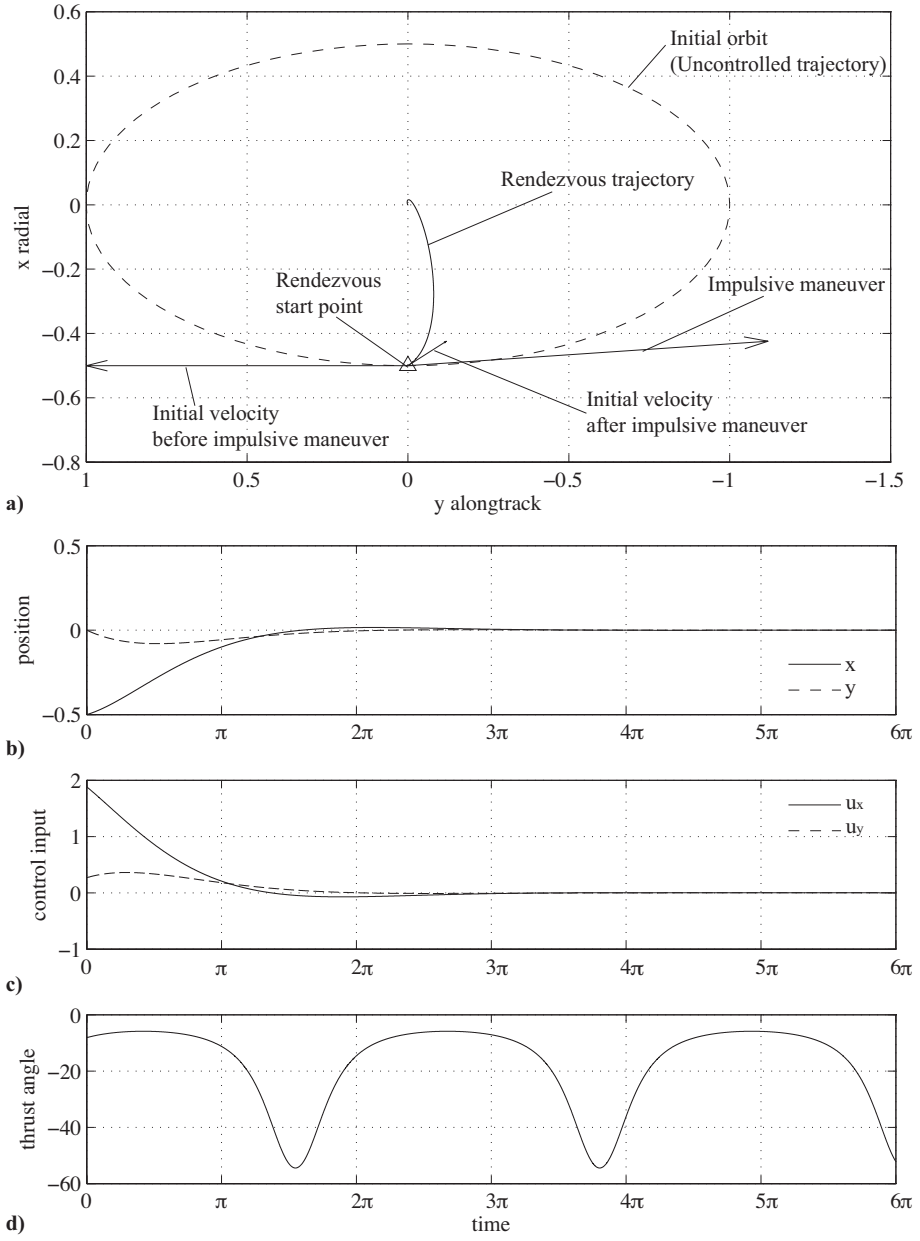

Figure 5.10: a) Rendezvous trajectory leaving $\lambda_2,\ \bar{\lambda}_2$ mode, b) Profiles in position $\boldsymbol{r}$, c) input $\boldsymbol{u}$, and d) thrust angle δ [°]. Parameter setting $q_r = q = 10,\ q_v = 0,\ \lambda_\alpha = \sqrt{0.9q},\ \varphi_0 = 180°$.

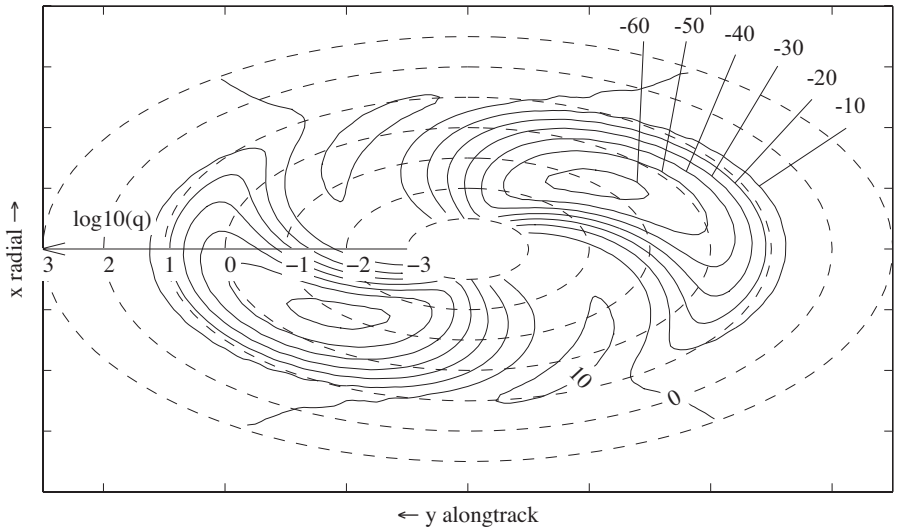

Figure 5.11: Initial δ [°] with optimal control when the initial state is in a periodic relative orbit.

that λ_2, λ_3 become a slowly damped mode and $|\delta|_\infty$ become small. However, case 2 has favorable characteristics in that it approaches the target quickly. In the following subsection, the case of an eccentric orbit and more concrete design parameters are explained regarding case 1.

5.6.2 Eccentric Orbit Case with Initial Periodic Orbit

Figure 5.17 shows the case of an eccentric orbit with $e = 0.3$. In this simulation, parameter setting case 1: $q_r = q,\ q_v = 0$ is selected and design parameters are set to $q = 0.1,\ \lambda = \sqrt{0.95q},\ \alpha = 30°$. The initial rendezvous state is chosen as $(x_0, y_0) = (0.5, 0)$ and $\theta_0 = 0$. Using Eq. (5.17), the free trajectory is shown in Fig. 5.17 by the dotted line. As stated in section V, the optimal control Eq. (5.63) and the CLF Eq. (5.68) are used for the satisficing control Eq. (5.62). Thrust angle at the final position, which is not predicted analytically if e cannot be approximated by $e \ll 1$, however, is found to be maintained practically if λ_α is set larger. The chaser also approaches stably to the target and the constraints on thrust direction are always satisfied in the case of an eccentric orbit.

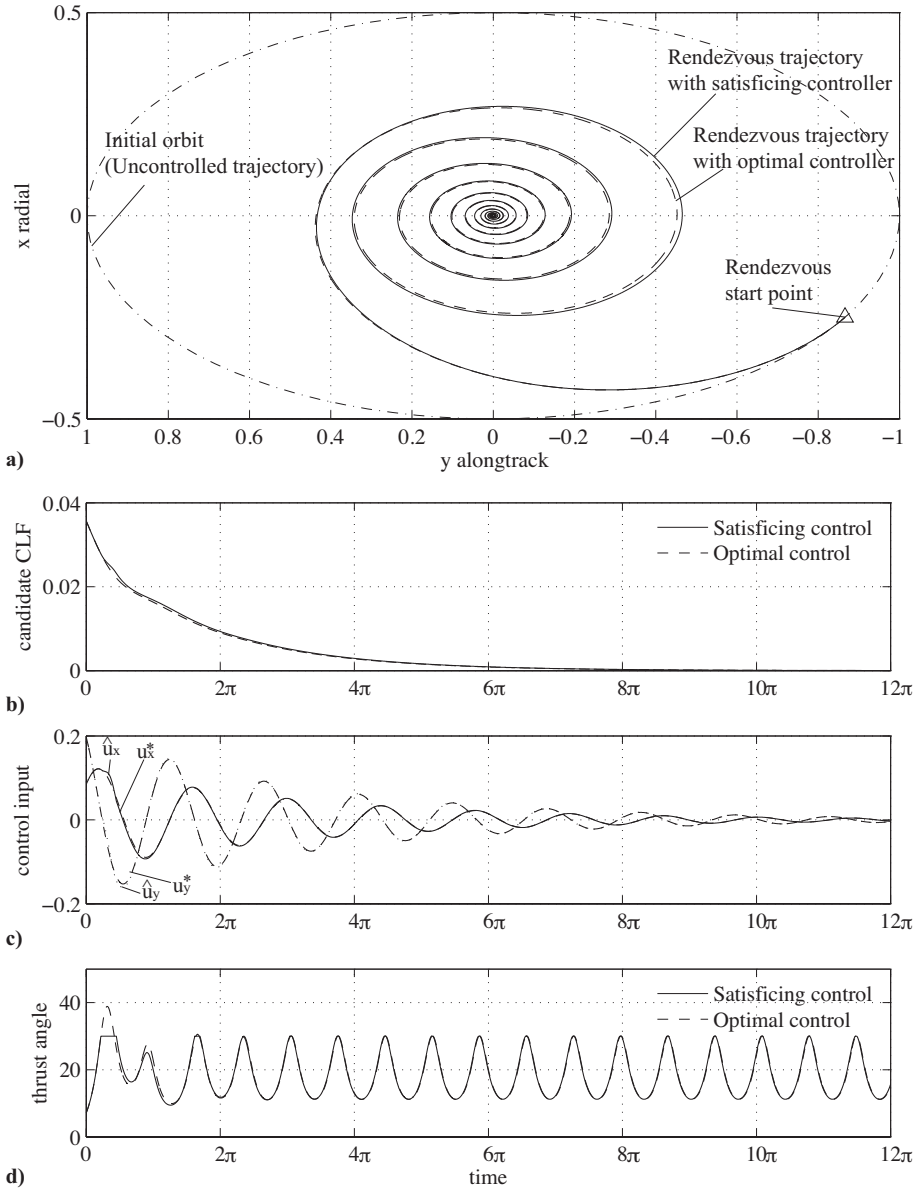

Figure 5.12: a) Rendezvous trajectories with satisficing and optimal control, b) Profiles in candidate CLF, c) input $\boldsymbol{u}$, and d) thrust angle δ. Parameter setting $q_r = q = 0.1,\ q_v = 0,\ \lambda_\alpha = \sqrt{0.9q},\ \varphi_0 = 120°,\ \alpha = 30°$.

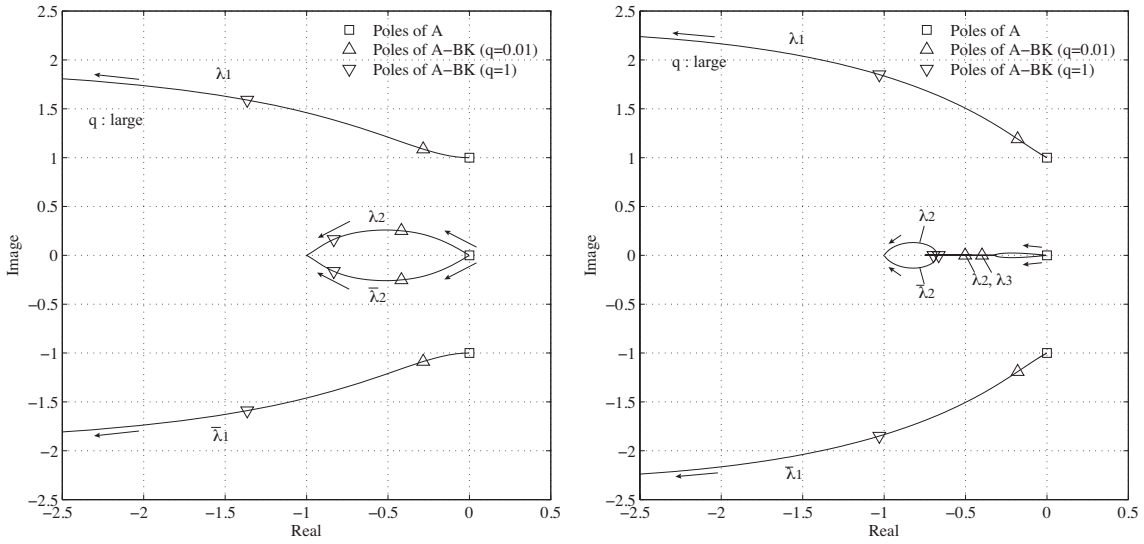

Figure 5.13: Closed-loop pole assignment in the case $q_r = q_v = q$ (Left: $\lambda_\alpha = 0$, Right: $\lambda_\alpha = \sqrt{0.9q}$).

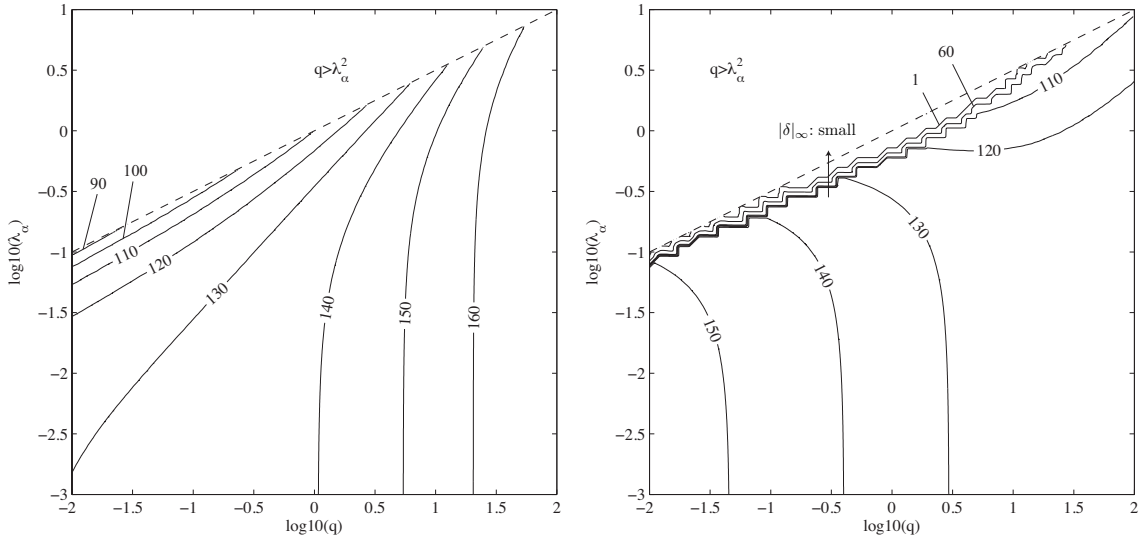

Figure 5.14: Estimation of $|\delta|_{\infty,\max}$ [°] as they approach the origin in the case $q_r = q_v = q$ (Left: $\lambda_1,\ \bar{\lambda}_1$ mode, Right: $\lambda_2,\ \bar{\lambda}_2$ mode or $\lambda_2,\ \lambda_3$ mode).

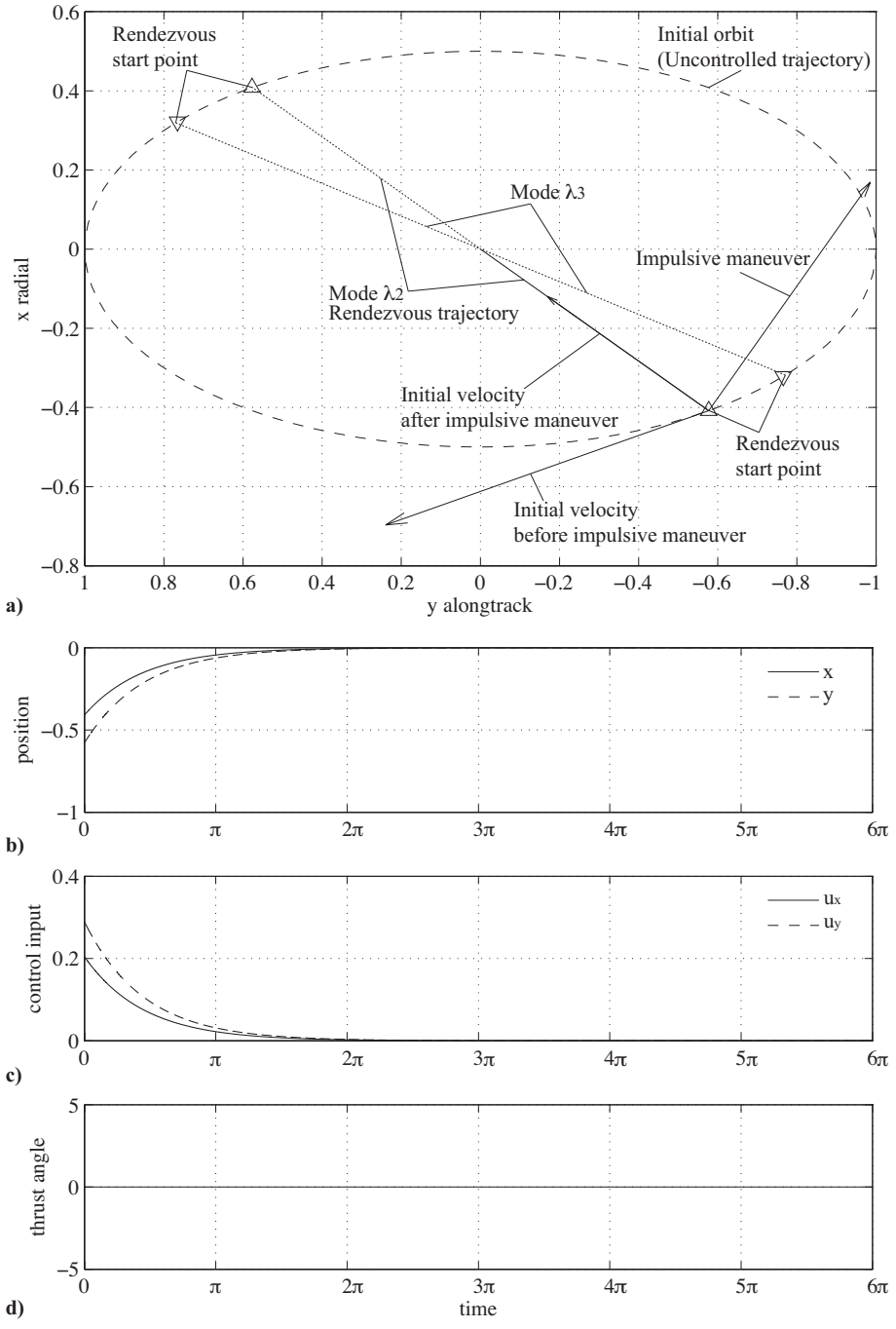

Figure 5.15: a) Rendezvous trajectory remaining only λ_2 or λ_3 mode, b) Profiles in position $\boldsymbol{r}$, c) input $\boldsymbol{u}$, and d) thrust angle δ. Parameter setting $q_r = q_v = 0.1,\ \lambda_\alpha = \sqrt{0.9q},\ \varphi_0 = 130.05°$.

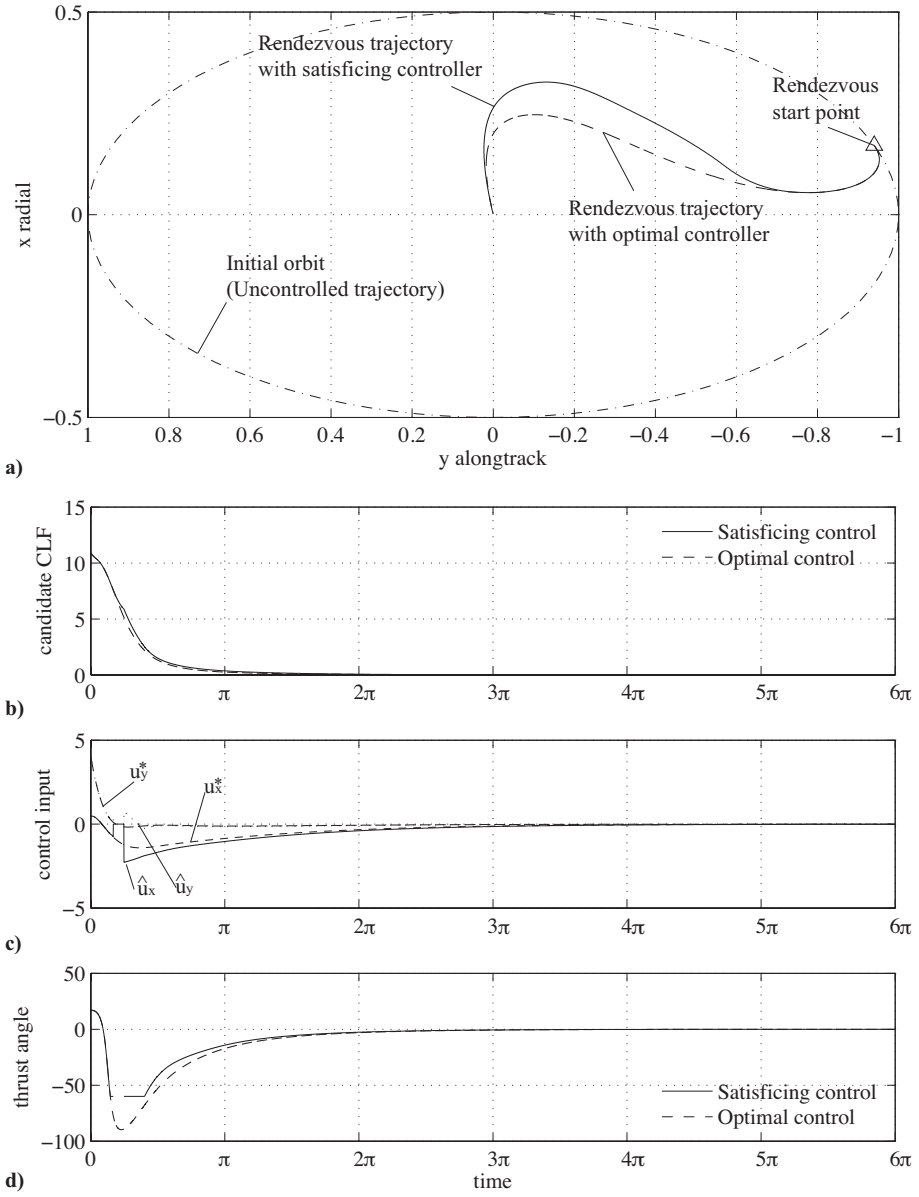

Figure 5.16: a) Rendezvous trajectories with satisficing and optimal control, b) Profiles in candidate CLF, c) input $\boldsymbol{u}$, and d) thrust angle δ. Parameter setting $q_r = q_v = 10,\ \lambda_\alpha = \sqrt{0.9q},\ \varphi_0 = 60°,\ \alpha = 60°$.

Table 5.2: Summary of control mode, initial condition and design parameters in examples.

Figure	Control mode	Initial condition	Design parameters case 1: $(q_r,\ q_v) = (q,\ 0)$ case 2: $(q_r,\ q_v) = (q,\ q)$
5.6.1 Circular orbit case, $e = 0$, $\boldsymbol{x}_0 = \boldsymbol{x}(\varphi_0) = (\cos\varphi_0/2, -\sin\varphi_0, y_0/2, -2x_0)$			
5.9	Leaving $\lambda_1, \bar{\lambda}_1$ mode	$\varphi_0 = 180°$	case 1: $q = 10,\ \lambda_\alpha = \sqrt{0.9q}$
5.10	Leaving $\lambda_2, \bar{\lambda}_2$ mode	$\varphi_0 = 180°$	case 1: $q = 10,\ \lambda_\alpha = \sqrt{0.9q}$
5.12	Satisficing with $\alpha = 30°$	$\varphi_0 = 120°$	case 2: $q = 0.1,\ \lambda_\alpha = \sqrt{0.9q}$
5.15	Leaving λ_2 or λ_3 mode	$\varphi_0 = 130.05°$	case 2: $q = 0.1,\ \lambda_\alpha = \sqrt{0.9q}$
5.16	Satisficing with $\alpha = 60°$	$\varphi_0 = 60°$	case 2: $q = 10,\ \lambda_\alpha = \sqrt{0.9q}$
5.6.2 Eccentric orbit case, $e = 0.3$, $\boldsymbol{x}_0 = \boldsymbol{x}(\theta_0) = \phi(\theta_0) \cdot [K_1\ K_2\ 0\ 0]^T$			
5.17	Satisficing with $\alpha = 30°$	$(x_0, y_0) = (0.5, 0)$, $\theta_0 = 0°$	case 1: $q = 0.1,\ \lambda_\alpha = \sqrt{0.95q}$

Table 5.3: Result of comparing cases 1 and 2.

	case 1 ($q_r = q, q_v = 0$)				case 2 ($q_r = q_v = q$)			
	mode 1	$\lvert\delta\rvert_\infty$	mode 2	$\lvert\delta\rvert_\infty$	mode 1	$\lvert\delta\rvert_\infty$	mode 2,3	$\lvert\delta\rvert_\infty$
$q < 0.1$	**slow**	**small**	fast	large	**slow**	large	fast	**small**
$q \sim 1$	**slow**	**small**	fast	large	fast	large	**slow**	**small**
$q > 10$	**slow**	**small**	fast	**small**	fast	large	**slow**	large

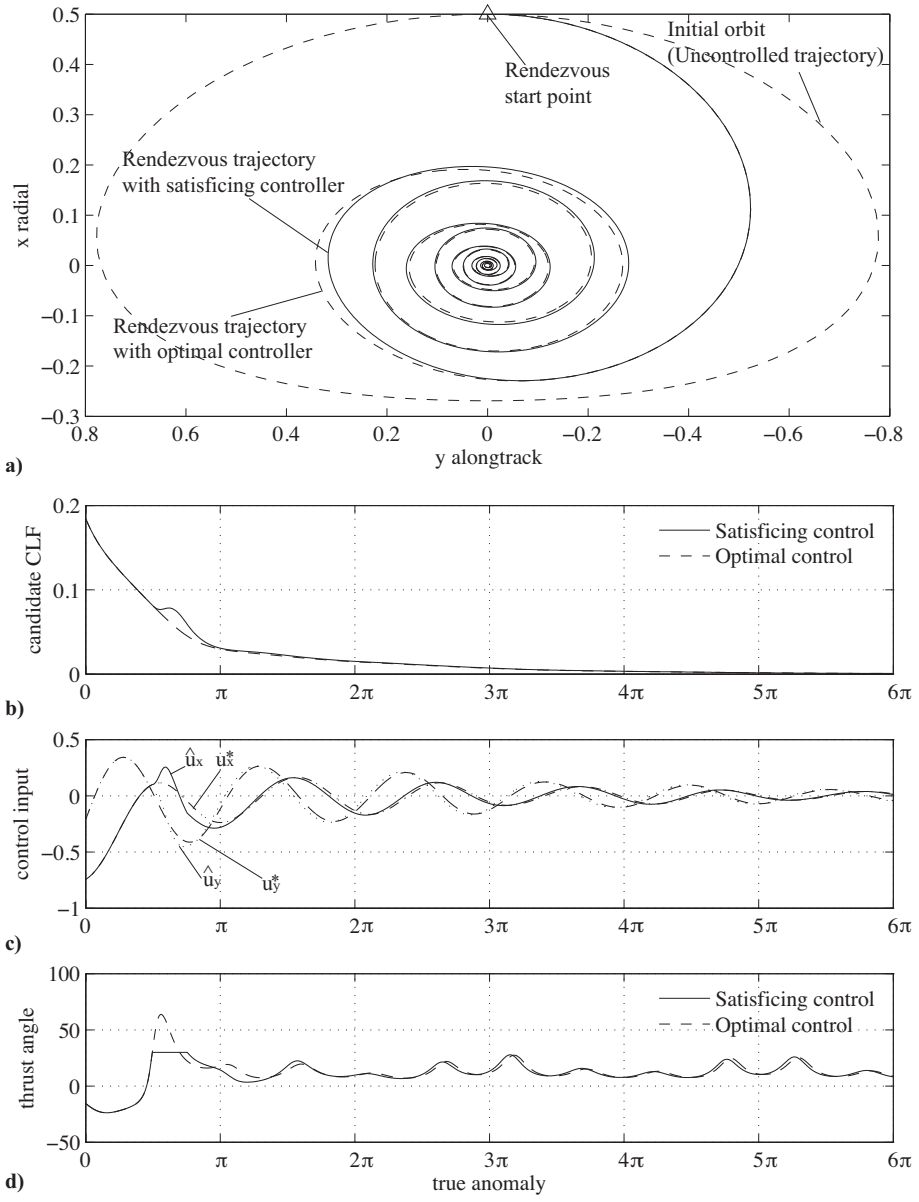

Figure 5.17: a) Rendezvous trajectories with satisficing and optimal control, b) Profiles in candidate CLF, c) input $\boldsymbol{u}$, and d) thrust angle δ. Parameter setting $q_r = q = 0.1,\ q_v = 0,\ \lambda_\alpha = \sqrt{0.95q},\ \theta_0 = 0,\ \alpha = 30°,\ e = 0.3$.

Table 5.4: $|\delta|$, eigenfrequency ω, J, ΔV, $|\boldsymbol{u}|_{\max}$ and convergence time T_{conv} for $q_r = q,\ q_v = 0,\ \lambda_\alpha = \sqrt{0.9q},\ \varphi_0 = 180°$.

q	λ_α	$\lvert\delta\rvert_{\min}$ - $\lvert\delta\rvert_{\max}$ [°]	$\omega/2\pi$	J	ΔV	$\lvert\boldsymbol{u}\rvert_{\max}$	T_{conv}
0.01	$\sqrt{0.9 \cdot q}$	10.2 - 32.9	0.188	0.0137	1.34	0.0869	95.9
0.1	$\sqrt{0.9 \cdot q}$	11.2 - 30.1	0.226	0.0700	2.00	0.316	48.6
1	$\sqrt{0.9 \cdot q}$	12.6 - 26.9	0.298	0.261	3.03	0.886	26.7
10	$\sqrt{0.9 \cdot q}$	14.0 - 24.1	0.425	0.522	4.11	1.82	14.2
100	$\sqrt{0.9 \cdot q}$	15.4 - 22.0	0.647	2.56	6.50	5.10	6.77

Table 5.5: $|\delta|$, eigenfrequency ω, J, ΔV, $|\boldsymbol{u}|_{\max}$ and convergence time T_{conv} for $q_r = 1,\ q_v = 0,\ \lambda_\alpha = \sqrt{\eta q},\ 0 \leq \eta < 1,\ \varphi_0 = 180°$.

q	λ_α	$\lvert\delta\rvert_{\min}$ - $\lvert\delta\rvert_{\max}$ [°]	$\omega/2\pi$	J	ΔV	$\lvert\boldsymbol{u}\rvert_{\max}$	T_{conv}
1	$\sqrt{0 \cdot q}$	66.5 - 113	0.253	0.856	0.860	0.993	6.56
1	$\sqrt{0.3 \cdot q}$	39.8 - 77.8	0.281	0.597	1.18	0.961	9.16
1	$\sqrt{0.5 \cdot q}$	31.2 - 63.2	0.288	0.494	1.41	0.942	11.9
1	$\sqrt{0.7 \cdot q}$	22.8 - 47.6	0.294	0.390	1.81	0.919	15.3
1	$\sqrt{0.9 \cdot q}$	12.6 - 26.9	0.298	0.261	3.03	0.886	26.7

5.6.3 Performance Index, Delta-V, and Maximum Acceleration Comparison

To study how to choose the design parameters, tendencies of J, ΔV, $|u|_{\max}$ by varying q, λ_α are examined. Table 5.4 shows the effects varying q, with $\lambda_\alpha = \sqrt{0.9 \cdot q}$ are set. J, ΔV, $|u|_{\max}$ become large when q is large and the LQR problem is narrowly defined. Convergence times become faster and the maximum thrust angle becomes smaller when q is larger. Table 5.5 shows the effects of varying λ_α and fixing q. $\lambda_\alpha = 0$ corresponds to a usual LQR problem. In this case, the thrust angle at the final phase is 113°. It is found that $|\delta|_{\max}$ become smaller when λ_α become larger under the condition of Eq. (5.31). Fuel consumption and convergence time become larger, whereas, $|\boldsymbol{u}|_{\max}$ is almost the same. Considering these things, the planning procedure to design a rendezvous trajectory from the actual design criteria are as follows: First, q is chosen from maximum thrust acceleration $|\boldsymbol{u}|_{\max}$. Next λ_α is chosen from the trade-off between thrust angle δ at the final phase and ΔV, T_{conv}. Using a contour plot, like the one shown in Fig. 5.11, the initial thrust angle is chosen to be small in the initial phase of the rendezvous. Figure 5.18 summarizes the proposed procedure for determining the design parameters.

1. Determine q from maximum acceleration $|\boldsymbol{u}|_{\max}$ using Eqs. (5.28) and (5.29).

$$|\boldsymbol{u}_0^*(q, \lambda_\alpha = 0)| \leq |\boldsymbol{u}|_{\max} \implies q^\# = q$$

Remark: One can adjust the penalty q for required specifications. If it is desirable to keep ΔV small, one could take small $|\boldsymbol{u}_0^*(q, \lambda_\alpha = 0)|$ for given $|\boldsymbol{u}|_{\max}$, which gives larger T_{conv}.

2. Determine λ_α from thrust constraint α using Eq. (5.38). (see Fig. 5.7)

$$|\delta|_\infty(q^\#, \lambda_\alpha) \leq \alpha \implies \lambda_\alpha^\# = \lambda_\alpha$$

Remark: Given smaller α, which gives larger λ_α near $\sqrt{q}$, ΔV and T_{conv} become larger.

3. If $|\delta|_0^{\text{impulse}}(q^\#,\ \lambda_\alpha^\#,\ \exists\varphi_0) \leq \alpha$ and additive $|\Delta V|^{\text{impulse}}(q^\#,\ \lambda_\alpha^\#,\ \exists\varphi_0)$ is admissible

   (a) Then, determine φ_0 parameter to minimize $|\Delta V|^{\text{impulse}}(q^\#,\ \lambda_\alpha^\#,\ \varphi_0)$ using Eqs. (5.44) and (5.45). (See Fig. 5.8)

$$\varphi_0^\# = \arg\min_{\varphi_0} |\Delta V|^{\text{impulse}}(q^\#,\ \lambda_\alpha^\#,\ \varphi_0)$$

   Perform impulsive maneuver $\Delta\boldsymbol{v} = \dot{\boldsymbol{x}}_0^{M_1} - \dot{\boldsymbol{x}}_0$ Eq. (5.45) at phase $\varphi_0^\#$ and optimal control $\boldsymbol{u}^*(q^\#, \lambda_\alpha^\#)$ Eq. (5.28) right after the impulsive maneuver.

   (b) Else, determine φ_0 from thrust constraint α using Eqs. (5.21) and (5.28). (See Fig. 5.11)

$$|\delta|_0(q^\#,\ \lambda_\alpha^\#,\ \varphi_0) = \arccos(-\boldsymbol{u}_0^{*T} \cdot \boldsymbol{r}_0 / |\boldsymbol{u}_0^*| \cdot |\boldsymbol{r}_0|) \leq \alpha \implies \varphi_0^\# = \varphi_0$$

   Perform satisficing control $\tilde{\boldsymbol{u}}(q^\#, \lambda_\alpha^\#)$ Eq. (5.62) at phase $\varphi_0^\#$.

Figure 5.18: Design procedure to determine the design parameters $q,\ \lambda_\alpha,\ \varphi$ under the constraint conditions $|\boldsymbol{u}|_{\max},\ \alpha,\ \Delta V,\ T_{\text{conv}}$.

5.7 Conclusions

This chapter examined how to maintain a small-magnitude thrust angle based on continuous optimal feedback control for the problem of satellite rendezvous. Considering the constraints on the parameters set in the general quadratic performance index, a control design process was proposed using modal analysis to make the thrust angle small at the initial and final phases. Using a candidate CLF by solving the Riccati equation for the performance index considered, a new control applying the satisficing method was devised to meet the constraints strictly from start to finish. If the limitation angle is small, the devised control may become null transiently because the candidate CLF is not a strictly defined CLF. However, this chapter showed that thrust angle can be practically maintained and the control law leads to convergence at the origin in some simulations. Extending the theory to an eccentric orbit and time-varying system was explained and numerical calculations showed effectiveness. Although the application of two-dimensional plane motion was discussed, this technique can be extended easily to the design method, including out-of-plane motion. This method can also be applied to nonlinear control problems and can be extended to multiple control constraints, such as sensor field of view and sun direction.

Chapter 6

Satisficing Nonlinear Rendezvous Approach Under Control Magnitude and Direction Constraints

6.1 Introduction

The satisficing method was applied to the rendezvous problem with control direction constraints in the previous chapter. This chapter takes over the main results in the previous chapter (Mitani and Yamakawa, 2010, 2011). In Chapter 5, a Lyapunov function for the general linear quadratic regulator (LQR) was chosen as a local constrained control Lyapunov function (CCLF)(Sznaier *et al.*, 2003). By performing modal analysis in a linear system (Khalil, 2002), the thrust angle in the final convergent phase can be analytically predicted. The trajectory becomes optimal once the trajectory enters the invariant set where these constraints are no longer binding. To treat the input constraint in the transient phase, a new satisficing set to guarantee closed-loop stability under input constraints on the magnitude and direction is proposed, inspired by the idea of a smoothing technique (Bertrand and Epenoy, 2002; Gil-Fernandez and Gomez-Tierno, 2010). Then, a proposed controller is chosen to minimize a pre-Hamiltonian from the given set. The proposed controller in the set resembles that in (Mitani and Yamakawa, 2010) from the perspective of having stability and satisficing constraints, except magnitude constraint consideration. However, the proposed controller would be more suitable for the following reasons: firstly, since a local CCLF is chosen for the value function in the nonbinding case, the proposed controller becomes a unique optimal control solution where the constraint condition is nonbinding. Secondly, on

the other hand, the proposed controller gives a projection solution onto the input constraint set where the constraint condition is binding. The projected controller would be sub-optimal because it is guaranteed that the projection vector of a negative signed Lawden's primer vector onto the constraint boundary is optimal (Sukhanov and Prado, 2007, 2008).

6.2 Problem Statement

6.2.1 Dynamic Equations

Consider two satellites subject to the gravitational force of the Earth, one of which is flying in a given circular orbit of radius R_0 and referred to as a target, and the other flying nearby is referred to as a chaser. The chaser satellite is equipped with a continuous-thrust propulsion system and mass changes of satellites due to propellant usage are not taken into account for analysis. Introduce a rotating right-hand reference frame $o - \{\boldsymbol{\mathcal{R}}, \boldsymbol{\mathcal{S}}, \boldsymbol{\mathcal{W}}\}$, where o is the center of mass of the target, $\boldsymbol{\mathcal{R}}$ is in the radial direction, $\boldsymbol{\mathcal{S}}$ is in the flight direction, and $\boldsymbol{\mathcal{W}}$ is the direction outward from the orbital plane. Let $\boldsymbol{r}$ be the position vector of the chaser relative to the target, and let $\boldsymbol{u}$ be the control acceleration vector. Set $\boldsymbol{r} = x\boldsymbol{\mathcal{R}} + y\boldsymbol{\mathcal{S}} + z\boldsymbol{\mathcal{W}}$ and $\boldsymbol{u} = u_x\boldsymbol{\mathcal{R}} + u_y\boldsymbol{\mathcal{S}} + u_z\boldsymbol{\mathcal{W}}$. The relative motion of the follower with respect to the target is given by Newton's equations of motion as follows (Wie, 1998);

$$\ddot{x} = 2n\dot{y} + n^2(R_0 + x) - \frac{\mu}{R^3}(R_0 + x) + u_x \tag{6.1}$$

$$\ddot{y} = -2n\dot{x} + n^2 y - \frac{\mu}{R^3}y + u_y \tag{6.2}$$

$$\ddot{z} = -\frac{\mu}{R^3}z + u_z \tag{6.3}$$

where $\dot{\boldsymbol{a}}$ is the derivative with respect to time t, μ is the gravitational parameter of the Earth, $n = (\mu/R_0^3)^{1/2}$ is the orbit rate of the target, and $R = [(R_0+x)^2+y^2+z^2]^{1/2}$. The out-of-plane motion concerning z is independent of the in-plane motion determined by x and y. Because the out-of-plane motion is relatively simple, only the in-plane motion will be discussed. Introducing $\sigma = R_0^2\alpha_{\max}/\mu$, $\bar{\boldsymbol{r}} = (\bar{x}, \bar{y}) = (x, y)/(\sigma R_0)$ and replacing the independent variable t by $\tau = nt$, Eqs. (6.1) and (6.2) are transformed into the affine form:

$$\bar{\boldsymbol{x}}'(\tau) = f(\bar{\boldsymbol{x}}) + g\bar{\boldsymbol{u}}(\tau) \tag{6.4}$$

$$f(\bar{\boldsymbol{x}}) = A\bar{\boldsymbol{x}} + f_2(\bar{\boldsymbol{x}}) \tag{6.5}$$

$$g = B \tag{6.6}$$

where differentiation with respect to τ is indicated by $'$, $\bar{\boldsymbol{x}}(\tau) = [\bar{\boldsymbol{r}}\ \bar{\boldsymbol{r}}']^T \in \mathbf{R}^4$, $\bar{\boldsymbol{u}}(\tau) = \boldsymbol{u}(\tau)/\alpha_{\max} \in \mathbf{R}^2$ is the normalized control acceleration vector of the chaser at τ, as expressed in the $(\boldsymbol{\mathcal{R}}, \boldsymbol{\mathcal{S}}, \boldsymbol{\mathcal{W}})$ frame, $\bar{\boldsymbol{u}}(\tau)$ satisfies $\|\bar{\boldsymbol{u}}(\tau)\| \leq 1$, $\|\cdot\|$ denotes the Euclidean norm, $\alpha_{\max}$ is the maximum control acceleration, and

$$A = \begin{bmatrix} 0 & 0 & 1 & 0 \\ 0 & 0 & 0 & 1 \\ 3 & 0 & 0 & 2 \\ 0 & 0 & -2 & 0 \end{bmatrix},\ B = \begin{bmatrix} 0 & 0 \\ 0 & 0 \\ 1 & 0 \\ 0 & 1 \end{bmatrix} \tag{6.7}$$

$$f_2(\bar{\boldsymbol{x}}) = B \begin{bmatrix} -3\bar{x} - \left(\frac{1}{\sigma} + \bar{x}\right)\left(\frac{1}{\sigma^3 \bar{R}^3} - 1\right) \\ -\bar{y}\left(\frac{1}{\sigma^3 \bar{R}^3} - 1\right) \end{bmatrix} \tag{6.8}$$

where $\bar{R} = [(1/\sigma + \bar{x})^2 + \bar{y}^2]^{1/2}$. The linearized equations around the origin $\bar{x} = \bar{y} = 0$ are given by setting the nonlinear term $f_2(\bar{\boldsymbol{x}})$ to 0, which are known as Hill-Clohessy-Wiltshire equations. $f(\bar{\boldsymbol{x}})$ and $g(\bar{\boldsymbol{x}})$ are locally Lipschitz functions and $f(\mathbf{0}) = \mathbf{0}$. Hereinafter, all formulations are executed using the nondimensional values obtained using τ, which corresponds to the mean anomaly of the target. Therefore, the bars over $\boldsymbol{x}$ and $\boldsymbol{u}$ are not shown in the following sections.

6.2.2 Rendezvous Problem under Control Magnitude and Direction Constraints

Assume that the chaser is in an eccentric orbit $\Gamma = (A_0, \boldsymbol{e})$ in the inertial frame, where A_0 is the semimajor axis and $\boldsymbol{e}$ is the eccentricity vector. If the X coordinate of the perigee is $A_0 - a$, then the eccentricity $e = ||\boldsymbol{e}|| = a/A_0$ (Bando and Ichikawa, 2009). Consider the problem of a chaser at time t_0 and in the initial state $x_0 \in \Gamma$ being guided towards the target. The terminal time is free and the thrust direction, which represents the angle between the direction vector toward the target $-\boldsymbol{r}$ and the control direction vector $\boldsymbol{u}$, is constrained within the angle $\pm\gamma$ $(0 \leq \gamma \leq \pi)$ from the view of the chaser in the direction away from the target. Notice that the direction of control input $\boldsymbol{u}$ is opposite to that of injection $-\boldsymbol{u}$. The thrust angle and control input constraints are defined by

$$||\theta(\boldsymbol{u}, \boldsymbol{x})|| \leq \gamma \tag{6.9}$$

where θ is the signed control direction which defined as

$$-\hat{\boldsymbol{r}}^T \hat{\boldsymbol{u}} = \cos\theta \tag{6.10}$$

$$\hat{\boldsymbol{r}} \times \hat{\boldsymbol{u}} = \sin\theta \boldsymbol{\mathcal{W}} \tag{6.11}$$

Combined with magnitude constraint, the constrained input set U_C is defined as

$$U_C = \{\boldsymbol{u} \in \boldsymbol{R}^2 : ||\boldsymbol{u}|| \leq 1,\ ||\theta(\boldsymbol{u}, \boldsymbol{x})|| \leq \gamma\} \tag{6.12}$$

6.3 Satisficing Set Considering Magnitude and Direction Constraints

6.3.1 Description of the Constraint-Satisficing Set

To solve this problem, a satisficing method is used to satisfy rigidly U_C Eq. (6.12). Initially, according to Definition 4.2.1, we define CLF V which is positive definite, radially unbounded, and

$$\inf_{\boldsymbol{u}} \dot{V} = \inf_{\boldsymbol{u}} V_x^T[f(\boldsymbol{x}) + g(\boldsymbol{x})\boldsymbol{u}] < 0 \tag{6.13}$$

for all $\boldsymbol{x} \neq 0$. Specifically, if $\boldsymbol{u} \in U_C \subset \boldsymbol{R}^m$, $V(\boldsymbol{x})$ is said to be a constrained CLF (CCLF) (Sznaier *et al.*, 2003). From Definition 4.2.2, we define the satisficing set as follows:

$$S_b(t, \boldsymbol{x}) = \left\{\boldsymbol{u} \in \boldsymbol{R}^m :\ p_s(t, \boldsymbol{u}, \boldsymbol{x}) > \frac{1}{b(t, \boldsymbol{x})} p_r(t, \boldsymbol{u}, \boldsymbol{x})\right\} \tag{6.14}$$

Associate the notion of selectability with stability, and that of rejectability with instantaneous cost. In particular, let

$$p_s(\boldsymbol{u}, \boldsymbol{x}) = -V_x^T(\boldsymbol{x})(f(\boldsymbol{x}) + g\boldsymbol{u}) \tag{6.15}$$

where V is a CLF. Note that stabilizing control values make $p_s = -\dot{V}$ positive. Choose the rejectability criterion to be

$$p_r(\boldsymbol{u}, \boldsymbol{x}) = \left[\frac{1}{2}\boldsymbol{x}^T Q \boldsymbol{x} + \frac{1}{2}\boldsymbol{u}^T \boldsymbol{u} + \boldsymbol{x}^T N \boldsymbol{u}\right] + \varepsilon_m F_m(\boldsymbol{u}) + \varepsilon_d F_d(\boldsymbol{u}) \tag{6.16}$$

$$\varepsilon_m F_m(\boldsymbol{u}) = -\varepsilon_m \log u(1-u) \tag{6.17}$$

$$\varepsilon_d F_d(\boldsymbol{u}) = -\varepsilon_d u \log[w(\boldsymbol{r}, \boldsymbol{u})] \tag{6.18}$$

$$w(\boldsymbol{r}, \boldsymbol{u}) = \frac{\cos\theta - \cos\gamma}{1 - \cos\gamma} \tag{6.19}$$

where $Q = Q^T$ is a nonnegative matrix and N matrix satisfies the relation $Q - NN^T > 0$. The first term of Eq. (6.16) is a convex integrand of performance index J in the LQR problem. Introducing the term $\boldsymbol{x}^T N \boldsymbol{u}$ helps make the thrust angle θ small (Mitani and Yamakawa, 2011). $\varepsilon_m F_m$ and $\varepsilon_d F_d$ are continuous functions satisfying

$$\varepsilon_m F_m(\boldsymbol{u}) \geq 0, \quad \varepsilon_m > 0, \quad u \in (0, 1) \tag{6.20}$$

$$\varepsilon_d F_d(\boldsymbol{u}) \geq 0, \quad \varepsilon_d > 0, \quad w > 0 \tag{6.21}$$

If u approaches one or zero and w approaches $+0$, then $\varepsilon_m F_m(\boldsymbol{u}) \to +\infty$ and $\varepsilon_d F_d(\boldsymbol{u}) \to +\infty$ respectively. Therefore F_m and F_d are referred to as a barrier function for the constraints on magnitude and direction respectively (Bertrand and Epenoy, 2002; Mitani and Yamakawa, n.d.). Adding barrier functions $\varepsilon_m F_m$ and $\varepsilon_d F_d$ to p_r is the first attempt of its kind among the satisficing theory. Note that the new definition of p_r is a convex set of $\boldsymbol{u}(u, \theta)$, which are expressed in polar coordinates. Additionally p_s is a linear function in $\boldsymbol{u}$ and is, hence, concave in $\boldsymbol{u}$. For these choices of p_s and p_r, therefore, the satisficing set

$$\begin{aligned} S_b(\boldsymbol{x}) = \{\boldsymbol{u} \in \boldsymbol{R}^m : -V_x^T(f + g\boldsymbol{u}) \\ > \frac{1}{b}(\frac{1}{2}\boldsymbol{x}^T Q\boldsymbol{x} + \frac{1}{2}\boldsymbol{u}^T\boldsymbol{u} + \boldsymbol{x}^T N\boldsymbol{u} - \varepsilon_m \log u(1-u) - \varepsilon_d u \log w)\} \end{aligned} \tag{6.22}$$

is guaranteed to be a convex set.

Although the proposed additional constraint S_b cannot be represented as explicit parameterization, the S_b contour can be described using a semi-analytic approach. Define the following variables

$$c \triangleq \boldsymbol{x}^T Q\boldsymbol{x}/2 + bV_x^T f \tag{6.23}$$

$$\boldsymbol{p}_N \triangleq bg^T V_x + N^T\boldsymbol{x} \tag{6.24}$$

$$h \triangleq \frac{1}{2}\boldsymbol{p}_N^T\boldsymbol{p}_N - c \tag{6.25}$$

By substituting these to Eq. (6.22) and completing the square

$$S_b = \{\boldsymbol{u} \in \boldsymbol{R}^m : -\frac{1}{2}||\boldsymbol{u} + \boldsymbol{p}_N||^2 + h > -\varepsilon_m \log u(1-u) - \varepsilon_d u \log w\} \tag{6.26}$$

When a certain fixed direction $\hat{\boldsymbol{u}}$ is considered, the crossing points u_A and u_B of the following two convex and concave curves can be obtained by numerical analysis:

$$y_1 = -\frac{1}{2}||\boldsymbol{u} + \boldsymbol{p}_N||^2 + h \tag{6.27}$$

$$y_2 = -\varepsilon_m \log u(1-u) - \varepsilon_d u \log w \tag{6.28}$$

Then, $u \in (u_A(\hat{\boldsymbol{u}}),\ u_B(\hat{\boldsymbol{u}}))$ is a member of S_b. If Equation $y_1 = y_2$ has multiple root solution $u_A = u_B$, such a $\hat{\boldsymbol{u}}$ corresponds to the tangential line of S_b. In addition, there is a sole point $\boldsymbol{u} \in S_b$ which maximizes p_s to p_r/b, denoted by $\boldsymbol{u}^\varepsilon$. In other words, $\boldsymbol{u}^\varepsilon$ is a control input, which is an extremal value of the pre-Hamiltonian function $H_b^\varepsilon \triangleq -bp_s + p_r$ at instant time.

The control input $\boldsymbol{u}^\varepsilon$ minimizes the following pre-Hamiltonian:

$$\begin{aligned} H_b^\varepsilon &= -b(\boldsymbol{x})p_s(\boldsymbol{u}, \boldsymbol{x}) + p_r(\boldsymbol{u}, \boldsymbol{x}) \\ &= bV_x^T(f + g\boldsymbol{u}) \\ &\quad + \left[\frac{1}{2}\boldsymbol{x}^T Q\boldsymbol{x} + \frac{1}{2}\boldsymbol{u}^T\boldsymbol{u} + \boldsymbol{x}^T N\boldsymbol{u} - \varepsilon_m \log u(1-u) - \varepsilon_d u \log w\right] \end{aligned} \tag{6.29}$$

Substituting Eqs. (6.23) and (6.24) to Eq. (6.29), Eq. (6.29) is transformed into

$$H_b^\varepsilon = \frac{1}{2}\boldsymbol{u}^T\boldsymbol{u} + \boldsymbol{p}_N^T\boldsymbol{u} + c - \varepsilon_m \log u(1-u) - \varepsilon_d u \log w \tag{6.30}$$

The necessary optimality conditions $\partial H_b^\varepsilon / \partial \boldsymbol{u} = 0$ under the input constraints can be treated analytically by introducing a polar coordinate $\boldsymbol{u}(u, \theta)$. The solutions can be derived in the same manner as (Mitani and Yamakawa, n.d.).

$$\hat{\boldsymbol{u}}^\varepsilon = (\sin\theta^\varepsilon \cot\beta - \cos\theta^\varepsilon)\hat{\boldsymbol{r}} - \sin\theta^\varepsilon \csc\beta \hat{\boldsymbol{p}}_N \tag{6.31}$$

θ^ε is the solution to

$$\sin(\theta^\varepsilon - \beta)(\cos\gamma - \cos\theta^\varepsilon) - \tilde{\varepsilon}_d \sin\theta^\varepsilon = 0 \tag{6.32}$$

and u^ε is the solution to

$$u^\varepsilon - \frac{\varepsilon_u(1-2u^\varepsilon)}{u^\varepsilon(1-u^\varepsilon)} - \tilde{p}_N = 0 \tag{6.33}$$

where $\tilde{\varepsilon}_d = \varepsilon_d / p_N$, $\tilde{p}_N = -\boldsymbol{p}_N^T\hat{\boldsymbol{u}} + \varepsilon_d \log w$ and β is defined as the thrust angle, $\hat{\boldsymbol{r}}^T\hat{\boldsymbol{p}}_N = \cos\beta$, $-\hat{\boldsymbol{r}} \times \hat{\boldsymbol{p}}_N = \sin\beta\boldsymbol{\mathcal{W}}$.

Since H_b^ε is minimized at $\boldsymbol{u} = \boldsymbol{u}^\varepsilon$, the condition for $S_b \neq \phi$ is guaranteed if and only if

$$H_b^\varepsilon(\boldsymbol{u}^\varepsilon) \leq 0 \tag{6.34}$$

Therefore, the lower limit of b or $\underline{b}$ is the solution to

$$H_b^\varepsilon(\boldsymbol{u}^\varepsilon) = 0 \tag{6.35}$$

Consider the condition that $\boldsymbol{u} \in S_b$ exists for the certain direction $\hat{\boldsymbol{u}}$ in the case that $b \geq \underline{b}$ is chosen. Since S_b is a convex set, a certain direction $\hat{\boldsymbol{u}}$ exists such that the direction is tangential of S_b boundary. It is clear that $u, \hat{\boldsymbol{u}}$ satisfy the conditions

$$H_b^\varepsilon(u, \hat{\boldsymbol{u}}) = 0 \tag{6.36}$$

$$\frac{\partial H_b^\varepsilon(u, \hat{\boldsymbol{u}})}{\partial u} = 0 \tag{6.37}$$

Based on the convexity of S_b, two solutions exist provided $b > \underline{b}$. $\boldsymbol{u} \in S_b$ exists and if the direction $\hat{\boldsymbol{u}}$ between the two solutions $\hat{\boldsymbol{u}}_1$ and $\hat{\boldsymbol{u}}_2$ is chosen. Such a direction can be given as

$$\hat{\boldsymbol{u}} = \frac{s\hat{\boldsymbol{u}}_1 + (1-s)\hat{\boldsymbol{u}}_2}{||s\hat{\boldsymbol{u}}_1 + (1-s)\hat{\boldsymbol{u}}_2||}, \quad 0 \leq s \leq 1 \tag{6.38}$$

6.3.2 Comparison between Constraint-free and Constraint- Satisficing Method

In Table 6.1, the differences in parameters between constraint-free satisficing (Curtis and Beard, 2004) and constraint one are summarized. Constraint-free satisficing corresponds to $\varepsilon = 0$, whereupon the condition for $S_b \neq \phi$ Eq. (6.34) becomes a quadratic inequality for b. The lower limit $\underline{b}$ can be obtained as follows

$$\underline{b} = \begin{cases} \dfrac{\tilde{\omega} + \sqrt{\tilde{\omega}^2 + p^2 \cdot \tilde{q}}}{p^2}, & \text{if } \boldsymbol{p} \neq \mathbf{0} \\ \dfrac{\tilde{q}}{-2\tilde{\omega}}, & \text{if } \boldsymbol{p} = \mathbf{0} \end{cases} \tag{6.39}$$

where $\boldsymbol{p} = g^T V_x$, $\tilde{\omega} = V_x^T f - V_x^T g N^T \boldsymbol{x}$, and $\tilde{q} = \boldsymbol{x}^T (Q - NN^T)\boldsymbol{x}$. Furthermore, if S_b is nonempty, it is given by

$$S_b = \left\{ -\boldsymbol{p}_N + \boldsymbol{\nu}\sqrt{2h} : \ ||\boldsymbol{\nu}|| < 1 \right\} \tag{6.40}$$

As discussed in Chapter 4, Equation (6.40) provides an explicit formula for control values which satisfy this condition whenever S_b is nonempty. When $b = \underline{b}$, the satisficing set has the input of Sontag's formula (Sontag, 1989). While the constraint-free satisficing set has $\boldsymbol{\nu}$ as a design parameter, the constraint-satisficing set has $\hat{\boldsymbol{u}}$ and $u \in [u_A(\hat{\boldsymbol{u}}) \ \ u_B(\hat{\boldsymbol{u}})]$ as design parameters.

Set $\varepsilon_m = \varepsilon_d = \varepsilon > 0$ for simplicity. Figures 6.1a and 6.1b show how to vary S_b according to selectivity index $b = 1$, 5 and 100 in the unconstrained case ($\varepsilon = 0$) and the constraint case ($\varepsilon = 1 \times 10^{-5}$ and $\gamma = 30°$). Note that nondimensional u is normalized as 1 through this chapter. It is assumed that CCLF, states at a certain instantaneous time, b and $\alpha_{\max}$ are all the same. The open white points P_b in Figs. 6.1a and 6.1b are the controller inputs $\boldsymbol{u}^\varepsilon$ on each b. Initially, in the case without constraints, the circler radius of S_b set rises with increasing b increases (see Fig. 6.1a). The selectivity index b plays a critical role in the size of $S_b(\boldsymbol{x})$. Subsequently, the larger value of b decreases the curvature of the $S_b(\boldsymbol{x})$ boundary to approach asymptotically the half-plane $S_\infty(\boldsymbol{x})$ which has the normal vector as $-g^T V_x$. Secondly, when input constraints are considered, the boundary shape of S_b becomes deformed as thus suppressed by the control input boundary of U_C (see Fig. 6.1b). In addition, S_b approaches gradually a mere intersection between S_b without constraints and the constraint input set U_C decreases as ε. However, the smoothness of the S_b boundary is retained provided $\varepsilon > 0$. Even if $-\boldsymbol{p}_N$ vector steps out of U_C, $\boldsymbol{u}_b^\varepsilon \in S_b \cap U_C$ can be adequately obtained provided $H_b^\varepsilon(\boldsymbol{u}^\varepsilon) \leq 0$ Eq. (6.34) holds true.

Table 6.1: Comparison between constraint-free S_b (Curtis and Beard, 2004) and proposed constraint S_b.

Item	Original Satisficing	Constraint-Satisficing
Selectivity, p_s	$-V_x^T(f+g\boldsymbol{u})$	$-V_x^T(f+g\boldsymbol{u})$
Rejectability, p_r	$\frac{1}{2}\boldsymbol{x}^T Q\boldsymbol{x}+\frac{1}{2}\boldsymbol{u}^T\boldsymbol{u}+\boldsymbol{x}^T N\boldsymbol{u}$	$\frac{1}{2}\boldsymbol{x}^T Q\boldsymbol{x}+\frac{1}{2}\boldsymbol{u}^T\boldsymbol{u}+\boldsymbol{x}^T N\boldsymbol{u}$ $-\varepsilon_m \log u(1-u)-\varepsilon_d u\log w$
Condition for $S_b\neq\phi$	$h\geq 0$	$H_b^\varepsilon(\boldsymbol{u}^\varepsilon)=\frac{1}{2}\|\|\boldsymbol{u}^\varepsilon+\boldsymbol{p}_N\|\|^2-h$ $-\varepsilon_m\log u^\varepsilon(1-u^\varepsilon)-\varepsilon_d u^\varepsilon\log w\leq 0$
Limit, $\underline{b}$	$\frac{\tilde{\omega}+\sqrt{\tilde{\omega}^2+p^2\cdot\tilde{q}}}{p^2}$, if $\boldsymbol{p}\neq\boldsymbol{0}$ $\frac{\tilde{q}}{-2\tilde{\omega}}$, if $\boldsymbol{p}=\boldsymbol{0}$	solution of $H_b^\varepsilon(\boldsymbol{u}^\varepsilon)=0$.
Control, $\boldsymbol{u}\in S_b$	$-\boldsymbol{p}_N+\boldsymbol{\nu}\sqrt{2h}$	$u\cdot\hat{\boldsymbol{u}}$
Design Parameters	$\nu\in\boldsymbol{R}^m, \|\|\boldsymbol{\nu}\|\|\leq 1$	$\hat{\boldsymbol{u}}=\frac{s\hat{\boldsymbol{u}}_1+(1-s)\hat{\boldsymbol{u}}_2}{\|\|s\hat{\boldsymbol{u}}_1+(1-s)\hat{\boldsymbol{u}}_2\|\|},\ 0\leq s\leq 1,\ \|\|\hat{\boldsymbol{u}}\|\|=1$ $u\in[u_A(\hat{\boldsymbol{u}})\ \ u_B(\hat{\boldsymbol{u}})]$ $\hat{\boldsymbol{u}}_1,\hat{\boldsymbol{u}}_2$; solutions of Eqs. (6.36) and (6.37) u_A,u_B; solutions of Eq. (6.36)
Sub-optimal controller	$\boldsymbol{u}^*=-\boldsymbol{p}_N\ (\boldsymbol{\nu}=\boldsymbol{0})$	$\boldsymbol{u}^\varepsilon=u^\varepsilon\cdot\hat{\boldsymbol{u}}^\varepsilon$ $\hat{\boldsymbol{u}}^\varepsilon=(\sin\theta^\varepsilon\cot\beta-\cos\theta^\varepsilon)\hat{\boldsymbol{r}}-\sin\theta^\varepsilon\csc\beta\hat{\boldsymbol{p}}$ θ^ε; solution to Eq. (6.32) u^ε; solution to Eq. (6.33)

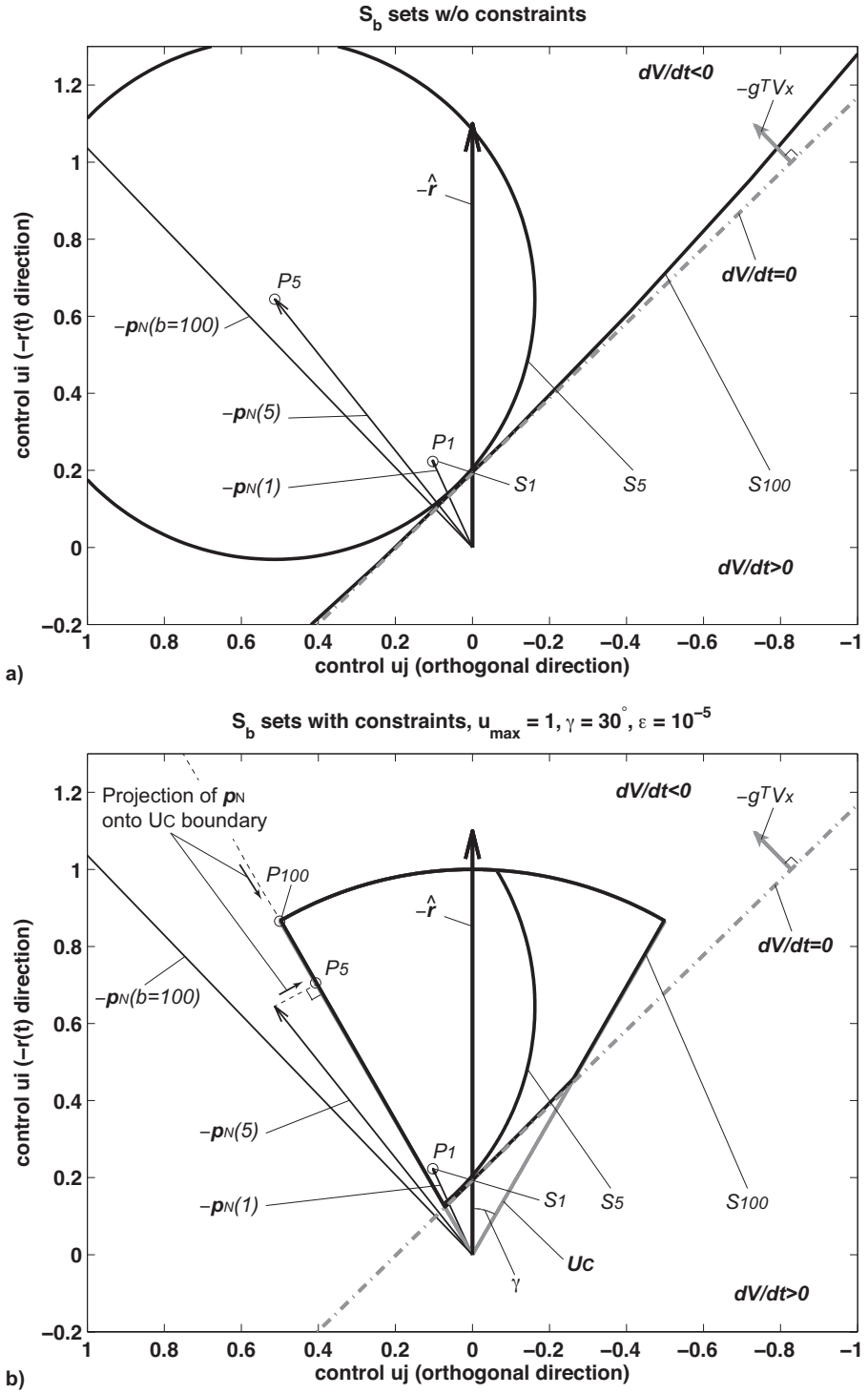

Figure 6.1: The comparison between a) S_b without constraints and b) S_b with input constraints, $\gamma = 30°$, $\varepsilon = 10^{-5}$.

6.4 Proposed Controller from the Constraint-Satisficing Set

6.4.1 Dual Control using the Satisficing Method

In the previous section, the constraint-satisficing set S_b was defined. If a "complete" CCLF that respects the input constraints in all states can be chosen, S_b is nonempty in all states. Subsequently, the state trajectory converges to the origin when any controller $\boldsymbol{u}(\boldsymbol{x}) \in S_b$, $b \geq \underline{b}$ is chosen. However, such CCLFs are generally extremely hard to devise. Therefore a local CCLF that respects the input constraints in restricted states is conventionally taken. In this case, if $\boldsymbol{u}(\boldsymbol{x}) \in S_b$ is inappropriately chosen, S_b falls into an empty set in some states and the state trajectory may not converge to the origin in the worst case.

Following the cases of success in MPC research, the generalized idea of specifying the terminal state constraint set X, including the origin (Maciejowski, 2002), is adopted and the controller is designed to have dual modes. The main design concept involves moving the state into X with one controller and continuously switching to another controller once the state goes into X. In this concept, the latter controller must guarantee that the state is stabilized at the origin once the state is included in X. Generally, it is assumed that all constraints are nonbinding in X, meaning an unconstrained ordinal controller would be adequate for the latter controller. In this section, it is shown that the controller $\boldsymbol{u}^{\varepsilon} \in S_b$ has both former and latter control mode properties if a local CCLF and control parameters are adequately chosen.

First, the quadratic formed Lyapunov function

$$V(\boldsymbol{x}) = \frac{1}{2}\boldsymbol{x}^T S \boldsymbol{x} \tag{6.41}$$

is employed as a local CCLF, where $S = S^T > 0$ is a unique nonnegative solution for the Algebraic Riccati Equation (ARE)

$$A^T S + SA - (SB + N)(B^T S + N^T) + Q = 0 \tag{6.42}$$

It is justified to choose V Eq. (6.41) as a candidate CCLF for the following lemmas:

Lemma 6.4.1 V($\boldsymbol{x}$) Eq. (6.41) is chosen as a local CCLF. The extremal controller $\boldsymbol{u}_{\mathrm{Proj}} = \lim_{\varepsilon \to 0} \boldsymbol{u}^{\varepsilon}$ satisfies the following properties:

1. When the constraint condition is nonbinding, $\boldsymbol{u}_{\mathrm{Proj}}$ is a state-feedback controller

$$-\boldsymbol{p}_N = -(bB^T S + N^T)\boldsymbol{x} \tag{6.43}$$

Specifically, $-\boldsymbol{p}_N$ is an optimal feedback controller that minimizes

$$J = \int_0^\infty \frac{1}{2}\boldsymbol{x}^T Q\boldsymbol{x} + \frac{1}{2}\boldsymbol{u}^T\boldsymbol{u} + \boldsymbol{x}^T N\boldsymbol{u}\ \mathrm{d}t \tag{6.44}$$

if $b(\boldsymbol{x}) = 1$ and the system dynamics are linear.

2. When the constraint condition is binding, $\boldsymbol{u}_{\mathrm{Proj}}$ becomes the projection of $-\boldsymbol{p}_N$ onto the boundary of U_C, and is smoothly connected to $-\boldsymbol{p}_N$ when no constraint condition is binding.

Proof: Substituting Eq. (6.41) to Eq. (6.24), $-\boldsymbol{p}_N$ reduces to Eq. (6.43) and $\boldsymbol{u}_{\mathrm{Proj}} = -\boldsymbol{p}_N$ when the constraint condition is nonbinding. As ε_m and ε_d approach 0, the explicit forms of the extremal controller $\boldsymbol{u}_{\mathrm{Proj}} = \lim_{\varepsilon\to 0}\boldsymbol{u}^\varepsilon$ are given as follows:

$$\hat{\boldsymbol{u}}_{\mathrm{Proj}} = \begin{cases} -\hat{\boldsymbol{p}}_N, & \beta \le \gamma \\ (\sin\gamma\cot\beta - \cos\gamma)\hat{\boldsymbol{r}} - \sin\gamma\csc\beta\hat{\boldsymbol{p}}_N, & \beta > \gamma \end{cases} \tag{6.45}$$

$$u_{\mathrm{Proj}} = \begin{cases} -\boldsymbol{p}_N^T\hat{\boldsymbol{u}}_{\mathrm{Proj}}, & -\boldsymbol{p}_N^T\hat{\boldsymbol{u}}_{\mathrm{Proj}} \le 1 \\ 1, & -\boldsymbol{p}_N^T\hat{\boldsymbol{u}}_{\mathrm{Proj}} > 1 \end{cases} \tag{6.46}$$

Therefore $\boldsymbol{u}_{\mathrm{Proj}}$ is the projection of $-\boldsymbol{p}_N$ vector onto the constraint boundary ∂U_C. □

In addition, the following lemma implies that the constraint condition is nonbinding with $\boldsymbol{u}_{\mathrm{Proj}}$ as $||\boldsymbol{x}||$ approaches 0 if the selectivity index b and the weight matrix parameters Q, N are adequately chosen.

Lemma 6.4.2 (Mitani and Yamakawa, 2011) The following parameter settings are considered:

$$Q = \mathrm{diag}(q, q, 0, 0) \tag{6.47}$$

$$N = \begin{bmatrix} \sqrt{\eta q} I_{2\times 2} \\ O_{2\times 2} \end{bmatrix} \tag{6.48}$$

The values $q > 0$ and $\eta \in [0\ 1)$ are independent design parameters in the performance index Eq. (6.44). Suppose that the controller $-\boldsymbol{p}_N$ is used. Given $\gamma \in (0, \pi]$, there is a parameter set (q, η, b) such that $||\boldsymbol{p}_N|| \le 1$ and the maximum thrust angle $||\theta||_{\max} < \gamma$ are satisfied when $||\boldsymbol{x}||$ approaches 0.

Proof: At first, $||\boldsymbol{p}_N|| \to 0$ as $||\boldsymbol{x}|| \to 0$ because $-\boldsymbol{p}_N$ is a state-feedback controller. For the linear system case, it is shown in Ref. (Mitani and Yamakawa, 2011) that if a parameter set (q, η, b) is adequately chosen, $||\theta||_{\max} < \gamma$ is satisfied when $||\boldsymbol{x}||$ approaches 0. For the nonlinear system, if a parameter set (q, η, b) is adequately chosen and the feedback controller $-\boldsymbol{p}_N$ is used, the state trajectory converges to the origin

without any binding of the constraints as $||\boldsymbol{x}||$ approaches 0 and nonlinearity become weak ($||f_2(\boldsymbol{x})|| \to 0$). $\square$

When reassigning the poles of the closed-loop with optimal state-feedback control $-\boldsymbol{p}_N$, eigenmodes divide into two groups: slowly and highly damped modes respectively. During the final approach phase, slowly damped modes mainly determine $||\theta||_{\max}$ (Mitani and Yamakawa, 2011). In other words, the state trajectory $\boldsymbol{x}$ converges to the subspace W spanned by eigenvectors of the slowly damped modes. Define the subset $X \in \boldsymbol{R}^4$ as

$$X = X_m \cap X_d \tag{6.49}$$

$$X_m = \{\boldsymbol{x} \in \boldsymbol{R}^4 : \boldsymbol{x}^T(bSB + N)(bB^TS + N^T)\boldsymbol{x} \leq k_m\} \tag{6.50}$$

$$X_d = \left\{\boldsymbol{x} \in \boldsymbol{R}^4 : \boldsymbol{x} = \boldsymbol{w} + \frac{k_d||\boldsymbol{w}||}{||\boldsymbol{w}_\perp||}\boldsymbol{w}_\perp,\ \boldsymbol{w} \in W, \boldsymbol{w}_\perp \in W_\perp\right\} \tag{6.51}$$

where $W_\perp$ is a complementary set of W (the subspace spanned by eigenvectors of the highly damped modes, and $W \oplus W_\perp = \boldsymbol{R}^4$). Clearly, the origin is included in X. Therefore X is the terminal state constraint set if $k_m(t_1), k_d(t_1) \in (0, 1]$ is adequately chosen to keep $\boldsymbol{x}(t)$ into X for $t > t_1$.

6.4.2 Superior Efficacy of the Controller

The proposed controller $\boldsymbol{u}_{\text{Proj}} = \lim_{\varepsilon \to 0} \boldsymbol{u}^\varepsilon$ resembles the authors' previous proposed controller considering the input constraint in (Mitani and Yamakawa, 2011). In this section, the difference and efficacy are briefly explained. In the previous method (Mitani and Yamakawa, 2011), the optimal controller without constraint is projected onto U_C along the half-plane boundary of S_∞, meaning the projected controller $\tilde{\boldsymbol{u}}$ will be included in S_∞ provided the control magnitude constraint $||\boldsymbol{u}|| \leq 1$ is not imposed on the system. However, when the boundary of U_C is closely parallel to the half-plane boundary of S_∞, the controller input becomes excessive. To avoid this problem, a controller is not activated in the case where the angle between the boundaries of U_C and S_∞ is less $\delta_{\text{margin}} > 0$. Conversely, the proposed controller $\boldsymbol{u}_{\text{Proj}}$ is the projection of $-\boldsymbol{p}_N$ onto the boundary of U_C. The magnitude of $\boldsymbol{u}_{\text{Proj}}$ is sure to be smaller than that of $-\boldsymbol{p}_N$. Figure 6.2 shows the difference in projection between $\tilde{\boldsymbol{u}}$ and $\boldsymbol{u}_{\text{Proj}}$ on the control space at a certain instantaneous time.

In addition, the proposed controller would be more suitable for the following reasons: At first, since a local CCLF is chosen for the unconstrained value function in the nonbinding case, the proposed controller becomes the sole optimal control solution according to Pontryagin's Minimum Principle, where the constraint condition is nonbinding. Second, on the other hand, the proposed controller gives a projection solution

onto the input constraint set where the constraint condition is binding. The projected controller would be sub-optimal because it is guaranteed that the projection vector of a negative signed Lawden's primer vector onto constraint boundary is optimal (Sukhanov and Prado, 2007, 2008).

Finally, the proposed controller has extensibility for various conditions on input constraints by selecting the perturbation parameters ε_m and ε_d. When $\varepsilon_m = \varepsilon_d = 0$, the constraint S_b set is completely identical to the original S_b set that Curtis proposed in (Curtis and Beard, 2004, 2002*a*,*b*). When $\varepsilon_m > 0$ and $\varepsilon_d = 0$, the S_b set reduces to the satisficing set only with magnitude constraint and when $\varepsilon_m = 0$ and $\varepsilon_d > 0$, the S_b set reduces to the satisficing set only with direction constraint. There is no need for geometric or condition branching consideration, solely the simple calculation of $\boldsymbol{u}^{\varepsilon}$.

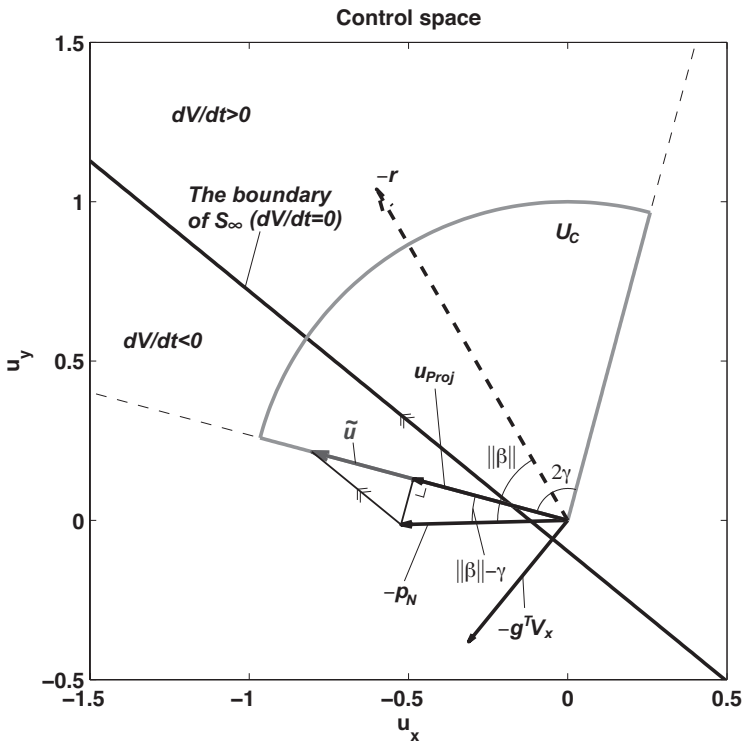

Figure 6.2: The difference in projection between $\tilde{\boldsymbol{u}}$ and $\boldsymbol{u}_{\mathrm{Proj}}$.

6.4.3 Stability Analysis

To generate the controller $\boldsymbol{u}_{\mathrm{Proj}}$, the optimal controller $-\boldsymbol{p}_N$ is projected orthogonally to U_C and an additional magnitude constraint is considered. Therefore the projected controller $\boldsymbol{u}_{\mathrm{Proj}}$ is not necessarily stable from the perspective of Lyapunov stability. In this section, the stability of the new proposed controller is investigated. $\boldsymbol{u}_{\mathrm{Proj}}$ in

another form is written as

$$\boldsymbol{u}_{\text{Proj}} = -(1-\chi)\cos\Delta\beta R(\Delta\beta)\boldsymbol{p}_N \tag{6.52}$$

where

$$R(\Delta\beta) = \begin{bmatrix} \cos\Delta\beta & -\sin\Delta\beta \\ \sin\Delta\beta & \cos\Delta\beta \end{bmatrix} \tag{6.53}$$

and

$$\Delta\beta = \begin{cases} 0 & \text{if } ||\beta|| - \gamma \leq 0 \\ \text{sign}(\beta)(||\beta|| - \gamma) & \text{if } 0 < ||\beta|| - \gamma \leq \pi/2 \\ \text{sign}(\beta)\pi/2 & \text{if } \pi/2 < ||\beta|| - \gamma \end{cases} \tag{6.54}$$

$$\chi = \begin{cases} 0 & \text{if } ||\boldsymbol{p}_N||\cos\Delta\beta \leq 1 \\ 1 - \dfrac{1}{||\boldsymbol{p}_N||\cos\Delta\beta} & \text{if } ||\boldsymbol{p}_N||\cos\Delta\beta > 1 \end{cases} \tag{6.55}$$

Introduced variables $(\chi, \Delta\beta)$ represent the degrees of deviation of $-\boldsymbol{p}_N$ from U_C.

Substitute Eqs. (6.43) and (6.52) to the linearized system equation $\dot{\boldsymbol{x}} = A\boldsymbol{x}$, whereupon the closed-loop system is formed as

$$\dot{\boldsymbol{x}}(t) = A_c(\chi, \Delta\beta)\boldsymbol{x}(t) \tag{6.56}$$

where

$$A_c(\chi, \Delta\beta) = A - (1-\chi)\cos\Delta\beta BR(\Delta\beta)(bB^TS + N^T) \tag{6.57}$$

When no constraint is binding, $(\chi, \Delta\beta) = (0, 0)$, then $A_c(0, 0)$ is the closed-loop matrix with a controller $-\boldsymbol{p}_N$. The poles of $A_c(\chi, \Delta\beta)$ represent the stability about the origin in global $\boldsymbol{x} \in \boldsymbol{R}^n$. It is noted that the optimal controller $-\boldsymbol{p}_N$ has 3 controller parameters: the values of LQR weight matrices q, η, and the sensitivity index $b(\boldsymbol{x})$. For example, Fig. 6.3 shows the trajectories of poles of $A_c(\chi, \Delta\beta)$ where $(q, \eta, b) = (0.01, 0.9, 1)$ and $\chi = 0$, varying $\Delta\beta$ from $-90°$ to $90°$. Starting from $\Delta\beta = -90°$, poles start at those of A since $\Delta\beta = -90°$ corresponds to zero input. From $-90°$ to $0°$, slowly damped modes have negative real parts but highly damped modes have positive real parts at first. Poles at $\Delta\beta = 0$ correspond to those of $A_c(0, 0)$, which is Hurwitz. From $0°$ to $90°$, in contrast, highly damped modes retain negative real parts but the modes slowly start having positive real parts. Both poles return to the poles of A since $\Delta\beta = 90°$ also corresponds to zero input.

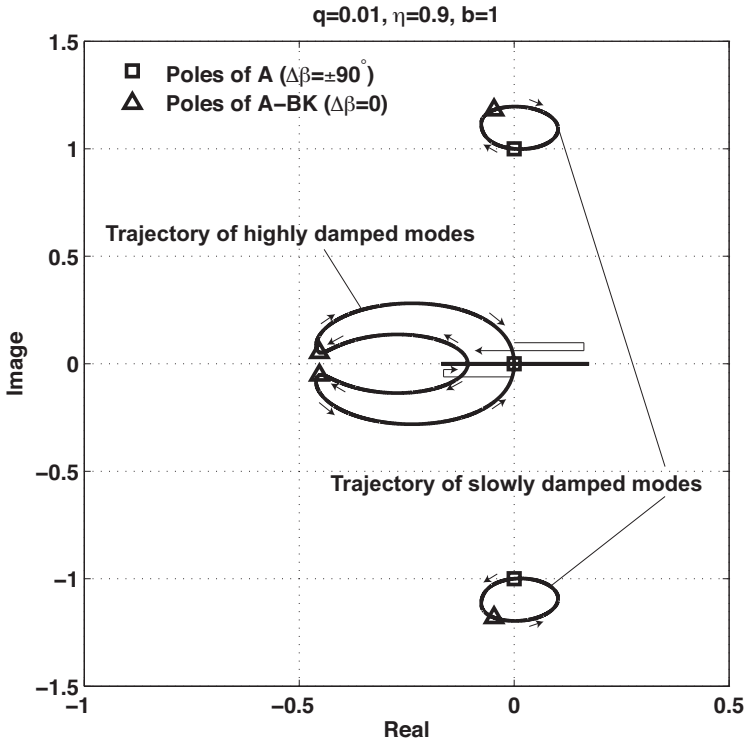

Figure 6.3: Trajectories of closed-loop pole assignments.

In this manner, examine how the stability region represented for the deviation parameters $(\chi, \Delta\beta)$ changes if the control parameters (q, η, b) are changed. It should be noted that

$$\begin{aligned} \dot{V} &= \boldsymbol{x}^T S[A\boldsymbol{x} + f_2(\boldsymbol{x}) - (1-\chi)\cos\Delta\beta BR(\Delta\beta)(bB^T S + N^T)\boldsymbol{x}] \\ &= \boldsymbol{x}^T S A_c(\chi, \Delta\beta)\boldsymbol{x} + \boldsymbol{x}^T S f_2(\boldsymbol{x}) \end{aligned} \tag{6.58}$$

then $A_c(\chi, \Delta\beta) < 0 \rightarrow \dot{V} < 0$ if the system is linear. Before the stability region is investigated, examine the physical meaning of poles in closed form more closely. The Jordan canonical form of A matrix J and its similarity transformation matrix V_J are

$$J = \begin{bmatrix} 0 & 1 & 0 & 0 \\ 0 & 0 & 0 & 0 \\ 0 & 0 & -j & 0 \\ 0 & 0 & 0 & j \end{bmatrix}, \; V_J = \begin{bmatrix} 0 & 4 & -3/2 & -3/2 \\ -6 & 0 & 3j & -3j \\ 0 & 0 & 3/2j & -3/2j \\ 0 & -6 & 3 & 3 \end{bmatrix} \tag{6.59}$$

Since the relation $V_J^{-1} A V_J = J$ holds, the free trajectory solution after the transformation $\boldsymbol{\xi} = V_J^{-1}\boldsymbol{x}$ is

$$\boldsymbol{\xi} = [a_\xi + b_\xi t, \; b_\xi, \; c_\xi e^{-jt}, \; \bar{c}_\xi e^{jt}]^T \tag{6.60}$$

where a_ξ, $b_\xi \in \boldsymbol{R}^1$, and $c_\xi \in \boldsymbol{C}^1$ are integral constants determined by the initial state. Therefore, this shows that highly damped modes correspond to constant and drift components, while slowly damped modes correspond to periodic components. Since highly damped modes converge first, the remaining trajectory tends to be periodic.

Stability dependency of parameter (q, η)

Fixing the controller parameters (q, η, b) and varying the deviation parameters $(\chi, \Delta\beta)$, the stability boundary lines between positive and negative real parts of both highly and slowly damped modes can be drawn respectively on the $(\chi, \Delta\beta)$ plot. At first, examine how to change the stability region when (q, η) are parametrically changed and b is fixed. Figure 6.4 shows the stability boundary lines of both highly and slowly damped modes in the case of q=0.01, 0.1, 1 and 10. The initial words "h" and "s" in the figure represent highly and slowly damped modes respectively. As q parameter increases, the region where both eigenmodes have negative real parts narrows.

Figure 6.5 shows the region where both eigenmodes have negative real parts in the case of q=0.01, 0.1, 1 and 10, which widens with decreasing parameter η. Note that highly damped modes have negative real parts in the wide region of $\Delta\beta = +90°$ side, as shown in Fig. 6.5, although both mode stabilized regions becomes narrow as η approaches 1, as shown in Fig. 6.5.

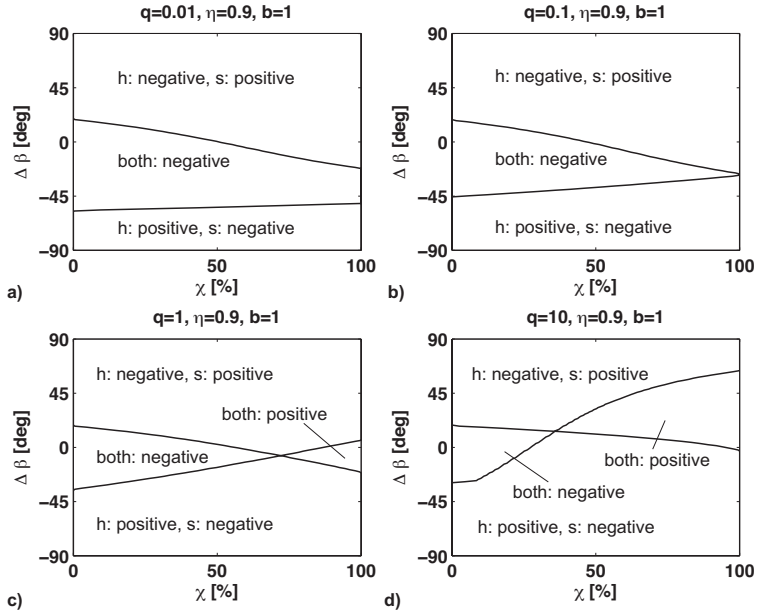

Figure 6.4: Stabilized limit in the case $\eta = 0.9$, and $b = 1$.

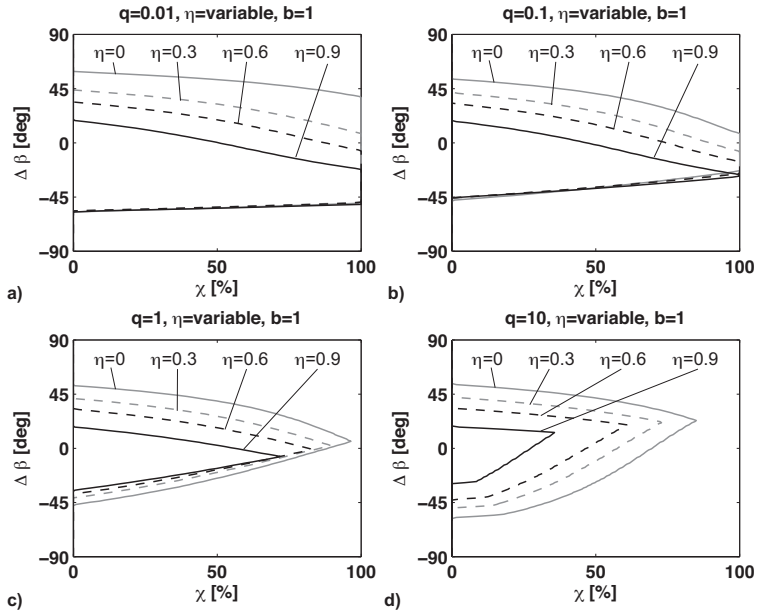

Figure 6.5: Stabilized limit in the case $b = 1$ varying η.

Stability dependency of the selectivity index b

Next, examine how to change the stability region when b is parametrically changed and (q, η) are fixed. The following lemma is satisfied:

Lemma 6.4.3 For any deviation parameter $\chi \neq 1$ and $\Delta\beta \neq \pm\pi/2$, there is $b_S > 0$ such that $A_c(\chi, \Delta\beta)$ is Hurwitz with (q, η) and $b > b_S$. And slowly damped modes converge to finite poles and highly damped modes diverge to the negative real axis.

The proof of Lemma 6.4.3 is shown in Appendix D. Figure 6.6 shows the stabilized region varying b in the case of $\eta = 0.9$, q=0.01, 0.1, 1 and 10. As shown in Lemma 6.4.3, the stabilized region is extended with increasing b.

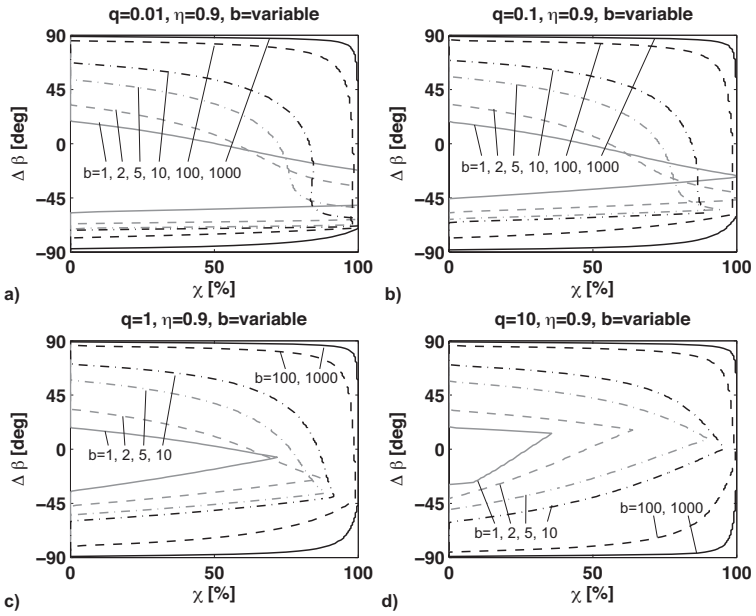

Figure 6.6: Stabilized limit in the case $\eta = 0.9$ varying b.

The final thrust angle dependencies of (q, η, b)

Figure 6.7 shows the maximum final thrust angle $||\theta||_\infty$, or $||\theta||_{\infty,\max}$ using Eq. (38) in (Mitani and Yamakawa, 2011) when varying (q, η). Each figure corresponds to the case in the selectivity index b =1, 2, 5, and 10 respectively. The case $b = 1$ (Fig. 6.7a), in which optimal control is applied, is essentially identical to Fig. 5.7 in Chapter 5 (Mitani and Yamakawa, 2011) although only slowly damped modes are shown here. Figure 6.7 shows that $||\theta||_{\infty,\max}$ declines for fixed q when a larger η is set. However, choosing a large b is not likely to be a suitable controller design for the meaning of keeping the

thrust angle small. Actually, as shown in Fig. 6.7, $||\theta||_{\infty,\max}$ tends to become larger than that in the case $b = 1$ for fixed q and η when a larger b is set. Therefore the b parameter should be set to trade off stability and the final thrust angle. Table 6.2 summarizes the control parameters (q, η, b) dependencies on the stability region and the final thrust angle.

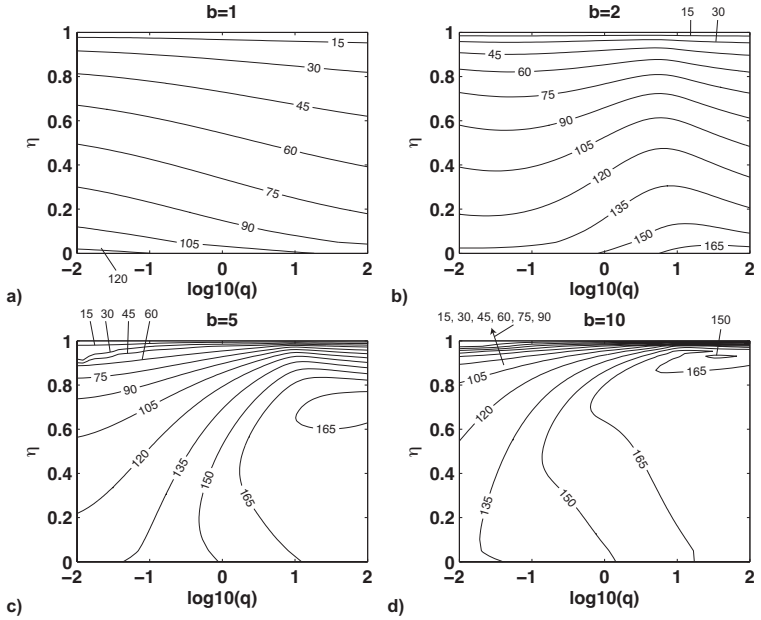

Figure 6.7: Estimation of $|\theta|_{\infty,\max}$ (in degrees) as they approach the origin.

Table 6.2: Constants and common parameters.

Parameter	Stability region	Fig.	Final thrust angle	Fig.
$q(0 \to \infty)$	$\searrow$ (narrow)	6.3	- (depend on η, b)	6.6
$\eta(0 \to 1)$	$\searrow$ (narrow)	6.4	$\searrow$ (small)	6.6
$b(0 \to \infty)$	$\nearrow$ (wide)	6.5	$\nearrow$ (large)	6.6

6.5 Example of Numerical Analysis

For numerical simulations, a Keplerian orbit of the target of the semimajor axis $A_0 = R_e + h_c$ km is considered, in which $h_c = 500$ km, the radius of the Earth R_e, and the gravitational constant of the Earth μ are given. Accordingly, the period of orbit is $T = 5,677$ s, and the orbital rate $n = 1.1068 \times 10^{-3}$ rad/s is considered (see Table

Table 6.3: Constants and common parameters.

Constants	Values
R_e	6,378.136 km
μ	398,601 $\mathrm{km}^3/\mathrm{s}^2$
h_c	500 km
n	1.1068×10^{-3} rad/s
T	5,677 s
$\alpha_{\max}$	0.02 $\mathrm{m/s}^2$
γ	60 deg

6.3). In addition, $\alpha_{\max} = 0.02$ $\mathrm{m/s}^2$ is considered to be the maximum acceleration of control.

6.5.1 Parameter-setting Case: LQR Control ($b = 1$)

Consider the problem of rendezvous to try the proposed method. The chaser flies around at 100 km in an eccentricity axis. Figure 6.8 shows an example of some designed rendezvous trajectories, setting the design parameters $(q, \eta, b) = (0.01, 0.9, 1)$, thrust constraint $\gamma = 60$ deg, and start rendezvous point $\varphi_0 = 60k$ $(k = 0, \cdots, 5)$ respectively. In Fig. 6.8, the chaser's initial periodical orbit before control is shown with a fine dotted line T_s and the rendezvous start point. A heavy solid line T_P and dotted lines T_O show the trajectory profiles with the proposed control $\boldsymbol{u}_{\mathrm{Proj}}$ Eqs. (6.45) and (6.46), and optimal control $-\boldsymbol{p}_N$ Eq. (6.43), respectively. The chaser approaches to the target from all start rendezvous points φ_0.

In Fig. 6.9, the controllers' profiles are represented in a rotational frame fixed to $-\boldsymbol{r}(t)$ direction. These figures facilitate understanding of the proposed control design concept and its advantage. A gray fan shape denoted by ∂U_C represents the boundary of input constraints on magnitude and direction U_C, while a gray dotted periodic curve denoted by Γ_u represents the control value of $-\boldsymbol{p}_N$ in the initial rendezvous state $\boldsymbol{x}_0(\varphi_0)$ $(0 \leq \varphi_0 \leq 2\pi)$ on a given periodic orbit Γ, where φ_0 represents the initial phase angle. Dotted straight lines represent asymptotic lines for the maximum and minimum thrust angle amplitude in the final phase $||\theta||_\infty$. $||\theta||_\infty$ oscillates at angular frequency ω, which is an imaginary part of eigenvalue in slowly damped modes (Mitani and Yamakawa, 2011). A dark-gray shape denoted by ∂U_S represents the boundary of stabilization, which is described by examining the poles' stability of closed-loop $A_c(\chi, \Delta\beta)$ Eq. (6.57).

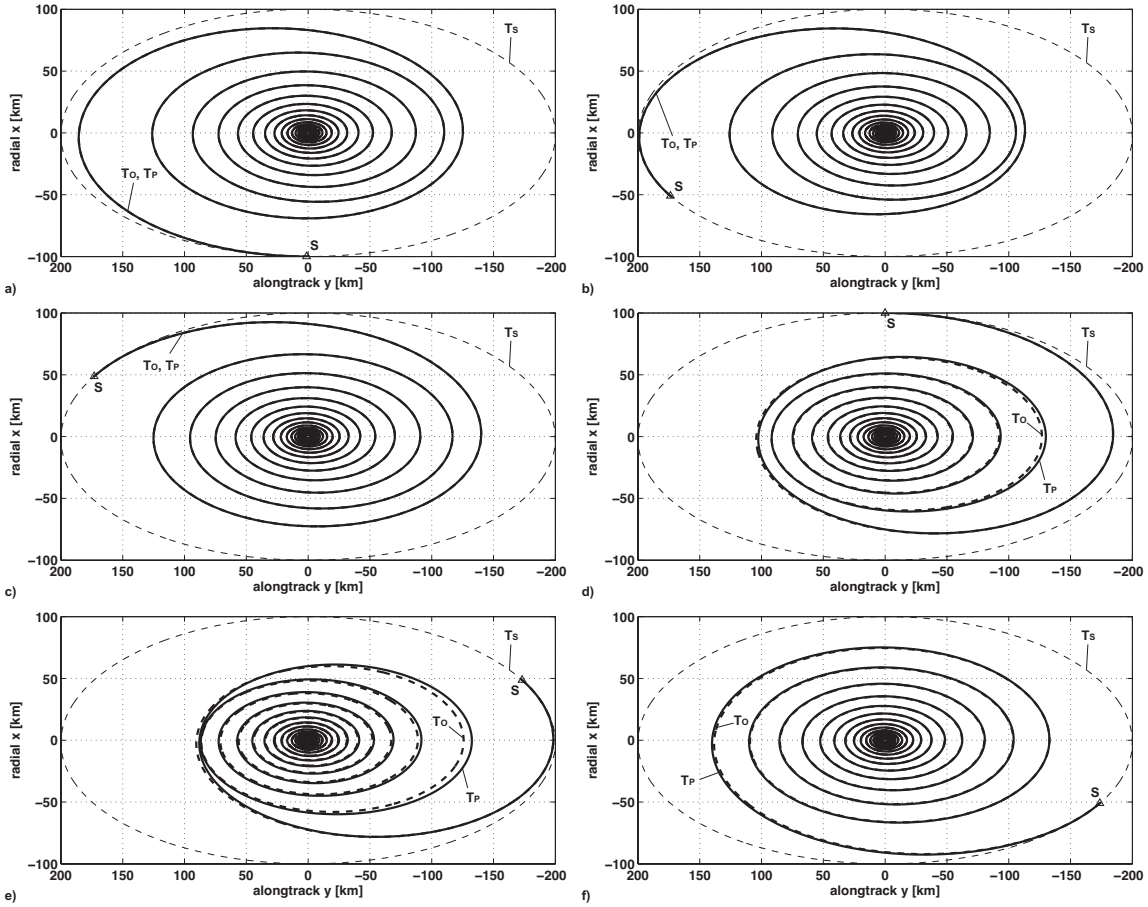

Figure 6.8: Plots of rendezvous trajectories with proposed and optimal control.

In Figs. 6.9, 3 types of control input trajectories are represented; First, the optimal controller denoted by $\boldsymbol{u}_O$, which minimizes J without the constraints (a fine solid line). Second, the proposed controller denoted by $\boldsymbol{u}_P$ (a heavy solid line), and finally, the optimal controller on $\boldsymbol{x}_P \triangleq \boldsymbol{x}(\boldsymbol{u}_P)$ at instantaneous time denoted by $\boldsymbol{u}_V \triangleq -\boldsymbol{p}_N(\boldsymbol{x}_P)$, which is the pre-calculated controller before projecting onto U_C (a fine chained line). If the trajectory of $\boldsymbol{u}_V$ is inside ∂U_S, the nonlinear system remains stable for all $t \in [0\ \infty]$. In some cases, such as $\varphi_0 = 180°$ and $240°$, however, $\boldsymbol{u}_V$ steps over ∂U_S (a bold line denoted by L shown in Figs. 6.9d and 6.9e. This fact means that $\boldsymbol{u}_P$ with parameters $(q,\ \eta,\ b)$ satisfies U_C but the linearized system has temporally unstable modes for some short time. However $\boldsymbol{u}_V$ reverts to the inside of ∂U_S again after a period of time and $\boldsymbol{u}_P$ resumes stability.

This mechanism can be explained as follows: the positive side of the instability region denoted by '+' shows the limitation of slowly damped modes as explained in Fig. 6.4. Since slowly damped modes correspond to periodic moving, the radius of the chaser's relative trajectory grows gradually wider. Conversely, highly damped modes, which correspond to constant and drift moving, decrease so that the property of reaching $||\theta||_\infty$ is still guaranteed for the period of time in question. If the controller enters the temporary instable zone ($\dot{V}(\boldsymbol{x}) \geq 0$), an input zero controller can be chosen. In these cases, $\boldsymbol{u}_P$ is totally included in the satisficing set S_∞ for all time and is therefore continuous. Even if $\dot{V}(\boldsymbol{x}) \geq 0$ but $\boldsymbol{u}_P$ is still chosen, $\boldsymbol{u}_P$ returns to the satisficing set in time. This is because the trajectory becomes periodic to some extent before reaching the instable zone and therefore $-\boldsymbol{r}$ vector rotates to come back to the satisficing set before the divergence for the residual constant and drift mode. After all, Fig. 6.9 shows that the constraints on thrust direction are rigorously satisfied using the proposed control, whereas the thrust angle exceeds γ at the transient phase using optimal control. In addition, θ at the final states is maintained as estimated in (Mitani and Yamakawa, 2011).

Table 6.4 summarizes the performance index J, total Delta-V ΔV, convergence time T^{conv} at each initial phase angle φ_0. Subscripts "O" and "P" represent the case of $\boldsymbol{u}_O$ ($b = 1$) and $\boldsymbol{u}_P$, respectively.

6.5.2 Parameter-setting Case: Sontag's formula

Choose $b = \underline{b}(\boldsymbol{x})$ Eq. (6.39), whereupon $\boldsymbol{u}_V$ becomes the input of Sontag's formula. The parameters $(q,\ \eta)$ are the same as those in the previous section. In this setting case, $\boldsymbol{u}_V$ is guaranteed to be included in S_∞ for a nonlinear system. The selectivity index b converges to 1 ($\underline{b}(\boldsymbol{x}) = 1$ in a linear system) by oscillating. Table 6.5 summarizes the maximum and minimum values of $b(\boldsymbol{x})$ in addition to J, ΔV, T^{conv} at each φ_0.

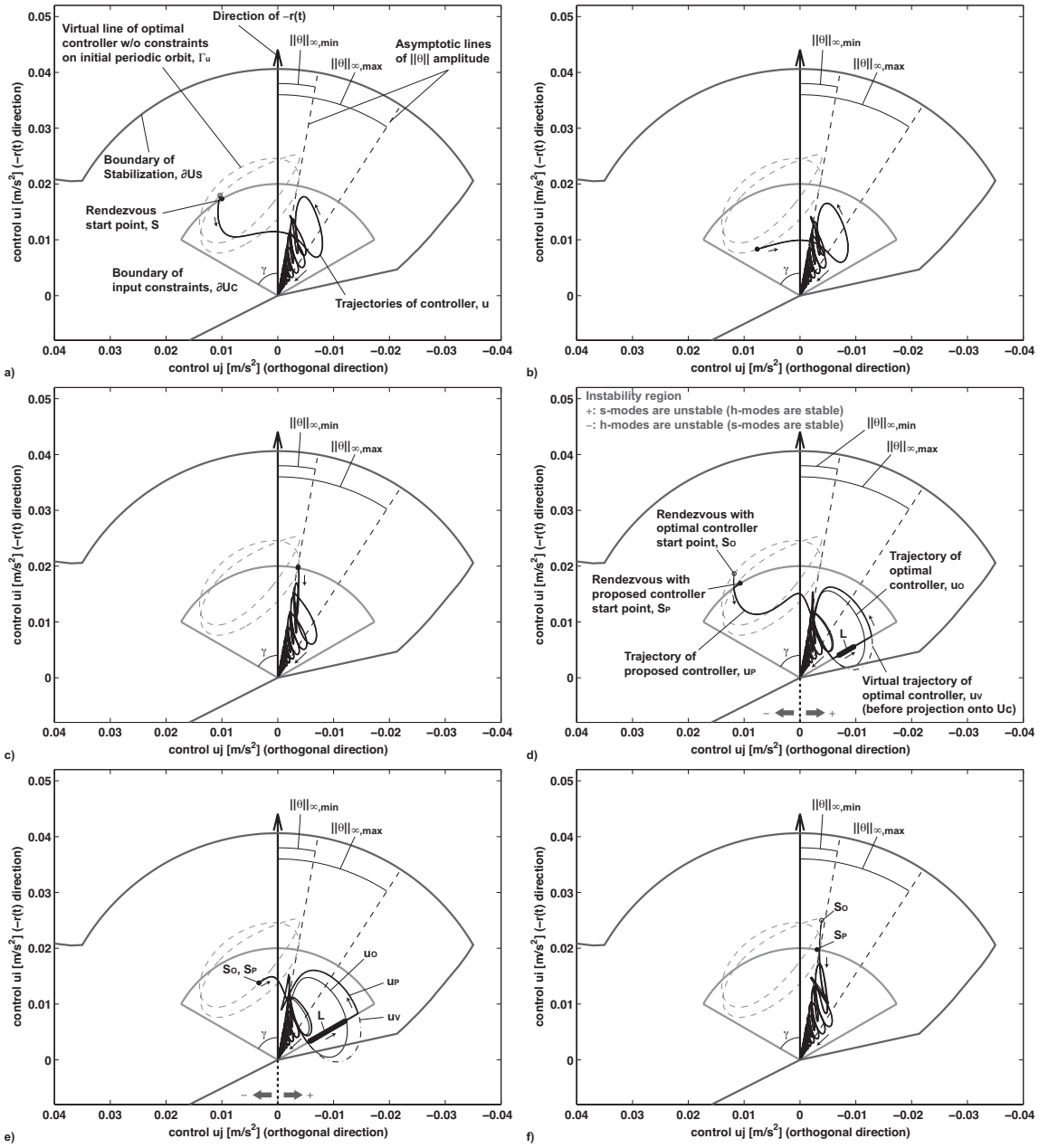

Figure 6.9: Plots of proposed and optimal control profiles in rotational coordinate fixed to $-\boldsymbol{r}(t)$ direction.

Table 6.4: φ_0 [deg], J, ΔV, and T^{conv}. Parameter settings $q = 0.01$, $\eta = 0.9$ and $b = 1$.

φ_0	J_O	J_P	ΔV_O	ΔV_P	T_O^{conv}	T_P^{conv}
0	1.06	1.06	17.0	17.0	63.8	63.8
60	1.03	1.03	15.7	15.7	62.9	62.9
120	0.682	0.682	16.5	16.5	62.0	62.0
180	1.04	1.05	15.8	16.0	61.2	61.2
240	1.03	1.05	14.5	14.9	60.2	60.2
300	0.685	0.684	16.5	16.6	62.0	62.1

Table 6.5: φ_0 [deg], J, ΔV, T^{conv}, and b. Parameter settings $q = 0.01$, $\eta = 0.9$ and $b = b(\boldsymbol{x})$.

φ_0	J_O	J_P	ΔV_O	ΔV_P	T_O^{conv}	T_P^{conv}	$\underline{b}_{\min}$ - $\underline{b}_{\max}$
0	1.21	1.20	17.6	17.6	63.8	63.8	0.436 - 2.29
60	1.11	1.11	15.8	15.9	60.4	62.8	0.467 - 2.01
120	0.731	0.731	15.9	15.9	62.0	62.0	0.438 - 2.26
180	1.15	1.14	14.3	14.8	58.7	61.1	0.421 - 1.79
240	1.10	1.08	13.9	14.4	57.8	60.2	0.512 - 1.80
300	0.745	0.746	15.9	15.9	62.0	62.0	0.402 - 2.52

Subscripts "O" and "P" represent the case of $\boldsymbol{u}_O$ ($b = \underline{b}(\boldsymbol{x})$) and $\boldsymbol{u}_P$, respectively. Compared to the case $b = 1$ (Table 6.4), ΔV diminishes by about 2.3 % on average due to optimization, although ΔV expands slightly at $\varphi_0 = 0°,\ 60°$. Again, $\boldsymbol{u}_P$ is totally included in the satisficing set S_∞ at all times and is therefore continuous.

6.6 Conclusions

In this chapter, the nonlinear rendezvous problem was considered under thrust magnitude and direction constraints. A constraint-satisficing scheme was newly proposed by introducing two barrier functions and it was shown that when the positive coefficients of both barrier functions approach zero, the constraint-satisficing set smoothly attained the intersection of the unconstrained satisficing and input constraint sets. A simple and effective nonlinear controller was proposed with the projected control as a member of the constraint-satisficing set. By adopting the value function in the constraint-free case as a constraint control Lyapunov function, and by choosing appropriate weight matrix parameters, the state trajectory converges to the origin; strictly satisfying the

input constraint in the final phase. For the proposed controller, linearized stability analysis was investigated using graphical description plot and used to assist in designing certain practical rendezvous trajectories. It was found that in the case starting from periodic orbit, the local subspace was widely covered by the region of attraction, provided highly damped modes were stable.

Although the effectiveness of the proposed design was verified in the nonlinear affine system, the same satisficing approach can be easily extended to a time-varying system when the target orbit is elliptic.

Chapter 7

Concluding Remarks

We treated the satellite formation and reconfiguration problem subject to constraints on control magnitude and direction. Firstly, the necessary condition of the optimal controller under these constraints was derived using a sequential smoothing method, in which a sequence of unconstrained optimal control problems was solved according to Pontryagin's Minimum Principle by introducing multiple barrier functions to the original performance index. By introducing the proposed additional barrier function concerning the constraints on control direction, the derived equations for the necessary condition with respect to optimal control magnitude and direction became decoupled, thereby facilitating their solution. The solutions converged toward solving the original problem and strictly satisfied the treated constraints as the perturbation coefficients of the barrier functions approached zero. Optimal controllers were successfully formulated in the L_1- and L_2-norm problems, and both solutions for the optimal control direction had the same form. These solutions are a natural extension of the solution with only the magnitude constraint. As the perturbation coefficients of the barrier functions approach zero, the smoothed optimal controller approaches the boundary of the inequality constraint near Lawden's primer vector, while the control, the primer, and the admissible direction vectors are coplanar. This extremal property is completely consistent with the result whereby the optimal thrust is directed along the projection of the primer vector onto the boundary of the restricting set. Numerical simulations demonstrated that the sequential optimal controller subject to such mixed constraint was obtained by solving the two-point boundary value problem with the shooting method in non-coplanar circular and coplanar eccentric orbits. In addition, the control angles of the derived solutions were confirmed as suppressed within the control direction constraint.

Secondly, we examined how to maintain a small-magnitude thrust angle based on continuous optimal feedback control for the problem of satellite rendezvous. Consider-

ing the constraints on the parameters set in the general quadratic performance index, a control design process was proposed using modal analysis to make the thrust angle small at the initial and final phases. Using a candidate control Lyapunov function (CLF) by solving the Riccati equation for the performance index considered, a new control applying the satisficing method was devised to meet the constraints strictly from start to finish. If the limitation angle is small, the devised control may become null transiently because the candidate CLF is not strictly defined. However, this paper showed that thrust angle can be practically maintained and that the control law leads to convergence at the origin in some simulations. Extending the theory to an eccentric orbit and time-varying system was explained and numerical calculations showed effectiveness. Although the application of two-dimensional plane motion was discussed, this technique can be easily extended to the design method, including out-of-plane motion. This method can also be applied to nonlinear control problems and extended to multiple control constraints, such as sensor field of view and sun direction.

In addition, we took steps to improve satisficing theory under input constraint. A constraint-satisficing scheme was newly proposed by introducing two barrier functions and it was shown that when the positive coefficients of both barrier functions approach zero, the constraint-satisficing set smoothly attained the intersection of the unconstrained satisficing and input constraint sets. A simple and effective nonlinear controller was proposed with the projected control as a member of the constraint-satisficing set. By adopting the value function in the constraint-free case as a constraint control Lyapunov function, and choosing appropriate weight matrix parameters, the state trajectory converged to the origin; strictly satisfying the input constraint in the final phase. For the proposed controller, linearized stability analysis was investigated using a graphical description plot and used to assist in designing certain practical rendezvous trajectories. It was found that when starting from periodic orbit, the local subspace was widely covered by the region of attraction, provided highly damped modes were stable.

Although the effectiveness of the proposed design was verified in the nonlinear affine system, the same satisficing approach can be easily extended to a time-varying system when the target orbit is elliptic.

Appendix A

Solving the L_2-norm problem

A.1 Solving $(\mathcal{P}_2)$ and $(\mathcal{P}_{m2})$

First, solving $(\mathcal{P}_2)$ is much easier than solving $(\mathcal{P}_{m1})$. The optimal control $\boldsymbol{u}_2(f)$ takes the following form Bryson and Ho (1975):

$$\boldsymbol{u}_2^*(f) = -\boldsymbol{p}(f) \tag{A.1}$$

Therefore, there is no bang-off-bang structure, and the magnitude of $\boldsymbol{u}_2$ is p. Next, consider $(\mathcal{P}_{m2})$. The control magnitude constraint can also be considered by introducing $\varepsilon_u F_u$ in Eq. (3.20). In order to apply PMP, build first the Hamiltonian function H_{m2}^{ε} defined as follows:

$$\begin{aligned} H_{m2}^{\varepsilon}(\boldsymbol{x}(f), \boldsymbol{u}(f), \boldsymbol{\lambda}(f)) &= L_2(u) + \varepsilon_u F_u + \boldsymbol{\lambda}^T(\boldsymbol{A}\boldsymbol{x} + \boldsymbol{B}\boldsymbol{u}) \\ &= \tfrac{1}{2}u^2 - \varepsilon_u \log u(1-u) + \boldsymbol{\lambda}^T\boldsymbol{A}\boldsymbol{x} + \boldsymbol{p}^T\boldsymbol{u} \end{aligned} \tag{A.2}$$

The extremal control $\boldsymbol{u}_{m2}^{\varepsilon}(f)$ is then given by $\arg\min_u H_{m2}^{\varepsilon},\ f \in (f_0, f_1)$. In order to obtain $\boldsymbol{u}_{m2}^{\varepsilon}(f)$, applying the Cauchy-Schwartz inequality to Eq. (A.2) yields

$$H_{m2}^{\varepsilon} \geq \tfrac{1}{2}u^2 - \varepsilon_u \log u(1-u) + \boldsymbol{\lambda}^T\boldsymbol{A}\boldsymbol{x} - pu \tag{A.3}$$

and the equality is obtained when

$$\boldsymbol{u}_{m2}^{\varepsilon} = -u_{m2}^{\varepsilon} \cdot \hat{\boldsymbol{p}} \tag{A.4}$$

where the magnitude $u_{m2}^{\varepsilon} \in (0,1)$ is the solution of

$$u - \varepsilon_u \frac{1-2u}{u(1-u)} - p = 0 \tag{A.5}$$

If $\varepsilon_u = 0$, $u = p$ clearly yields $\boldsymbol{u}_{m2}^* = -\boldsymbol{p}$ for Eq. (A.1), which is the solution of $(\mathcal{P}_2)$. If $\varepsilon_u > 0$, Eq. (A.5) becomes a cubic equation with respect to u, and the

solution $u^{\varepsilon}_{m2} \in (0,1)$ is obtained using the Tartaglia-Cardano formula Burnside and Panton (2005). Three real roots are derived in order to satisfy $u_1 < 0 < u_2 < 1 < u_3$. Therefore, a single root $u^{\varepsilon}_{m2} \in (0,1)$ in Eq. (A.5) exists because the other roots of Eq. (A.5) do not satisfy $u \in (0,1)$.

A.2 Solving $(\mathcal{P}_{md2})$

Using $\partial L_2(u)/\partial u = u$, Eq. (3.37) reduces to

$$u - \frac{\varepsilon_u(1-2u)}{u(1-u)} - \tilde{p} = 0 \tag{A.6}$$

which is the same equation as Eq. (A.5) except that p is displaced by $\tilde{p}$ Eq. (3.51). If $\varepsilon_u = 0$, u becomes simply $\tilde{p}$. If $\varepsilon_u \neq 0$, u^{ε}_{md2} can be also derived as the same manner.

Appendix B

Proof of $\nabla^2 H^{\varepsilon}_{mdj} > 0$ at $\boldsymbol{u} = \boldsymbol{u}^{\varepsilon}_{mdj}$

The matrix of the second partial derivatives of H^{ε}_{mdj}, known as the Hessian, is defined as follows:

$$\nabla^2 H^{\varepsilon}_{mdj} = \begin{bmatrix} \frac{\partial^2 H^{\varepsilon}_{mdj}}{\partial u^2} & \frac{\partial^2 H^{\varepsilon}_{mdj}}{\partial u \partial \theta} & \frac{\partial^2 H^{\varepsilon}_{mdj}}{\partial u \partial \varphi} \\ \frac{\partial^2 H^{\varepsilon}_{mdj}}{\partial \theta \partial u} & \frac{\partial^2 H^{\varepsilon}_{mdj}}{\partial \theta^2} & \frac{\partial^2 H^{\varepsilon}_{mdj}}{\partial \theta \partial \varphi} \\ \frac{\partial^2 H^{\varepsilon}_{mdj}}{\partial \varphi \partial u} & \frac{\partial^2 H^{\varepsilon}_{mdj}}{\partial \varphi \partial \theta} & \frac{\partial^2 H^{\varepsilon}_{mdj}}{\partial \varphi^2} \end{bmatrix} \tag{B.1}$$

Since $\nabla^2 H^{\varepsilon}_{mdj}$ exists for all $\boldsymbol{u} \in \mathcal{D}$ and is continuous on $\mathcal{D}$, H^{ε}_{mdj} is twice continuously differentiable on $\boldsymbol{u} \in \mathcal{D}$. Hence, the Hessian is a symmetric matrix

$$\frac{\partial^2 H^{\varepsilon}_{mdj}}{\partial \alpha_1 \partial \alpha_2} = \frac{\partial^2 H^{\varepsilon}_{mdj}}{\partial \alpha_2 \partial \alpha_1}, \quad \text{forall } \alpha_1, \alpha_2 = u, \theta, \varphi \tag{B.2}$$

From Eqs. (3.42) and (3.43),

$$\hat{\boldsymbol{u}}^{\varepsilon}_{mdj} = \frac{\sin\beta}{\sin\theta} \left(\frac{\tilde{\varepsilon}_b}{\hat{\boldsymbol{\xi}}^T \hat{\boldsymbol{u}} + \cos\gamma} \hat{\boldsymbol{\xi}} - \hat{\boldsymbol{p}} \right) \tag{B.3}$$

In addition, $\hat{\boldsymbol{u}}_{\theta\theta} = \hat{\boldsymbol{u}}_{\varphi\varphi} = -\hat{\boldsymbol{u}}^{\varepsilon}_{mdj}$, $\hat{\boldsymbol{u}}_{\theta\varphi} = \boldsymbol{0}$, $\hat{\boldsymbol{\xi}}^T \hat{\boldsymbol{u}}_{\theta} = \sin\theta$, and $\hat{\boldsymbol{\xi}}^T \hat{\boldsymbol{u}}_{\varphi} = \boldsymbol{0}$. Then, substituting these values into Eq. (B.1), the matrix elements are given by

$$\left.\frac{\partial^2 H^{\varepsilon}_{mdj}}{\partial u^2}\right|_{\boldsymbol{u}^{\varepsilon}_{mdj}} = \varepsilon_u \left[\left(\frac{(1-2u)}{u(1-u)}\right)^2 + \frac{2}{u(1-u)}\right] > 0 \tag{B.4}$$

$$\left.\frac{\partial^2 H^{\varepsilon}_{mdj}}{\partial u \partial \alpha}\right|_{\boldsymbol{u}^{\varepsilon}_{mdj}} = \left(-\frac{\varepsilon_b}{\hat{\boldsymbol{\xi}}^T \hat{\boldsymbol{u}} + \cos\gamma}\hat{\boldsymbol{\xi}} + \boldsymbol{p}\right)^T \cdot \hat{\boldsymbol{u}}_{\alpha} = 0 \tag{B.5}$$

$$\begin{aligned}\left.\frac{\partial^2 H^{\varepsilon}_{mdj}}{\partial \alpha^2}\right|_{\boldsymbol{u}^{\varepsilon}_{mdj}} &= u\left[\left(-\frac{\varepsilon_b}{\hat{\boldsymbol{\xi}}^T \hat{\boldsymbol{u}} + \cos\gamma}\hat{\boldsymbol{\xi}} + \boldsymbol{p}\right)^T \cdot \hat{\boldsymbol{u}}_{\alpha\alpha} + \frac{\varepsilon_b (\hat{\boldsymbol{\xi}}^T \hat{\boldsymbol{u}}_{\alpha})^2}{(\hat{\boldsymbol{\xi}}^T \hat{\boldsymbol{u}} + \cos\gamma)^2}\right] \\ &= u\left[p\frac{\sin\theta}{\sin\beta} + \frac{(\boldsymbol{p}^T \hat{\boldsymbol{u}}_{\alpha})^2}{\varepsilon_b}\right] > 0 \end{aligned} \tag{B.6}$$

$$\left.\frac{\partial^2 H^{\varepsilon}_{mdj}}{\partial \theta \partial \varphi}\right|_{\boldsymbol{u}^{\varepsilon}_{mdj}} = u\left[\left(-\frac{\varepsilon_b}{\hat{\boldsymbol{\xi}}^T \hat{\boldsymbol{u}} + \cos\gamma}\hat{\boldsymbol{\xi}} + \boldsymbol{p}\right)^T \cdot \hat{\boldsymbol{u}}_{\theta\varphi} + \frac{\varepsilon_b (\hat{\boldsymbol{\xi}}^T \hat{\boldsymbol{u}}_{\theta})(\hat{\boldsymbol{\xi}}^T \hat{\boldsymbol{u}}_{\varphi})}{(\hat{\boldsymbol{\xi}}^T \hat{\boldsymbol{u}} + \cos\gamma)^2}\right] = 0 \tag{B.7}$$

where $\alpha = \theta, \varphi$. Therefore,

$$\nabla^2 H^{\varepsilon}_{mdj}\big|_{\boldsymbol{u}^{\varepsilon}_{mdj}} > 0 \tag{B.8}$$

Appendix C

Analytical unconstraint L_2 optimal solution

This appendix summarizes a general solution to $(\mathcal{P}_2)$ for dealing with elliptic dynamics derived by Cho Cho *et al.* (2009). The analytical solution to $(\mathcal{P}_2)$ is summarized as follows:

$$\begin{aligned}
\boldsymbol{x}(f) &= \boldsymbol{\Phi}(f)(\boldsymbol{\Phi}^{-1}(f_0)\boldsymbol{x}(f_0) + \boldsymbol{C}^{-1}\boldsymbol{S}(f)\boldsymbol{S}^{-1}(f_1)\boldsymbol{C}\boldsymbol{K}) && \text{(C.1)}\\
\boldsymbol{\lambda}(f) &= -\boldsymbol{\Psi}(f)\boldsymbol{S}^{-1}(f_1)\boldsymbol{C}\boldsymbol{K} && \text{(C.2)}\\
\boldsymbol{u}_2^*(f) &= b_c(f)\boldsymbol{\Phi}_A(f)\boldsymbol{S}^{-1}(f_1)\boldsymbol{C}\boldsymbol{K} && \text{(C.3)}\\
J_2^* &= \boldsymbol{K}^T\boldsymbol{C}^T\boldsymbol{S}^{-1}(f_1)\boldsymbol{C}\boldsymbol{K} && \text{(C.4)}
\end{aligned}$$

where

$$\begin{aligned}
\boldsymbol{\Phi}(f) &= \begin{bmatrix} \boldsymbol{\Phi}_A(f) \\ \boldsymbol{\Phi}'_A(f) \end{bmatrix}, \quad \boldsymbol{\Psi}(f) = \begin{bmatrix} \boldsymbol{A}_2\boldsymbol{\Phi}_A - \boldsymbol{\Phi}'_A \\ \boldsymbol{\Phi}_A(f) \end{bmatrix} && \text{(C.5)}\\
\boldsymbol{S}(f) &= \int_{f_0}^{f} b_c^2(\nu)\boldsymbol{\Phi}_A^T(\nu)\boldsymbol{\Phi}_A(\nu)\mathrm{d}\nu && \text{(C.6)}\\
\boldsymbol{K} &= \boldsymbol{\Phi}^{-1}(f_1)\boldsymbol{x}_1 - \boldsymbol{\Phi}^{-1}(f_0)\boldsymbol{x}_0 && \text{(C.7)}\\
\boldsymbol{C} &= \boldsymbol{\Psi}^T(f)\boldsymbol{\Phi}(f) \\
&= \boldsymbol{\Phi}_A^T(f)\boldsymbol{\Phi}'_A(f) - (\boldsymbol{\Phi}_A^T(f)\boldsymbol{\Phi}'_A(f))^T - \boldsymbol{\Phi}_A^T(f)\boldsymbol{A}_2\boldsymbol{\Phi}_A(f) && \text{(C.8)}\\
b_c(f) &= \frac{R_0^2(f)}{\rho(f)}\frac{\alpha_{\max}}{\mu} && \text{(C.9)}
\end{aligned}$$

In addition, $\boldsymbol{\Phi}(f)$ is referred to as the fundamental matrix associated with matrix $\boldsymbol{A}(f)$, which can be written as Yamanaka and Ankersen (2002)

$$\boldsymbol{\Phi}(f) = \begin{bmatrix} \boldsymbol{\Phi}_A(f) \\ \boldsymbol{\Phi}'_A(f) \end{bmatrix} = \left[\begin{array}{cccccc} s & c & 0 & 2-3es\Omega & 0 & 0 \\ (1+1/\rho)c & -(1+1/\rho)s & 0 & -3\rho^2\Omega & 1 & 0 \\ 0 & 0 & c/\rho & 0 & 0 & s/\rho \\ \hline s' & c' & 0 & -3e(s'\Omega + s/\rho^2) & 0 & 0 \\ -2s & -2c+e & 0 & -3(1-2es\Omega) & 0 & 0 \\ 0 & 0 & -s/\rho & 0 & 0 & c/\rho \end{array}\right]_f \tag{C.10}$$

where $\rho(f) = 1 + e\cos f$, $s(f) = \rho\sin f$, $c(f) = \rho\cos f$, and

$$\Omega = \frac{n(t-t_0)}{(1-e^2)^{\frac{3}{2}}} = \int_{f_0}^{f} \frac{\mathrm{d}\nu}{\rho(\nu)^2} \tag{C.11}$$

Note that $\boldsymbol{K}$ is a constant matrix calculated from a given boundary condition $\boldsymbol{x}(f_0)$, $\boldsymbol{x}(f_1)$, f_0, and f_1, and $\boldsymbol{C}$ is a skew-symmetric constant matrix Carter (1998). Once the matrix $\boldsymbol{C}$ is determined from Eq. (C.8), the inverse of $\boldsymbol{\Phi}$ is readily obtained by $\boldsymbol{\Phi}^{-1} = \boldsymbol{C}^{-1}\boldsymbol{\Psi}^T$. Since the fundamental matrix $\boldsymbol{\Phi}$ has already been revealed, the symmetric matrix S is readily calculated.

Appendix D

Proof of Lemma 6.4.3

If $\chi \neq 1$ and $\Delta\beta \neq \pi/2$, $b' \triangleq b(1-\chi)\cos\Delta\beta \to \infty$ when $b \to \infty$. Therefore the closed-loop matrix $A_c(\chi, \Delta\beta)$ Eq. (6.57) is stabilized as $b \to \infty$ since vector $-g^T V_x = -B^T S\boldsymbol{x}$ is a stable direction. Then $A_c(\chi, \Delta\beta)$ approaches

$$\lim_{b\to\infty} A_c(\Delta\beta, \chi) = \begin{bmatrix} O_2 & I_2 \\ -b'R(\Delta\beta)S_{21} & -b'R(\Delta\beta)S_{22} \end{bmatrix} \tag{D.1}$$

where S_{21}, $S_{22} = S_{22}^T \in \boldsymbol{R}^{2\times 2}$ are submatrices of S:

$$S = \begin{bmatrix} * & * \\ S_{21} & S_{22} \end{bmatrix} \tag{D.2}$$

The characteristic equation of the matrix Eq. (D.1) becomes

$$|\lambda I_2 + b'R(\Delta\beta)S_{22} + \frac{b'}{\lambda}R(\Delta\beta)S_{21}| = 0 \tag{D.3}$$

for $\lambda \neq 0$ where $|A|$ represents determinant of matrix A. Equation (D.3) has two kinds of asymptotic solutions which satisfy the following equations

$$|S_{21}|\left(\frac{1}{\lambda}\right)^2 + \left[\begin{vmatrix} s_{31} & s_{34} \\ s_{41} & s_{44} \end{vmatrix} - \begin{vmatrix} s_{32} & s_{33} \\ s_{42} & s_{43} \end{vmatrix}\right]\left(\frac{1}{\lambda}\right) + |S_{22}| = 0 \tag{D.4}$$

$$\left(\frac{\lambda}{b'}\right)^2 + \mathrm{tr}\left[R(\Delta\beta)S_{22}\right]\left(\frac{\lambda}{b'}\right) + |S_{22}| = 0 \tag{D.5}$$

where s_{ij} is (i,j) component of S. Equation (D.4) has the finite roots which have no relation with $(\chi, \Delta\beta)$. On the other hand, Eq. (D.5) has the roots $\lambda = k(\chi, \Delta\beta)b'$ which diverge to the negative real axis. □

As an example, Fig. D.1 shows the trajectories of poles about $A_c(0,0)$ varying b from 1 to infinity. Slowly damped modes converges to finite poles and highly damped modes diverges to the negative real axis. And Fig. D.2 shows the real part of both modes in this case. The asymptotic solution for solving Eq. (D.4) and (D.5) are also shown on the same plots.

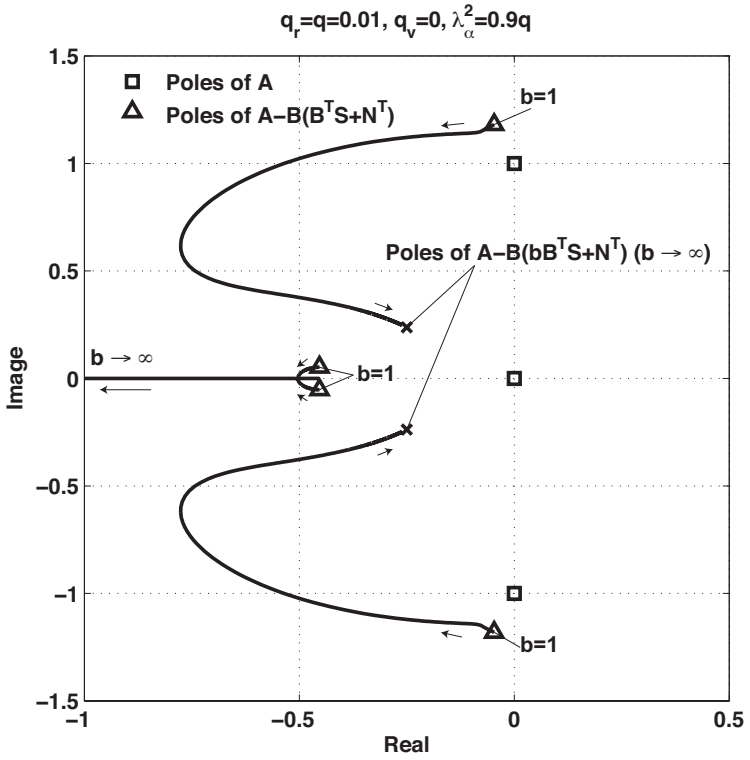

Figure D.1: Trajectories of closed-loop pole assignment in the case $(q, \eta) = (0.01, 0.9)$ and $(\chi, \Delta\beta) = (0, 0)$ varying the selectivity index b from 1 to infinity.

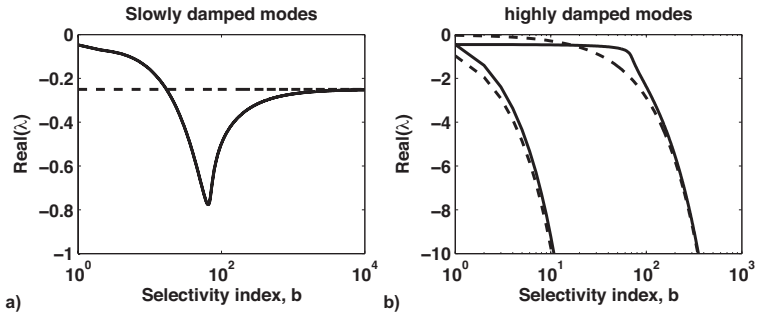

Figure D.2: Real part of both modes varying b. a) slowly damped modes and b) highly damped modes. The parameters are same as Fig. D.1. The dotted lines are asymptotic lines.

Bibliography

Alfriend, K.T., S.R. Vadali, P. Gurfil, J.P. How and L.S. Breger (2010). *Spacecraft Formation Flying: Dynamics, Control and Navigation*. Elsevier, Oxford, U.K.

Artstein, Z. (1983). Stabilization with relaxed control. *Nonlinear Analysis* **7**(11), 1163–1173.

Bando, M. and A. Ichikawa (2009). Periodic Orbits of Nonlinear Relative Dynamics and Satellite Formation. *Journal of Guidance, Control, and Dynamics* **32**(4), 1200–1208.

Bertrand, R. and R. Epenoy (2002). New Smoothing Techniques for Solving Bang-bang Optimal Control Problems - Numerical Results and Statistical Interpretation. *Optimal Control Applications and Methods* **23**(4), 171–197.

Betts, J.T. (1998). Survey of Numerical Methods for Trajectory Optimization. *Journal of Guidance, Control, and Dynamics* **21**(2), 193–207.

Boltz, F.W. (1991). Orbital Motion Under Continuous Radial Thrust. *Journal of Guidance, Control, and Dynamics* **14**(3), 667–670.

Boltz, F.W. (1992). Orbital Motion Under Continuous Tangential Thrust. *Journal of Guidance, Control, and Dynamics* **15**(6), 1503–1507.

Bryson, A.E. and Y. Ho (1975). *Applied Optimal Control, Revised Printing*. Taylor and Francis.

Burnside, W.S. and A.W. Panton (2005). *The Theory of Equations: with an Introduction to the Theory of Binary Algebraic Forms*. University of Michigan Library, MI.

Carter, T.E. (1998). State Transition Matrices for Terminal Rendezvous Studies: Brief Survey and New Example. *Journal of Guidance, Control, and Dynamics* **21**(1), 148–155.

Cho, H., S. Park and K. Choi (2009). Analytic Solution for Fuel-Optimal Reconfiguration in Relative Motion. *Journal of Optimization Theory and Applications* **141**(3), 495–512.

Clohessy, W.H. and R.S. Wiltshire (1960). Terminal Guidance System for Satellite Rendezvous. *Journal of Guidance, Control, and Dynamics* **27**(5), 653–658.

Conway, B.A. (2010). *Spacecraft Trajectory Optimization*. Cambridge University Press, NY.

Curtis, J.W. (2003). CLF-based Nonlinear Control with Polytopic Input Constraints. *42nd IEEE International Conference on Decision and Control* **3**, 2228–2233.

Curtis, J.W. (2005). An Input-to-state Stabilizing Control Lyapunov Function for Autonomous Guidance and Control. *AIAA Guidance, Navigation, and Control Conference, San Francisco, California*.

Curtis, J.W. and R.W. Beard (2001). A Model-Predictive Satisficing Approach to A Nonlinear Tracking Problem. In: *Decision and Control, 2001. Proceedings of the 40th IEEE Conference on*. Vol. 1. IEEE. pp. 491–495.

Curtis, J.W. and R.W. Beard (2002*a*). A Complete Parameterization of CLF-based Input-to-state Stabilizing Control Laws. *Automatica*.

Curtis, J.W. and R.W. Beard (2002*b*). Ensuring Stability of State-dependent Riccati Equation Controllers via Satisficing. *Proceedings of the 41st IEEE Conference on Decision and Control* **3**, 2645–2650.

Curtis, J.W. and R.W. Beard (2004). Satisficing: A New Approach to Constructive Nonlinear Control. *IEEE Transactions on Automatic Control* **49**(7), 1090–1102.

Enright, P.J. and B.A. Conway (1991). Optimal Finite-Thrust Spacecraft Trajectories Using Collocation and Nonlinear Programming. *Journal of Guidance, Control, and Dynamics* **14**(5), 981–985.

Epenoy, R. (2011). Fuel Optimization for Continuous-Thrust Orbital Rendezvous with Collision Avoidance Constraint. *Journal of Guidance, Control, and Dynamics* **34**(2), 493–503.

Epenoy, R. and C. Ferrier (2001). Optimal Control for Engines With Electro-Ionic Propulsion Under Constraint of Eclipse. *Acta Astronautica* **48**(4), 181–192.

Freeman, R.A. and J.A. Primbs (1996). Control Lyapunov Functions: New Ideas From an Old Source. *Proceedings of 35th IEEE Conference on Decision and Control* **4**(2), 3926–3931.

Freeman, R.A. and P.V. Kokotovic (1996). *Robust Nonlinear Control Design: State-Space and Lyapunov Techniques* . Birkhauser Boston.

Gergaud, J. (1989). Résolution Numérique de Probléms de Commande Bang-bang par des Méthods Homotopiques Simpliciales. *Ph.D. Thesis, Institut National Polytechnique de Toulouse (in French).*

Gil-Fernandez, J. and M.A. Gomez-Tierno (2010). Practical Method for Optimization of Low-Thrust Transfers. *Journal of Guidance, Control, and Dynamics* **33**(6), 1927–1931.

Goodrich, M.A., W.C. Stirling and R.L. Frost (1998). A Theory of Satisficing Decisions and Control. *IEEE Transactions on Systems, Man, and Cybernetics - Part A: Systems and Humans* **28**(6), 763–779.

Ichikawa, A. and H. Katayama (2001). *Linear Time-Varying Systems and Sampled-Data Systems*. Springer-Verlag, London.

Ichikawa, A. and M. Bando (2009). Satellite Formation and Reconfiguration with Restricted Control Interval. *The Seventh Asian Control Conference*.

Ichimura, Y. and A. Ichikawa (2008). Optimal Impulsive Relative Orbit Transfer Along a Circular Orbit. *Journal of Guidance, Control, and Dynamics* **31**(4), 1014–1026.

Irvin Jr., D.J., R.G. Cobb and T.A. Lovell (2009). Fuel-Optimal Maneuvers for Constrained Relative Satellite Orbits. *Journal of Guidance, Control, and Dynamics* **32**(3), 960–973.

Keerthi, S.S. and E.G. Gilbert (1988). Optimal Infinite-horizon Feedback Laws for a General Class of Constrained Discrete-time Systems: Stability and Moving-horizon Approximations. *Journal of Optimization Theory and Applications* **57**(2), 265–293.

Khalil, H.K. (2002). *Nonlinear Systems, 3rd ed.*. Prentice Hall, NJ.

Krstić, M. and H. Deng (1998). *Stabilization of Nonlinear Uncertain Systems*. ser. Communication and Control Engineering. London, U.K., Springer-Verlag.

Kuhn, H. and A. Tucker (1961). *Nonlinear Programming*. In Proc. 2nd Berkeley Symposium on Mathematical Statistics and Probability. Berkeley, California.

Lawden, D.F. (1963). *Optimal Trajectories for Space Navigation*. Butterworths, London.

Maciejowski, J. (2002). *Predictive Control with Constraints, Chapter 6*. Prentice Hall.

Massari, M. and F. Bernelli-Zazzera (2009). Optimization of Low-Thrust Reconfiguration Maneuvers for Spacecraft Flying in Formation. *Journal of Guidance, Control, and Dynamics* **32**(5), 1629–1638.

Mayne, D.Q., J.B. Rawlings, C.V. Rao and P.O.M. Scokaert (2000). Constrained Model Predictive Control: Stability and Optimality. *Automatica* **36**, 789–814.

Mitani, S. and H. Yamakawa (2010). A Novel Nonlinear Rendezvous Guidance Scheme with Control Direction Constraints. *Proceedings of the 20th AAS/AIAA Space Flight Mechanics Meeting, San Diego, CA*.

Mitani, S. and H Yamakawa (2011). Novel Nonlinear Rendezvous Guidance Scheme Under Constraints on Thrust Direction. *Journal of guidance, control, and dynamics* **34**(6), 1656–1670.

Mitani, S. and H. Yamakawa (n.d.). Continuous-thrust Transfer with Control Magnitude and Direction Constraints Using Smoothing Techniques. *Journal of guidance, control, and dynamics, Accepted*.

Palmer, P. (2006). Optimal Relocation of Satellites Flying in Near-Circular-Orbit Formations. *Journal of Guidance, Control, and Dynamics* **29**(3), 519–526.

Pontryagin, L. (1961). Optimal Regulation Processes. *American Mathematical Society Translations* **18**, 17–66.

Primbs, J.A. (1999). Nonlinear Optimal Control: A Receding Horizon Approach. *Ph.D. Thesis, California Institute of Technology, Pasadena, CA*.

Ren, W. and R.W. Beard (2004). Trajectory Tracking for Unmanned Air Vehicles With Velocity and Heading Rate Constraints. *IEEE Transactions on Control Systems Technology* **12**(5), 706–716.

Richards, A., T. Schouwenaars, J.P. How and E. Feron (2002). Spacecraft Trajectory Planning with Avoidance Constraints Using Mixed-Integer Linear Programming. *Journal of Guidance, Control, and Dynamics* **25**(4), 755–764.

Saaty, T.L. and J. Bram (1981). *Nonlinear Mathematics*. Dover Publications, NY.

Schaub, H. and J.L. Junkins (2003). *Analytical Mechanics of Space Systems*. AIAA Education Series.

Scheeres, D.J., Park, C. and Vincent Guibout (2003). Solving Optimal Control Problems with Generating Functions. *Advances in the Astronautical Science, AAS 03-575*.

Shibata, M. and A. Ichikawa (2007). Orbital rendezvous and flyaround based on null controllability with vanishing energy. *Journal of Guidance, Control, and Dynamics* **30**(4), 934–944.

Sontag, D.E. (1989). A "Universal" Construction of Artsteins Theorem on Nonlinear Stabilization. *Applied optics*.

Stirling, W.C. (2003). *Satisficing Games and Decision Making: with applications to engineering and computer science*.

Sukhanov, A.A. and A.F.B.de A. Prado (2007). Optimization of transfers under constraints on the thrust direction: I. *Cosmic Research* **45**(5), 417–423.

Sukhanov, A.A. and A.F.B.de A. Prado (2008). Optimization of Transfers under Constraints on the Thrust Direction: II. *Cosmic Research* **46**(1), 49–59.

Sznaier, M., R. Suarez and J. Cloutier (2003). Suboptimal Control of Constrained Nonlinear Systems via Receding Horizon Constrained Control Lyapunov Functions. *International Journal of Robust and Nonlinear Control* **13**(3-4), 247–259.

Tschauner, J. (1967). Elliptic Orbit Rendezvous. *AIAA Journal* **5**(6), 1110–1113.

Tschauner, J. and P. Hempel (1964). Optimale Beschleunigeungsprogramme fur das Rendezvous Manover. *Astronautica Acta* **10**(5-6), 296–307.

Wie, B. (1998). *Space Vehicle Dynamics and Control*. AIAA, Reston, VA.

Woffinden, D.C., M.B. Rose and D.K. Geller (2008). Trigger Angle Targeting for Orbital Rendezvous. *The Journal of the Astronautical Sciences* **56**(4), 495–513.

Yamakawa, H. and I. Funaki (2008). Radially Accelerated Periodic Orbits in the Clohessy-Wiltshire Frame. *The Journal of the Astronautical Sciences* **56**(1), 1–16.

Yamanaka, K. and F. Ankersen (2002). New State Transition Matrix for Relative Motion on an Arbitrary Elliptical Orbit. *Journal of Guidance, Control, and Dynamics* **25**(1), 60–66.

Publication List

Journal Papers

- Shinji Mitani and Hiroshi Yamakawa, Novel Nonlinear Rendezvous Guidance Scheme Under Constraints on Thrust Direction, Journal of Guidance, Control, and Dynamics, Vol. 34 No. 6, pages 1656-1671, 2011

- Shinji Mitani and Hiroshi Yamakawa, Continuous-thrust Transfer with Control Magnitude and Direction Constraints Using Smoothing Techniques, Journal of Guidance, Control, and Dynamics, (accepted)

- Shinji Mitani and Hiroshi Yamakawa, Satisficing Nonlinear Rendezvous Approach Under Control Magnitude and Direction Constraints, Journal of Guidance, Control, and Dynamics, (submitted)

Conference and Workshop Papers

- Shinji Mitani and Hiroshi Yamakawa, A Novel Nonlinear Rendezvous Guidance Scheme with Control Direction Constraints, Proceedings of the 20th AAS/AIAA Space Flight Mechanics Meeting, AAS 10-178, Vol. 136, Pt. II, pages 1181-1198, San Diego, CA, 2010

- Shinji Mitani and Hiroshi Yamakawa, Rendezvous Trajectory Planning with Safety Considerations, Proceedings of ISAS Workshop on Astrodynamics and Flight Mechanics, 2009

- Shinji Mitani and Hiroshi Yamakawa, Rendezvous trajectory planning with practical constrained conditions, Proceedings of the 53th Space Sciences and Technology Conference, 1I17, Kyoto, 2009 (*in Japanese*)